Landslide Geoanalytics Using LiDAR-derived

Digital Elevation Models

by

Saeid Pirasteh

A thesis

presented to the University of Waterloo

in fulfilment of the

thesis requirement for the degree of

Doctor of Philosophy

in

Geography

Waterloo, Ontario, Canada, 2018

Examining Committee Membership

The following members served on the Examining Committee for this thesis. The decision of the Examining Committee is by majority vote.

External Examiner   NAME: Baoxin Hu

                                                               Title: Professor

Supervisor(s)   NAME: Jonathan Li

                                                                 Title: Professor

Internal Member   NAME: Ellsworth LeDrew

                                                                  Title: Professor

Internal-external Member   NAME: Shoufa Lin

                                                                 Title: Professor

Other Member(s)   NAME: Michael Chapman

                                                                  Title: Professor

Author's Declaration

This thesis consists of material all of which I authored or co-authored: see Statement of Contributions included in the thesis. This is a true copy of the thesis, including any required final revisions, as accepted by my examiners.

I understand that my thesis may be made electronically available to the public.

Statement of Contributions

The doctoral thesis is compiled under the manuscript option, following the guidelines provided by the joint Waterloo-Laurier Graduate Program in Geography. Three manuscripts published in refereed journals and two manuscripts in the process of publication, as listed below, are presented in Chapters 3 to 6, respectively. Please note that the manuscripts are modified with some minor changes for consistent formatting.

[1] **Pirasteh Saied***, and Li, J. (2016). Landslides investigations from geo-informatics perspective: Quality, challenges, and recommendations. *Geomatics, Natural Hazards and Risk*, 1-18. doi:10.1080/19475705.2016.1238850. (Chapter 2)

[2] **Pirasteh Saied***, Li, J., and Chapman, M. (2017a). Use of LiDAR-derived DEM and a stream length-gradient index approach to investigation of landslides in Zagros Mountains, Iran. *Geocarto International,* 1-15. doi:10.1080/10106049.2017.1316779. (Chapter 3)

[3] **Pirasteh Saied***, and Li, J. (2017a). Probabilistic frequency ratio (PFR) model for quality improvement of landslide susceptibility mapping from LiDAR point clouds. *Geoenvironmental Disaster*. 4:9. doi: 10.1186/s40677-017-0083-z. (Chapter 4)

[4] **Pirasteh Saied***, Li, J., and Chapman, M. (2017b). An approach of semi-automated geometric analysis and classification of landslides incorporating LiDAR-derived DEMs. *Environmental Earth Sciences*, in press. (Chapter 5)

[5] **Pirasteh Saied***, and Li, J. (2017b). An approach of landslide deformation simulation-modeling and flow direction using LiDAR-derived DEMs and UAV images. *International Journal of Digital Earth*, under review. (Chapter 6)

In the above-mentioned five manuscripts, I am the first author and corresponding author, and my supervisor Professor Dr. Jonathan Li is co-author. These manuscripts are dominated by my intellectual effort. The roles of co-authors are explained in detail below.

The ideas in the five manuscripts were conceived by me and guided by Dr. Li. I carried out the work, including database design, field visits, data processing and analysis, development of algorithms, implementation, manuscript writing, and revision. Dr. Li actively participated in the discussion of the results and in the reviewing and revision of the manuscripts. The other co-author participated in providing insights for analytical approaches. Professor Dr. Michael Chapman provided critical suggestions on analytical design and reference choice. Signatures of co-authors indicate they are in agreement with the statements above.

Jonathan Li_____ Michael Chapman_____

Thesis Contributions

This doctoral dissertation aimed to make the following contributions: (a) landslide investigations and assessments from Light Detection And Ranging (LiDAR)-derived Digital Elevation Models (DEMs) and Geographical Information System (GIS) techniques by implementing empirical, ground truth, and analytical approaches of tectonic geomorphology features; (b) an analysis of PFR model for landslide susceptibility mapping by using LiDAR-derived DEMs as well as for validation and updating of the existing inventory dataset; (c) a geoanalytical approach for developing algorithms and codes or a software platform for semi-automated geometric and deformation analysis as well as classification of landslides that can possibly be implemented into a future platform like a web-GIS for landslide prediction; (d) an introduction of a classification of landslides based on landslide geometry; and (e) identification of the challenges and quality of remote sensing data and techniques for landslide investigations in Iran.

Abstract

Landslides are natural hazards that contribute to tremendous economic loss and result in fatalities if there is no well-prepared mitigation and planning. Assessing landslide hazard and optimizing quality to improve susceptibility maps with various contributing factors remain a challenge when working with various geospatial datasets. Also, the system of updating landslide inventories which identify geometry, deformation, and type of landslide with semi-automated computing processes in the Geographic Information System (GIS) can be flawed. This study explores landslide geoanalytics approaches combined with empirical approach and powerful analytics in the Zagros and Alborz Mountains of Iran. Light Detection And Ranging (LiDAR)-derived Digital Elevation Models (DEMs), Unmanned Aerial Vehicle (UAV) images, and Google Earth images are combined with the existing inventory dataset. GIS thematic data in conjunction with field observations are utilized along with geoanalytics approaches to accomplish the results.

The purpose of this study is to explore the challenges and techniques of landslide investigations. The study is carried out by studying stream length-gradient (SL) index analysis in order to identify tectonic signatures. A correlation between the stream length-gradient index and the graded Dez River profile with slopes and landslides is investigated. By building on the previous study a quantitative approach for evaluating both spatial and temporal factors contributing to landslides for susceptibility mapping utilizing LiDAR-derived DEMs and the Probability Frequency Ratio (PFR) model is expanded. Furthermore, the purpose of this study is to create an algorithm and a software package in MATLAB for semi-automated geometric analysis to measure and determine the length, width, area, and volume of material displacement and flow direction, as well as the type of landslide. A classification method and taxonomy of landslides are explored in this study. LiDAR-derived DEMs and UAV images help to

characterize landslide hazards, revise and update the inventory dataset, and validate the susceptibility model, geometric analysis, and landslide deformation.

This study makes the following accomplishments and contributions: 1) Operational use of LiDAR-derived DEMs for landslide hazard assessment is estimated, which is a realistic ambition if we can continue to build on recent achievements; 2) While a steeper gradient could potentially be a signature for landslide identification, this study identifies the geospatial locations of high-gradient indices with potential to landslides; 3) An updated inventory dataset is achieved, this study indicates an improved landslide susceptibility map by implementing the PFR model compared to the existing data and previous studies in the same region. This study shows that the most effective factor is the lithology with 13.7% positive influence; and 4) This study builds a software package in MATLAB that can a) determine the type of landslide, b) calculate the area of a landslide polygon, c) determine and measure the length and width of a landslide, d) calculate the volume of material displacement and determine mass movement (i.e. deformation), and e) identify the flow direction of a landslide material movement. In addition to the contributions listed above, a class taxonomy of landslides is introduced in this study. The relative operating characteristic (ROC) curve method in conjunction with field observations and the inventory dataset are used to validate the accuracy of the PFR model. The validation of the result for susceptibility mapping accuracy is 92.59%. Further, the relative error method is applied to validate the performance of relative percentage of error of the selected landslides computing in the proposed software package. The relative percentage of error of the area, length, width, and volume is 0.16%, 1.67%, 0.30%, and 5.50% respectively, compared to ArcGIS. Marzan Abad and Chalus from Mazandaran Province of Iran and Madaling from Guizhou Province of China are used for validating the proposed algorithm.

Acknowledgements

with the Department of Geography and Environmental Management at University of Waterloo

for helping me in various ways.

Finally, and most importantly, I am deeply indebted to my parents and my wife for their

love, patience, understanding, and support.

Dedication

This Ph.D. thesis is dedicated to everyone around the world, including students, professionals, and volunteers, who work in the field of landslide hazards planning. Their dedication, sacrifice, and skill are the inspiration that motivated me to pursue this study. For their work they deserve the best technologies and tools for hazards prevention and the future development of a smart system for hazards forecasting.

Table of Contents

xiii

List of Figures

List of Tables

List of Abbreviations

ASTER	Advanced Spaceborne Thermal Emission and Reflection
DEM	Digital Elevation Model
DIP	Digital Image Processing
FOV	Field of View
GCPs	Ground Control Points
GIS	Geographical Information System
GPS	Global Positioning System
HRF	Hierarchy Robust Filter
HZ	High Zagros
InSAR	Interferometric Synthetic Aperture Radar
ISO	Iranian Survey Organization
LiDAR	Light Detection And Ranging
NDVI	Normalized Difference Vegetation Index
NITR	Numerical Integral Trapezoidal Rule
PFR	Probability Frequency Ratio
RMSE	Root Mean Square Error
ROC	Relative Operating Characteristic
RTK	Real Time Kinematic
SSZ	Sanandaj Sirjan Zone
UAV	Unmanned Aerial Vehicle
UTM	Universal Transverse Mercator
ZFB	Zagros Fold Belt
ZSB	Zagros Structural Belt
ZT	Zagros Thrust

Chapter 1

Introduction

1.1 Introduction to Landslides

Landslide is a general term used to describe the downslope movement of materials such as soil and rock under the effects of gravity. A landslide is a very common phenomenon of the geological and geomorphological process (Varnes, 1984; Cruden, 1991; Highland and Bobrowsky, 2008) on the Earth's surface that occurs on a wide range of spatial and temporal scales. Landslides can change landscapes; for example, a recent massive landslide on a California highway went into the Pacific Ocean, hit a Californian community, and added to a record cost of one billion dollars in highway damage from one of the state's wettest winters in decades (Canadian Press, 2017). Landslides are natural hazards that contribute to tremendous economic loss and result in fatalities if they are not recognized, assessed, and monitored with a well-prepared mitigation and loss-reduction program. The term "landslide" denotes events such as ground movement, rock fall, failures of slopes, topples, slides, spreads, and flows. Also, it may involve debris flows, mudflows, or mudslides. Landslides happen rapidly in the world every year, particularly in Asia (Figure 1.1). These landslide events have drawn the interest of non-geologists based on the need to practice catastrophic and visible mass movements that are widely recognized by other disciplines. Landslides cause several thousand deaths worldwide often. However, the long-term average of spatiotemporal distribution and the impacts on the environment and people may still be underestimated due to the non-availability of data as well as outdated inventory datasets to reinforce the foundation for smart decision-making (Petley, 2012; Sassa, 2017a; Sassa, 2017b; Sassa, 2017c; UN-GGIM, 2017). One global dataset of fatalities

from tectonic actives and non-seismically triggered landslides resulting in loss of life and worldwide data recorded during a seven-year period indicated 2,620 fatal landslides causing a total of 32,322 recorded fatalities. Environmental impacts and human losses from landslides have mostly occurred in Asia, especially along the Himalayan Arc, China, and certain regions of Iran in the Alborz and Zagros Mountains and parts of the Himalayas.
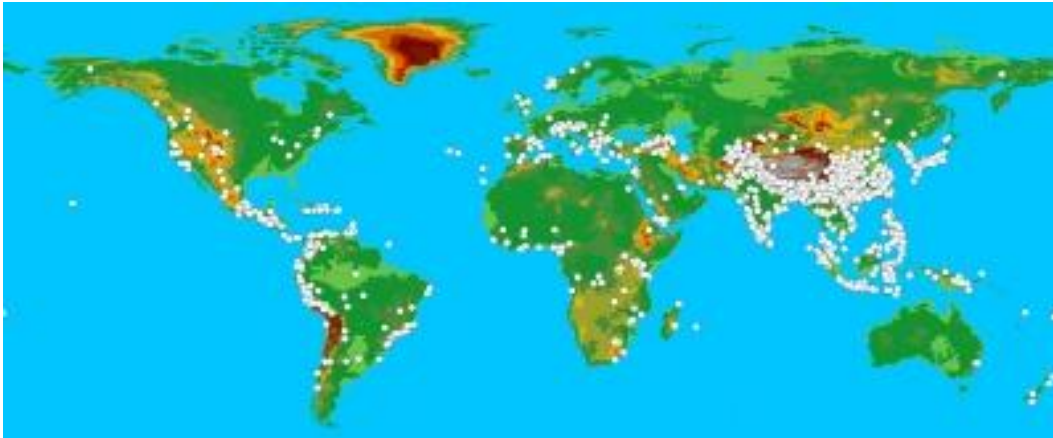
Figure 1.1: Fatal landslides from 2004-2010 with white dots. Source: NASA-http://www.nature.com/news/death-toll-from-landslides-vastly-underestimated-1.11140.

In this study, geoanalytics are used to interpret location-based landslide data combined with powerful analytics and logical correlation among objects. Geoanalytics provides a new context for and perspective of data with a complex mathematical calculation and topological relationships to investigate a landslide in a way which cannot be presented with tables and charts. Developing methods to map susceptible landslide areas with acceptable accuracy, extract the geometry of a landslide polygon automatically, and simulate the material displacement and mass movement flow direction of deformation require a geoanalytical and modelling approach. Geoanalytic is the location-based data, combined with powerful analytics puts a wealth of information at fingertips. Modelling is also the act of building a model that has been carried out in this research for landslide study. Also, geodata is information about all geographic locations of

landslide or any object that is stored in a format and can be used with a geographical information system (GIS).

Although an semi-automated classification of landslides is challenging, the goal of this thesis is (a) to investigate the challenges, quality, and issues of the landslide study in the Zagros and Alborz Mountains of Iran; (b) to improve landslide susceptibility mapping and update the inventory dataset; and (c) to develop a solution package consisting of semi-automated landslide geometry extraction for determining the length, width, area, volume, and landslide type as well as the deformation pattern and flow direction of the material movement simulation. In this study, utilizing Light Detection And Ranging (LiDAR)-derived DEMs and high resolution of orthoimages could prove reliable for upgrading inventory datasets in real-world applications. In addition, the proposed landslide geometry and deformation pattern algorithm and code could probably be used for establishing a platform for data collection and sharing data based on the future direction of the United Nation Global Geospatial Information and Resources Management (UN-GGIM) sustainable development goals (http://ggim.un.org/).

Following the introduction, this chapter describes the general thesis and motivation in Section 1.2; the problem statement, research assumptions and core research issues in Section 1.3; the objectives of thesis in Section 1.4; and the thesis organization in Section 1.5.

1.2 Motivation

In the last decades, we have observed the following: (1) Remote sensing technologies have been used from the realm of research for operational use in natural hazards. Furthermore, satellite images and DEMs are useful for reducing and preventing damages in conjunction with Geographical Information System (GIS) techniques for susceptibility modelling and mapping. (2) Private industries, government agencies, and public/private stakeholder consortiums are

planning or may have recently formed their intentions to work with large-scale acquisitions data of LiDAR data utilizing Unmanned Aerial Vehicle (UAV) for natural hazard studies as well as landslide investigations (Pirasteh and Li, 2016). In developed countries, this will likely take place before 2020 (Evans et al., 2009); and in developing countries such as Iran, this will likely take place before 2030 (UN-GGIM, 2015). (3) LiDAR data acquisition, digital processing, quality, updating, and validation of landslide inventory dataset. Also, optimization of utilizing a DEM in landslide investigation and semi-automated extraction of landslide geometry and landslides classification are elements to encourage the author to study. In addition to the aforementioned, determining the volume of mass movement and landslide deformation pattern simulation have remained a challenge and a key interest of researchers in defining unlimited applications such as landslide monitoring and assessment. (4) Furthermore, LiDAR and user-driven products for decision-makers and consistent standards in project planning have not yet been probably well-introduced in some applications, as they are still undiscovered across multiple disciplines.

By considering the issues outlined above, it is concluded that remote sensing products such as DEM particularly with a high-resolution in pixel size are increasingly being used in the landslide community. These products are becoming an essential tool for landslide studies. Thus, this study may expect that in a few years, LiDAR sensors and UAV will have likely become standard tools for landslide investigations, susceptibility mapping, and monitoring. However, remote sensing products may still require practical recommendation to the users and applications of investigations of geometric analysis, deformation analysis, classification, quality, updating, and validity of the existing inventory landslides dataset. The real challenge is to not only use and benefit from the products of LiDAR and UAV technologies such as high resolution DEMs and satellite images, but also to develop more methods and technical computing algorithms and

codes to assess recent landslides, update inventory dataset, prediction, geometry analysis, deformation analysis, and classification. Also, researchers have not yet notably attempted to extract DEM derivatives with new information (Pirasteh and Li, 2016).

Therefore, the motivation of this research is not only to explore the use of DEM derivatives accompanying satellite images in landslide recognition and GIS techniques for susceptibility modelling and mapping, but also to (a) develop an algorithm for semi-automated extraction of landslides geometry, (b) conduct deformation analysis, and (c) determine the landslide type from the updated inventory dataset in conjunction with LiDAR and UAV technologies to optimize the quality of data. More concretely speaking, this study aims at building and advancing semi-automated extraction of landslide geometry and deformation patterns simulation, modelling, and mapping with MATLAB. The two proposed MATLAB codes not only enable generating of geometric representation and report, but also support the validation of landslide deformation description within the inventory dataset. The proposed algorithm and the MATLAB codes compute the geographical coordinates of the landslide polygon, slope angle (θ), length, width, area, and classification of a landslide. These data are supported and identified by high resolution satellite images of Google Earth, UAV orthoimages, LiDAR-derived DEMs, and an inventory dataset in conjunction with field observations. Also, this proposed algorithm enables simulating, modelling, and mapping of before and after landslides for deformation, volume, and failure material displacement direction.

1.3 Research Assumptions and Core Research Issues

1.3.1 Research Assumptions

This study observes that: (1) Landslide assessment is a very important issue in deformation of environment and the Earth's surface, and such assessment is useful for reducing and preventing damages; (2) Conventional surveying techniques can only provide data measurements with very

low sampling and may not provide detailed information for landslide deformation description, particularly for a large geographical area being monitored object; (3) Satellite images may not be a desirable choice for generating a high-resolution of a DEM to study the landslide, but may be used for geologic and geomorphologic interpretation to identify influential parameters such as vegetation, faults, folds, and drainage networks for landslides assessment; (4) LiDAR and UAV have alternative advantages in capturing high-density 3D point cloud data and images that open substantial potential for landslide ; and (5) The utilization of the probability frequency ratio (PFR) model (see Chapter 4) in the GIS environment accompanied with the LiDAR-derived DEM, temporal Google Earth images, and UAV images of the high-resolution data can enrich the extraction of DEM derivatives such as slope, aspect, and drainage density with qualitative and detailed information for landslide susceptibility mapping. They may also increase the quality of geometric analysis such as volume of materials displacement, length, width, and area measurement of a landslide. This study presumes that these techniques could possibly validate and update any existing landslide inventory dataset. Also, these techniques may result in identifying more precise evaluation in ranking the landslide contributing factors such as lithology, land use, drainage, vegetation, and lineaments in the grid form.

1.3.2 Core Research Issues

In general, this research looks at landslide investigations from two perspectives: (1) inside the landslide boundary, and (2) outside the landslide boundary. Therefore, the research focuses on (a) assessing the quality of landslide assessment (i.e. both inside and outside the landslide boundary) and exploring the tectonic geomorphology features utilizing a LiDAR-DEM for landslide investigations; (b) evaluating geodata analytics and empirical approaches of landslide assessment by implementing PFR model for susceptibility mapping of a large to small area (i.e.

outside the landslide boundary); and (c) developing an algorithm as well as codes for semi-automated geometric analysis (i.e. for inside the landslide boundary), deformation simulation, modelling, and mapping. This study also focuses on a classification of landslides using LiDAR-derived DEMs, Google Earth images, UAV images, and the existing inventory dataset in conjunction with field observations to support the quality and validation of the landslide analysis. The following questions and problems are answered in this Ph.D. research thesis:

- *Problem-1*: How are landslides assessed using LiDAR-derived DEM and GIS techniques by implementing empirical and analytical approaches? What are the factors influencing a landslide in the Alborz Mountains? This research focuses on the use of the LiDAR-derived DEMs, Google Earth images, and UAV images to represent an improved landslide susceptibility map, support validation, and update the inventory dataset. This study explores and identifies empirical and geoanalytics methods which enable the extraction of tectonic geomorphology features and susceptible hazard-prone areas for landslide investigations from the DEMs and PFR model.

- *Problem-2*: What are the different geometric types of landslides? How can a semi-automated algorithm be developed to determine the type of landslide? Which algorithm can be used in developing a software tool to determine length, width, area, and volume of a landslide? ArcGIS software has limitation in detecting and determining landslide length, width, or type. In addition, it cannot determine length (long side) and width (short side), and also type of a landslide. In this study, the researcher must first understand the phenomenon of landslide and identify the main modelling analysis requirements to represent a landslide's geometry and classification. Moreover, this study needs to understand the length, width, deformation, and classification of landslides. Furthermore, this study needs to determine which equation might be used to evaluate and measure the length, width, and area of a landslide polygon as well as the

volume of a mass movement. Of course, this automatic computing technical process should benefit from evaluating and analyzing the landslide investigations mentioned in Problem-1.

1.4 Objectives of the Thesis

The objectives of this research are:

1) To apply LiDAR-derived DEMs and user-driven products such as drainage network and to determine stream length-gradient index anomalies for undiscovered approaches of landslide identification and assessment by determining the value of the stream length-gradient index and the river topography profile;

2) To evaluate the inventory datasets by applying PFR model for quality improvement and landslide susceptibility mapping using LiDAR-derived DEMs;

3) To develop a semi-automated algorithm to extract landslide geometry and analyze deformation patterns using LiDAR-derived DEMs and UAV imaging system; and

4) To develop a semi-automated algorithm and to determine landslide type.

1.5 Thesis Organization

This thesis is organized into seven chapters including this introduction chapter.

Chapter 2 presents the general methodology of this thesis, including descriptions of the study area and the whole research work shares in common, and defines how the following chapters connect to geoanalytics for susceptibility mapping and the semi-automated extraction of landslide geometric analysis and deformation simulation using scripting and coding associated with remote sensing and GIS technologies. Moreover, this chapter outlines the advantages and disadvantages of the various techniques and models from previous studies based on challenges, quality, and recommendations using LiDAR-derived DEMs for the landslide assessment.

Chapter 3 presents the stream gradients analysis in the RiverTools and ArcGIS software to identify signatures, interpret, and improve landslide investigations and mapping. Moreover, this chapter identifies the correlation between stream length-gradient index and the graded topographic profile with slopes and landslides.

Chapter 4 describes the integrations of LiDAR-derived DEMs, ASTER DEMs, and GIS-based analysis in conjunction with the inventory dataset and field observations and applies the PFR model for landslide susceptibility mapping.

Chapter 5 presents a semi-automated algorithm for extraction of landslide geometry, including landslide polygon extraction, and determination of the length, width, and area of a landslide, and use of MATLAB for generation of geometric representation and reports and validation of an updated landslide deformation description.

Chapter 6 describes an algorithm to simulate and model the material displacement volume and flow direction as well as landslide classification. This chapter also presents a landslide classification method based on the geographical coordinates, slope angle (θ), and geometry of landslides..

Chapter 7 presents the conclusions from the thesis and recommendations for future work.

Chapter 2

Description of Methodology

This chapter describes the general methodology of this thesis and attempts to show the relationships among the chapters. Section 2.2 presents the skeleton of the strategic research design of the thesis. Section 2.3 details the study area, and Section 2.4 presents the data acquisition and the datasets used. Section 2.5 describes the accessibility and quality of data, determining datasets for landslide investigations, geoanalytics approaches based on data availability, as well as past occurrence of catastrophic landslides. Section 2.6 demonstrates the proposed approach of a tectonic geomorphological analysis utilizing remote sensing and GIS techniques for landslide investigations of the Zagros Mountains. Section 2.7 presents the PFR model and improvement of landslide susceptibility mapping based on the existing and updated inventory datasets and LiDAR-derived DEMs in conjunction with field observations. Section 2.8 presents an algorithm for semi-automated extraction of the length, width, and area of a landslide polygon. Section 2.9 describes an algorithm for simulation of volume material displacement, deformation pattern, and flow direction. Section 2.10 summarizes this chapter.

2.1 Introduction

Landslide investigations, which involve several qualitative or quantitative approaches, are discussed in many scholarly research papers (Wu and Sidle, 1995; Pack et al., 1998; Lee et al., 2002; Zhou et al., 2003; Schulz, 2007; Watts, 2004; Pradhan et al., 2006; Yilmaz and Yildrim, 2006; Ercanoglu et al., 2008; Yalkin, 2008; Pradhan and Buchroithner, 2010; Pradhan and Pirasteh, 2010; Yilmaz, 2010; Goetz et al., 2011; Choi et al., 2012; Solaimani et al., 2013; Zarea et al., 2013; Jebur et al., 2014; Lee et al., 2014; Su et al., 2015). Moreover, the amount and the quality of available data such as DEM, appropriate methodology of analysis, and modelling are

significant elements of landslide susceptibility mapping (Carrera et al., 1991; Montgomery and Dietrich, 1994; Dai and Lee, 2002; Huabin et al., 2005; Evans et al., 2009; Mehrdad et al., 2010; Guzzetti et al., 2012; Konstantinos et al., 2016).

Researchers have implemented the diagnosis of landslide processes by means of geographical distribution of landslides, by developing algorithms and codes, and by generating susceptibility maps and models. Also, some researchers have attempted the semi-automated approach by identifying landslide-contributing factors, measuring accuracy performance, forming a geological and engineering perspective, utilizing remote sensing technologies, and considering early warning systems (Wu and Sidle, 1995; Zhou et al., 2003; Watts, 2004; Jebur et al., 2014; Lee et al., 2014; Su et al., 2015; Siyahghalat et al., 2016).

There are three major remote sensing techniques used in landslide investigations. They are (1) aerial photography, which is considered an early technique (Su and Stohr, 2000); (2) interferometric synthetic aperture radar (InSAR) (Travelletti et al., 2008; Jaboyedoff et al., 2012; Bianchini et al., 2016); and (3) LiDAR (Su and Bork, 2006). All of these techniques have advantages, disadvantages, and limitations.

2.2 Research Design

This thesis investigates the relationship between tectonic geomorphology and landslide hazards, and explores the modelling, simulating, and mapping of landslides using LiDAR-derived DEMs (5m).

Figure 2.1 illustrates the relationships among chapters, datasets, and methods used in this thesis. In this study, data availability and data quality for modelling, simulating, mapping, and geometric analysis have been determined, and challenges have been identified. Some recommendations are provided in Section 2.5. Landslide influencing factors have been studied and a new technique of assessing landslides has been developed by investigating the stream

length-gradient index and empirical interpretations of the Dez River profile in conjunction with field observations (see Chapter 3).

The quality of landslide susceptibility evaluation was improved by applying the PFR model to consider the effects of landslide-related and predisposing factors associated with the existing inventory dataset, LiDAR-derived DEMs, Google Earth images, and field observations (see Chapter 4). An algorithm and three codes for semi-automated extraction of geometric analysis, deformation simulation, and classification of the landslide were developed by implementing the proposed approaches (see Chapters 5 and 6). Throughout this entire development process, empirical data and analytical data have been used for investigating, simulating, modelling, and mapping landslides using RiverTools, ArcGIS, and the MATLAB.
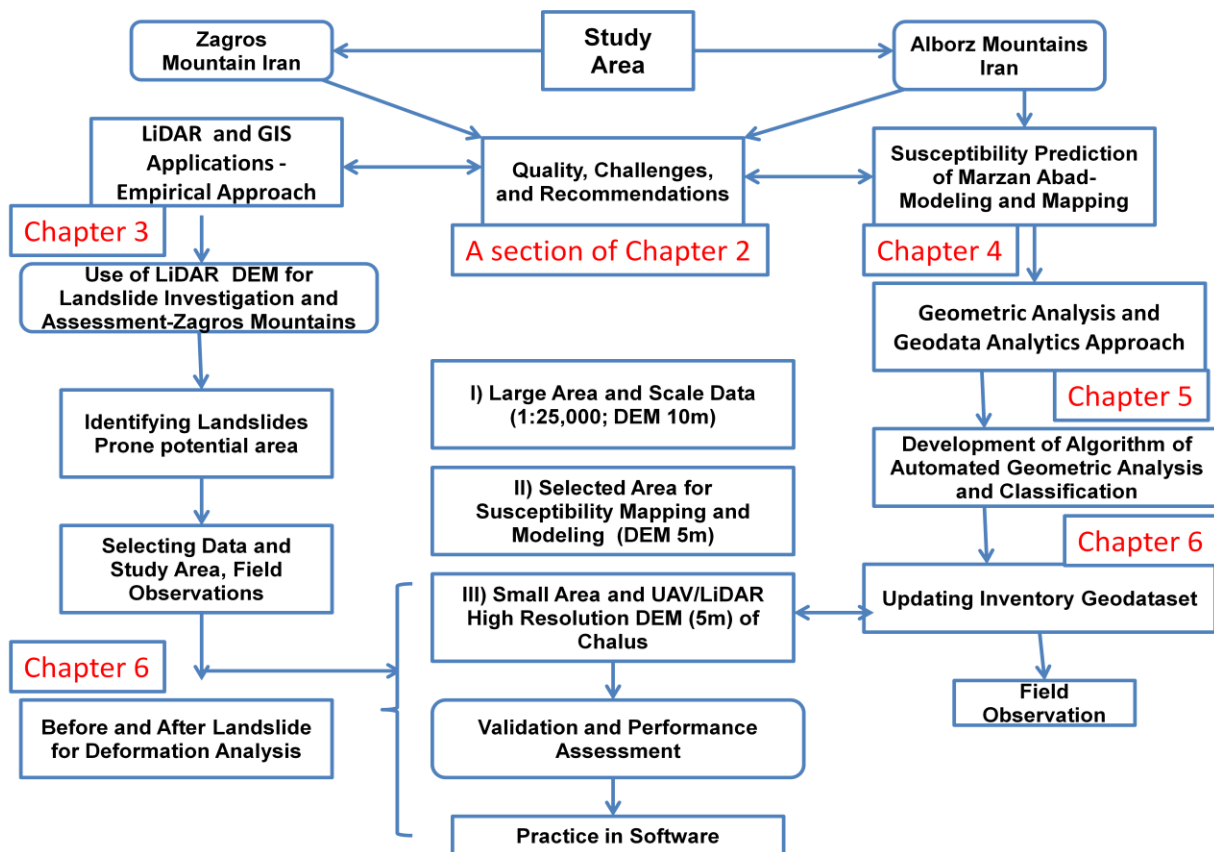
Figure 2.1: Skeleton of strategic research plan and relationships among chapters.

2.3 Study Area

The study area is comprised of parts of the Himalaya mountain range which covers the Zagros and Alborz Mountains of Iran.

A) The Zagros Mountains extend from northwestern to southeastern Iran and end at the strait of Hormoz in the Persian Gulf. This mountain range has the lithostratigraphy such as Bakhtiyari Formation with conglomerates, Kashkan Formation with marls, and Papdeh Formation with sandstones, and also geomorphology features such as steep slopes, hogbacks, scarps, and knickpoints with rugged topography, high tectonic activities, and potential for landslide hazards. It is situated in the Zagros Fold Belt (ZFB) in Iran's southwest (Figure 2.2). This part of the study area is bounded by Longitude 47º 58' 10.42" - 49º 18' 50.63" E and Latitude 32º 21' 40.94" – 34º 29' 10" N. The elevation, which varies from 142 m to 4,200 m, covers a high density of canopy in the spring and winter. The temperature varies between 49°C to -5°C. Geologically, the study area consists of various lithological units ranging from the Cretaceous age at the Sanandaj Sirjan Zone (SSZ) contact in the northeast (dominated by calcareous strata), and Sub-recent and Recent age in the Zagros Structural Belt (ZSB) in the south. The closure of the Zagros Basin during the Cretaceous-Miocene time period has generated diverse styles of folding and faulting. These structures, especially in the ZFB, exhibit tight, NW-SE trending folds with closely-spaced fracture systems which explain the potential acceleration of landslide hazards occurrence.

B) The Iranian plateau is the part of the Eurasian Plate that is wedged between the Arabian and Indian plates. The Alborz Mountains extend from northwestern to northeastern Iran and cover the Central Alborz from the Mazandaran Province of Iran. This part of the study area is located in the Central Alborz close to the Caspian Sea in the north and Tehran in the south. The study area is located in the Central Alborz at a distance of 30 km from the Caspian Sea in

the north, and 100 km from the capital city of Tehran in the south. The study area, which is approximately 1,048 km^2, is located between Latitudes 36°15'00" N to 36°35'00" N and Longitudes 51°07'30" E to 51° 27'30" E (4014000N-4048000N and 511184E-541004E in UTM). High tectonic activities have created an immature and rugged topography with high slopes and scarps in various locations that are indicators of susceptible landslides (Figure 2.2). The study area covers forests with a high density of vegetation. The elevation of the study area decreases from the south (by approximately 4000 m) to the north in the runoff of Chalus River. Chalus River, which is one of the most important rivers in the Central Alborz because it cuts the area in the northeast to form a deeply incised valley. This river transfers water from the highlands with an annual precipitation of less than 400 mm to the lowlands to the south of the Caspian Sea with annual precipitation of more than 1000 mm.
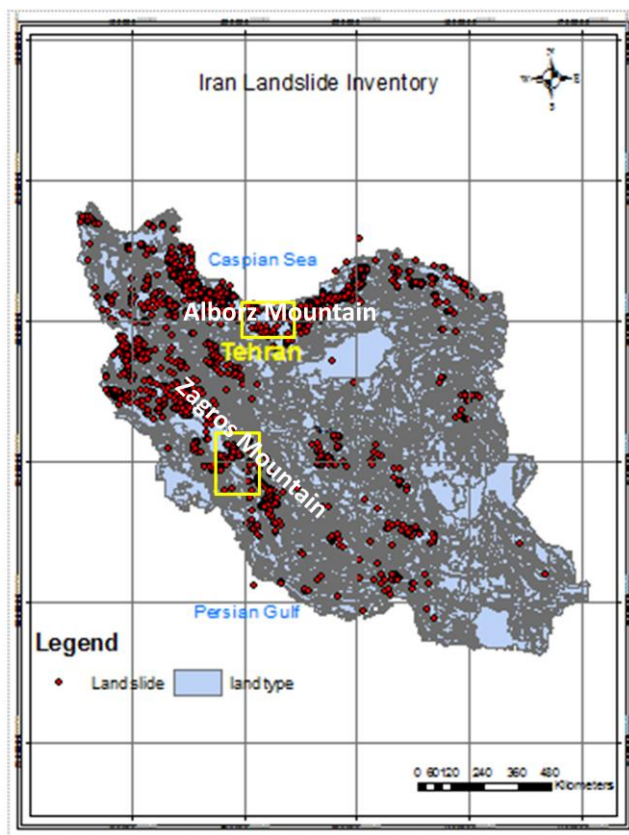
Figure 2.2: Study areas in the Zagros and Alborz Mountains.

14

2.4 Data Acquisition

Data quality and challenges for landslide investigations from geo-informatics perspective have been measured to understand the limitations of future study directions. Data collection and preparation are the first fundamental and essential steps of landslide investigations including susceptibility mapping, geometry analysis, and deformation and mass movement simulation. Table 2.1 depicts the GIS data layer of landslide studies as well as the source of the data for this study. In general, this study has organized the GIS database into five parts:

I.   Generating a 5 m resolution LiDAR-derived DEM and a 30 m resolution DEM of short wave infra red (SWIR) from the ASTER;

II.   Google Earth images and UAV images;

III.   Landslide inventory map which was developed by the Natural Resources of Iran from aerial photography collected from 1990-2010 for the Zagros and Alborz Mountains (Source: Natural Resources of Iran);

IV.   Thematic layers and landslide predisposing factors such as geology, geomorphology, soil, land use, seismic activity, vegetation, drainages, and topographic maps, and

V.   Global Positioning System (GPS) for data collection from field observations. The landslide inventory spatial dataset is composed of points and polygons. The Google Earth images (dated in December of 2009, 2010, 2011, 2012, 2013, 2014, 2015, and 2016) and 5 m resolution LiDAR-derived DEMs in conjunction with field observations have been acquired.

These components have assisted in drawing new landslide polygons in the ArcGIS 10.4 software using ArcBruTile tool. This study used the GPS Real Time Kinematic (RTK) smartnet. The UAV has been used for a case study in the Chalus District of the study area to characterize landslide hazards and capture new landslide data. The 20 cm resolution UAV images can aid in improving the existing landslide inventory map as well as in verifying some of the landslide

polygons associated with field observations. The eBee sensefly UAV with 16mb camera with 4000 pixel × 4000 pixel and RGB camera was used to take images of Chalus area. The weight of the UAV is 1.2 kg. The technical specification of this UAV is provided at https://www.sensefly.com/drones/ebee-plus.html.

Table 2.1: GIS data layer of landslide studies.

Data layers	Remote sensing/source	GIS data type
Landslide data	Collected from field and GPS, geospatial distribution collected from database	Point coverage
Slope	DEM derivative derived from ALS, SRTM, aerial photographs	GRID
Aspect	DEM derivative derived from ALS, SRTM, aerial photographs	GRID
Curvature	DEM derivative derived from ALS, SRTM, aerial photographs	GRID
Distance from drainage	DEM derivative derived from ALS, SRTM, aerial photographs Developed in GIS environment, buffer	GRID
Geology (litho types)	Extracted from satellite images based on digital and visual interpretation and digital image processing, collected from field and GPS, geospatial distribution collected from database	GRID
Distance from lineaments	Extracted from satellite images based on digital and visual interpretation and digital image processing, collected from field and GPS, geospatial distribution collected from database, developed in GIS environment, buffer	GRID
Soil types	Extracted from satellite images based on digital and visual interpretation and digital image processing, collected from field and GPS, geospatial distribution collected from database, developed in GIS environment	GRID
Land cover	Extracted from satellite images based on digital and visual interpretation and digital image processing, collected from field and GPS, geospatial distribution collected from database, developed in GIS environment	GRID
Normalized Difference Vegetation Index (NDVI)	Extracted from satellite images based on digital image processing, geospatial distribution collected from database, developed in ENVI environment	GRID
Rainfall data	Non-spatial data collected from stations	GRID

Ninety-five landslides were selected from the updated inventory spatial dataset to test the proposed algorithm. These landslide were selected based on accessibility to the ground observation, type of landslide, location, and the type of available data (i.e. point type or polygon

type). The RiverTools 3.0 software was used to extract the tectonic geomorphologic parameters such as the stream gradient-length index and the Dez River profile which are amended in landslide investigations and landslide hazards assessment.

Furthermore, some landslide points and polygons from the landslide inventory dataset were chosen. Required analyses of quality, conversion, field observations, and updating have been applied to identify specifications of the program for designing the architecture of the proposed algorithm in the MATLAB platform. The ArcGIS 10.4 software was used in conjunction with field observations and traditional measurements and simulation to validate and evaluate the performance assessment of the proposed algorithm's results.

2.5 Accessibility and Quality of Data

Although this study contains a detailed literature review of the remote sensing of landslide investigations, this section describes the accessibility of data and data preparation with acceptable quality in the study of landslides.

The availability of data, data preparation, quality, and challenges of landslide investigations were studied. This study is carried out based on the motivations, available data, and the presumption of occurrence of landslides. A peer review of review literature and data were implemented by studying available data as an object to see how it works and therefore enhance the studying of other objectives of the research based on the designed strategic research plan (Pirasteh and Li, 2016). Therefore, this study could aid in determining:

- The type of data to be used in this research and to create significant outcomes;

- The study area, which has a significant impact on and contribution to landslide assessment and investigation;

- Existing methods (i.e. algorithms, software, and hardware) and the gaps of landslide studies including both within and beyond landslide boundary; and

17

- The future direction of this study.

For landslide assessment and investigation in the Zagros and Alborz Mountains, the available data include landslide inventory datasets; moderate to high resolution of satellite images; Google Earth images; various spatial maps such as geology, geomorphology, land use, soil, vegetation, lineaments, and UAV images; LiDAR-derived DEMs; and DEMs' derivatives were used. Some available data were checked in conjunction with field observations and then analyzed by ENVI software, Rivertool software, as well as ArcGIS software. Throughout the collection of data, it was realized that some of the data would be derived or updated while other data were not of a good quality and form to be used further either due to being old and traditional data or geospatially incorrect or inconsistent data lacking standardization (Pirasteh and Li, 2016). It is because most of the data were in analog form or sometimes were required to be regenerated.

Nevertheless, this method of evaluating and analyzing accessibility of data and data preparation with an acceptable quality helped to prepare the fundamental landslide investigations in Zagros and Alborz Mountains using LiDAR and UAV. It allowed for the expansion of the problem and solution through further studies on modelling, simulating, and mapping of a landslide. Therefore, the following sections show the required connections through the entire study.

2.6 Remote Sensing Investigations of Landslides

2.6.1 Mapping Challenges

Landslide mapping and modelling have been developed in many parts of the world; however, most cases consist of prototypic approaches. Numerous methods have focused on generating landslide investigations (Pike, 1988; Wu et al., 1995; Pack et al., 1998; Lee et al., 2002; McKean and Roering, 2003; McKean and Roering, 2004; Hodgson and Bresnahan, 2004; Yilmaz and Yildrim, 2006; Glen et al., 2006; Streutker and Glenn, 2006; Su and Bork, 2006; Mahdavifar et

al., 2006; Oppikofer et al., 2009; Pradhan and Pirasteh, 2010; Rau et al., 2011; Goetz et al., 2011; Spaete et al., 2011; Niethammer et al., 2012; Choi et al., 2012; Solaimani et al., 2013; Ren et al., 2014; Mohamed et al., 2015; Mohamed et al., 2016; Yousef et al., 2015; Su et al., 2015; Lee et al., 2014). Nevertheless, previous studies have discovered that a number of shortcomings need to be overcome (Pirasteh and Li, 2017).

This section of the thesis has been published in Geomatics, Natural Hazards and Risk Journal in 2016 because to cover a review of literature; and to identify challenges and quality of data that to be used further in this study. The following challenges were identified:

(1) It may not be surprising that a complex interrelationship causes landslides, and that agreement about how to influence variable factors involved in landslide hazard assessment is not uniform among the researchers. Clearly, no general agreement has been reached on the scope, techniques, and methodologies for landslide hazard investigations.

(2) Previous studies have discovered that structural features and geomorphologic analysis play an important role in landslide assessment (Ali and Pirasteh, 2004; George et al., 2012). However, no study notably has identified the interface of thrust fault, scarp, strike-slip fault, fold, hogback, lineament density, drainage density, elevation drop, water gap, net erosion, channel slope, sinuosity, straight-line length, and stream gradient index in a rugged topography to assess landslides utilizing LiDAR-derived DEM.

(3) It seems that LiDAR permits the improvement of geological mapping as well as landslide inventory mapping. It also seems that increasing the resolution of the landslide contours leads to the identification of geomorphologic features such as scarps and displaced material. These conceptual methods are usually employed to detect landslides in different climates and environments such as tropical and mountainous regions (Keaton and DeGraff, 1996; Soeters and VanWesten, 1996). Some morphological features of landslides are easily

19

extracted while others cannot be delineated from DEMs or hillshades produced only by photogrammetry techniques, satellite images, and LiDAR. Limitations vary from technique to technique, and depend upon the resolution of the images, topography, climate, and environmental conditions. However, one of the main issues in laser scanning is vegetation removal either by automatic methods or manually (Hopkinson et al., 2004). Nevertheless, any remote sensing approach does not replace field investigations. However, remote sensing approaches change the fieldwork methods and can be considered part of the validation process of a landslide inventory produced by high resolution DEMs.

2.6.2 Feature Extraction and Analysis

This study presents a detailed method of landslide investigations in the Zagros Mountains in Chapter 4. This section explores how empirical and analytical tectonic geomorphology analysis and modelling using LiDAR-derived DEMs of the Zagros Mountains have been studied. This study (Chapter 4) explores an empirical and interpretational method of landslide investigation, particularly for a high tectonic active region such as the Zagros Mountains.

In this study, 5 m resolution LiDAR-derived DEMs, slope, stream gradient-length index, Dez River profile, and river network of the Zagros Structural Belt (ZSB) were considered for landslide investigations and assessments. Pre-processing techniques were applied to the LiDAR point clouds data to achieve a certain level of quality before using the data for tectonic geomorphological analysis, visual interpretation, and landslide investigations. The LiDAR-derived DEMs of the ZSB are the most useful representation of terrain in the GIS for the spatial analysis and stream length-gradient index. The stream length-gradient index (Figure 2.3) is a signature that is sensitive enough to analyze the reach scale variability of tectonic function, rock resistance, and topography associated with landslide processes. The Dez River tends to flow over the rocks and soils in the Zagros Mountains and attain equilibrium with distinct longitudinal

profiles and hydraulic geometries (Bull, 2007). Geospatial analysis was applied on the stream length-gradient index in the GIS environment. By employing visual interpretation techniques of geotechnical elements such as drainage, slope, and vegetation, the relative tectonic activity in the Dez River basin (Dar et al., 2014) that influences the potential for landslide phenomenon was estimated. The Dez River network and the Dez River profile (Figure 2.4) were extracted by using the river network and channel profile functions in the RiverTools 3.0 software, respectively. The morphometric parameters were converted to the ArcGIS format, in which the stream length-gradient index map was generated and assessed for landslide investigations.

This landslide investigation in the Zagros Mountains developed the motivation to study the Alborz Mountain comparatively with a Probabilistic Frequency Ratio (PFR) of an analytical approach. It is because most of the available methods have limitations in some extend depending on their implementation in various environments (Safaie et al. 2010; Pirasteh and Li, 2016). Therefore, the following section and Chapter 5 explore landslide susceptibility mapping in the Alborz Mountains. The Zagros Mountain is rugged topography with high tectonic activities while the Alborz Mountain is covered by forests and tectonically active. In the Zagros Mountains, the tectonic geomorphology analysis has employed as a tool to the landslide investigation while in the Alborz Mountain the Probability Frequency Ratio (PFR) was implemented to landslide susceptibility mapping. Generally speaking, the south of Iran is connecting the north by rail and road, and major crude and gas pipelines crossing the Zagros mountains and streams are under influence of active landslides hazards while in the Alborz Mountain this is not the case. The most of available data have limitations in some extend depending on their implementation in various environments (Safaie et al. 2010; Pirasteh and Li, 2016). In addition to above, the author was interested in experiencing different environmental conditions. The Zagros Mountain contains sedimentary rocks while the Alborz Mountain

consists of tuffs, igneous, sedimentary, and metamorphic rocks with a very dense forest. Perhaps, the author could show how to investigate the landslide in a tectonic active region with limited data (i.e., only DEM) while in the Alborz Mountain some predisposing factors are considered to landslide susceptibility mapping. However, the review literature (Pirasteh and Li, 2016) evidenced that the researchers have not used 5m resolution in the Zagros and Alborz Mountains.

2.7 Landslide Susceptibility Mapping, Data Analysis and PFR Model

By building on the previous section's discussion of the LiDAR-derived DEMs and tectonic geomorphology techniques to assess landslides in the Zagros Mountains, PFR modelling and susceptibility mapping of landslides in the Alborz Mountains are explored. This approach delivers an updated landslide inventory dataset and improved susceptibility mapping using LiDAR-derived DEMs as compared to previous studies using Fuzzy or logistic regression (Lee et al. 2004; Mahdavifar et al. 2006; Safaiee et al. 2010; Lee et al. 2014) and DEMs in lower resolution than 5m. This susceptibility mapping in conjunction with LiDAR-derived DEMs (5m) and UAV images promote the elaboration of further research on the selected landslides including the revising and updating of the landslide inventory dataset, analyzing the geometry of a landslide, simulating a landslide deformation, and classifying landslides (see Chapter 5 and Chapter 6).

Data analysis and the PFR model are followed by strategic research design (Figure 2.1). This allows for a study area to be selected from the Central Alborz Mountains in Mazandaran Province of Iran's north, adjacent to the Caspian Sea.

The PFR model has been adopted to consider the effects of landslide-related factors associated with Google Earth high resolution images and field observations. Some ground control points (GCPs) were used in the ENVI 4.2 software to georeference the Landsat Thematic Mapper (TM) satellite images and to extract landslide marks by using geotechnical and

photographic elements of the interpretational method. ENVI 4.2 software allows for the operation of digital image processing (DIP) such as geometric correction, enhancement, and filtering on Google Earth images. The geomorphology map was created based on the geological and topographic map in 1:25000 scales associated with the ASTER DEM. The PCI Geomatica 9.1 was used to generate ASTER DEMs. Also, image interpretation was applied on the available ASTER DEM (30 m); it is supported and enhanced by LiDAR-derived DEMs (5 m) to detect landslides in the study area.
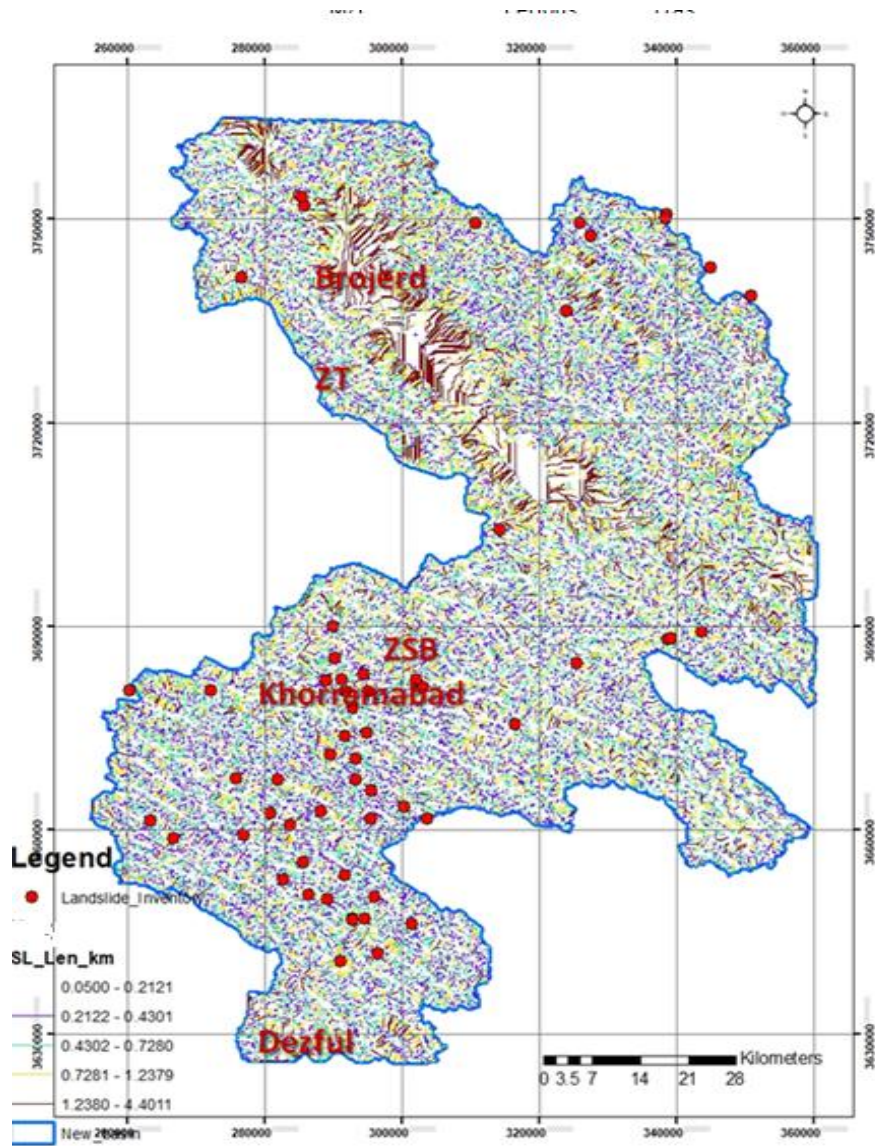
Figure 2.3: Stream length map. ZT: Zagros Thrust, ZSB: Zagros Structural Belt.

23
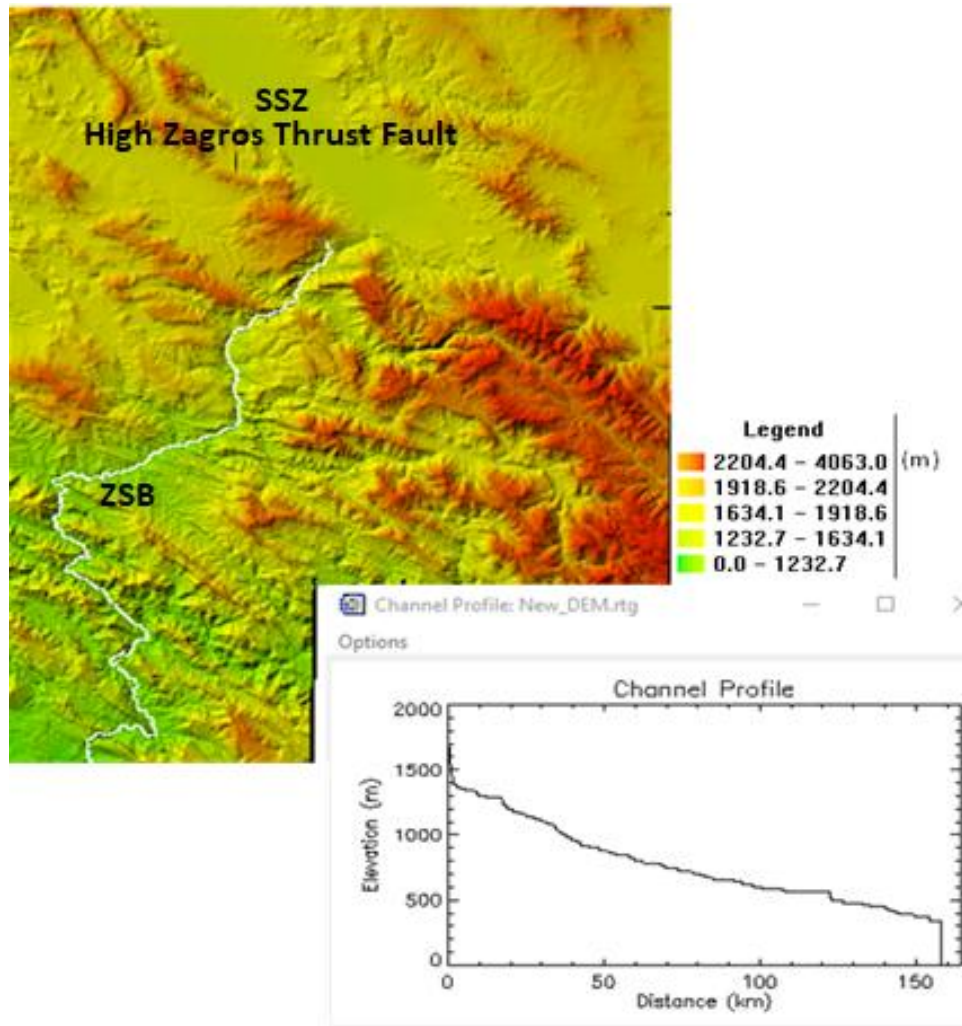
Figure 2.4: Dez River profile on LiDAR-derived DEM of the Zagros Mountains.

In this study, LiDAR-derived DEMs and existing landslide inventory dataset were used. The LiDAR point clouds data in the LAS format allowed for the creation of high resolution DEMs in the ArcGIS environment. The pre-processing technique to the point cloud data was applied to achieve a certain level of quality before using the data for landslide susceptibility mapping in ArcGIS software. The slope map and hillshade map (Figure 2.5) were extracted from the 5 m resolution LiDAR-derived DEMs.

The Ministry of Natural Resources of Iran provided the soil map of the study area in 1:25000 scale. To verify the soil map, this study attempted a field survey. By using the

24

topography map of the study area (National Cartographic Center organization) of 1:25000 scale, the road and drainage maps were extracted in the GIS environment. The land use thematic map and the Normalized Difference Vegetation Index (NDVI) of the study area were collected from the Natural Resources of Mazandaran Province.

The GIS-based analysis allowed for the performance of high quality landslide susceptibility assessments using inventory datasets as compared to the previous studies. Because existing studies have rarely used high resolution DEMs, predisposing factors were considered in this study. A spatial database of landslide-related factors was constructed in the GIS platform to apply the PFR model. In this study, factors such as geology, geomorphology, land use, soil, slope, and distance from roads and drainage were evaluated to represent, manipulate, and analyze landslide contributing factors. Also, this study evaluated the performance success of the rate curve of landslide hazards prediction. A detailed methodology of landslide susceptibility mapping is provided in Chapter 4.

This study analyzed the development of a semi-automated extraction of the geometry inside a landslide boundary from the selected landslides in a particular area (Chapter 5) of Mazandaran Province in the Central Alborz Mountains. The process of updating the inventory dataset of landslides is presented in Chapter 4 and Chapter 5.

2.8 Extraction of Landslides Geometry and Computing and Analysis

Developing an algorithm and a code for semi-automated extraction of landslide geometry (length, width, and area) required a technical computing Geoanalytics approach. The general flowchart methodology of the algorithm is depicted in Figure 2.6.

The Numerical Integral Trapezoidal Rule (NITR) method was implemented and the 5 m resolution LiDAR-derived DEMs were utilized in the Alborz Mountains to support and enhance

the on screen digitization of landslide polygons for a better certainty than previous studies (Lee et al. 2004; Poiraud, 2014; Shirzadi et al. 2017). The LiDAR-derived DEMs in conjunction with field observations and the Google Earth images were assisted the revision and updating of the available inventory datasets.

In order to perform computing and analysis of landslides, every landslide polygon from the landslide inventory dataset was calculated in ArcGIS environment. The algorithm and codes were developed in the MATLAB platform, and the scripts were implemented through an analytics process.
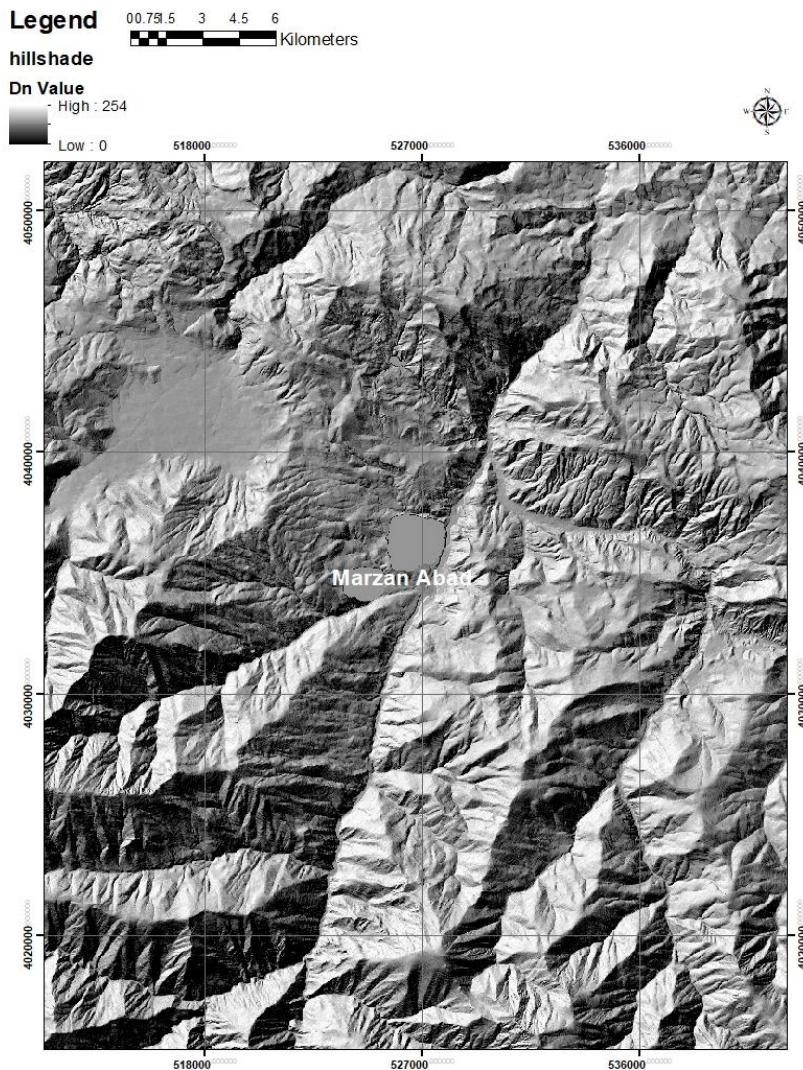
Figure 2.5: Hillshade of the study area extracted from the 5 m LiDAR-derived DEM.

26
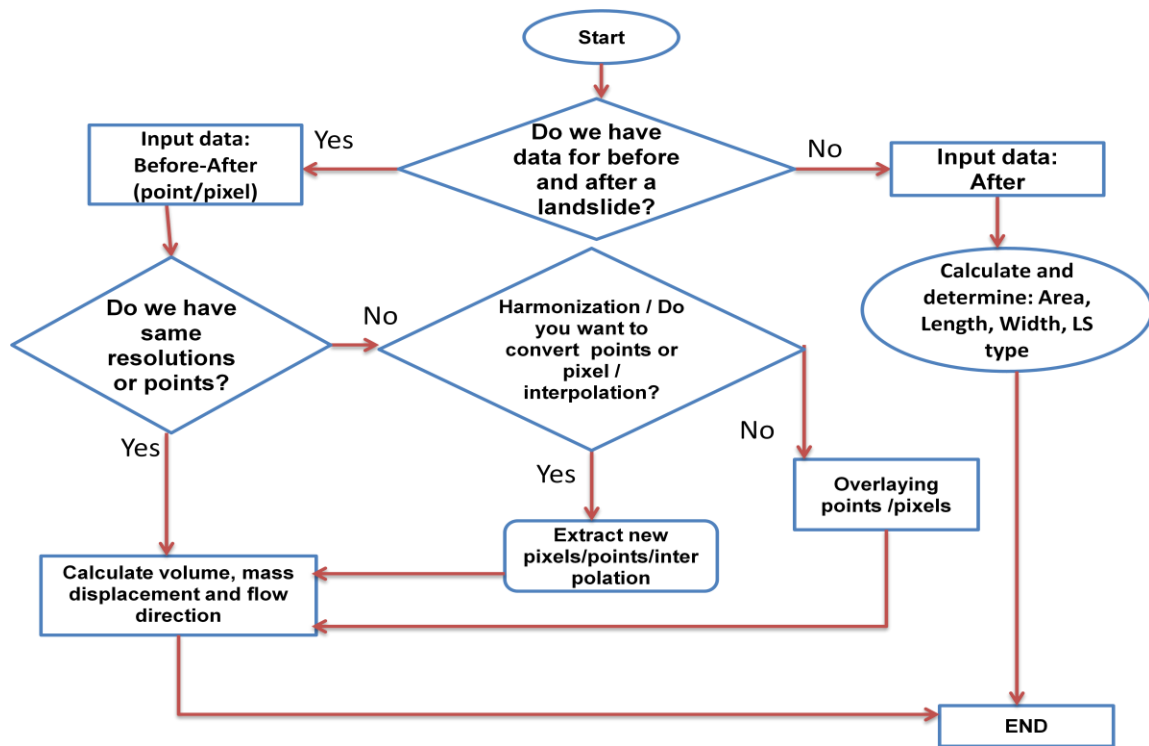
Figure 2.6: Flowchart of the algorithm.

The following steps are considered when writing the code for developing semi-automated extraction of a landslide geometry:

a. Input data;

b. Find maximum and minimum X and Y;

c. Calculate $d_1=(l_1)$ and $d_2=(w_1)$ and their slopes;

d. Determine a landslide type;

e. For a wide landslide, recognize top and bottom points and sort them into two separate matrices;

f. Calculate the area under the top and bottom curves;

g. Identify, measure, and determine width (Alpha angle between length and width);

h. Calculate area and print output (type, length, width, and area);

i. For a long landslide, recognize right and left points and sort them into two separate matrices;

27

j. Calculate the area under right and left curves;

k. Identify, measure, and determine width (Alpha angle between length and width); and

l. Calculate area and print output (type, length, width, and area).

This semi-automated geometric analysis code allows the simulation and modelling of a landslide polygon by introducing geographical coordinate systems of polygons or points in the MATLAB platform (Figure 2.7). The algorithm is based on the geographical coordinates system (Universal Transverse Mercator [UTM]), slope angle (θ), and geometry (i.e. length and width) of a landslide. The analytical and numerical approaches compute the data and divide the landslides into four geometric classes automatically (see Chapter 6). The result performance and validation of the algorithm were conducted through field observations and tested in conjunction with ArcGIS software. The mean error percentage of measurement was determined from the selected landslide polygons. The basis for error is zero% defined from relative error equation (Erwin Kreyszig, 2011), 10 Edition, page 794, chapter Numerics in General. It means that as we get closer to zero, then the relative error is more précised. In this study, the relative error and validation of the output results of MATLAB code have been attempted with ArcGIS, GPS-RTK Smartnet ground truth (for simulation), and also check with the existing inventory dataset. The findings of this study overcome the shortcomings of the previous efforts by other researchers (Booth et al. 2009; Niculit, 2016) to analyze the length and width of the landslides computed using GIS techniques. When working with landslide polygons, the analysis of the length and width of the landslides computed using usual GIS techniques (like bounding boxes) can be flawed. Niculitˇa (2016) determined the length and width of a landslide using a boundary rectangle box in which the four space' corners of rectangle are missing and impacts the accuracy of the output result for measuring the length and width. In this study, the trapezoidal method was used to measure and calculate all parts of a polygon. Also, Niculitˇa (2016) algorithm cannot detect and determine the

length, width, volume, and type of a landslide automatically. However, the proposed algorithm in the MATLAB platform contributes the following while the previous studies can only determine and measure the length and width of a landslide within a boundary box:

•   Determining the landslide type;

•   Calculating the area of a landslide polygon;

•   Determining and measuring the length and width of a landslide;

•   Calculating the volume of material displacement and determining mass movement (deformation); and

•   Identifying the flow direction of a landslide material movement.

This proposed method of semi-automated geometric analysis of a landslide is followed by exploring an algorithm and two codes including a) semi-automated volume material displacement (i.e. deformation) and flow direction simulation, as well as b) determining the type of a landslide. This method also introduced a class taxonomy of landslides (see Chapter 6). This study used semi-automated term because some of the process allows to calculate geometry of a landslide without a human action in MATLAB environment.

The basis for error measurement was the Natural Resources of Iran inventory dataset and the ground measurement the author attempted. In this study, the precision refers to the level of measurement and exactness of the GIS database. The field measurements were done by using the RTK for simulation purposes. Then the measuring tape was used on the ground to see the error. The validation is through comparing field observation and measurement. The ArcGIS was used to measure the collected RTK points and later the same points were processed and measured by the proposed algorithm. In general, the study was done by a) ground truth measurement aand measuring tape, b) RTK, c) ArcGIS output, and d) the proposed algorithm's output. As for

landslide inventory dataset of the Alborz Mountain, the output result was validated by (1) using the inventory dataset, and (2) field observations. The data were collected from the Natural Resources of Iran. The author also collected the data from the ground measurement for the simulation of some of the landslide polygons.
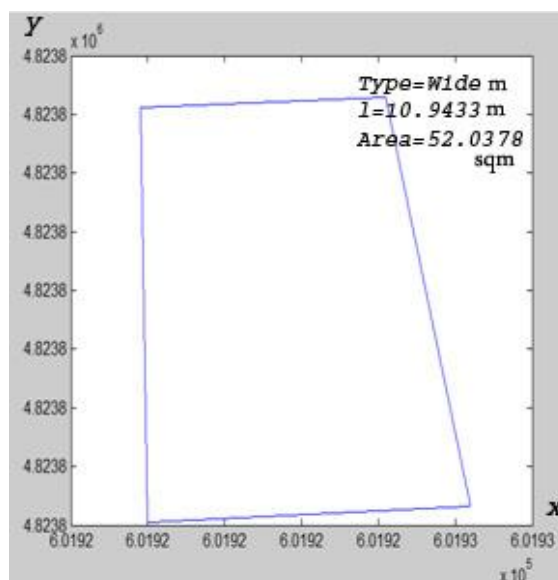
Figure 2.7: Simulation of a landslide polygon in MATLAB.

Chapter 5 presents a detailed explanation of the method of the semi-automated extraction of the geometric parameters of a landslide.

2.9 Deformation and Classification

Simulation and modelling of landslide deformation are required data in the form of points or pixels before and after the event. This is the fundamental data and structure to develop an algorithm and a code that determine the volume of material displacement and flow direction. In this study, the two different DEMs (5m and 30m) of a particular selected landslide before and after occurrence in Madaling, Guizhou Province of China help to model and simulate the deformation of a mass movement. It is because to test and validate the performance of the proposed algorithm in different environment condition.

The updated landslide inventory dataset was amended to the selected landslide polygons to investigate the landslide classification. Also, this study incorporates the geographical coordinates system, slope angle (θ), and geometry (i.e. length and width) of a landslide to determine the landslide type.

2.9.1 Simulation of Deformation and Modelling

To semi-automatically and incrementally extract deformation of the landslide, this study considered the "pixel" or "point" into deformation simulation and modelling. This thesis built on the previous study of landslide geometry analysis and it is done by expanding the previous scripts to determine the volume of the mass movement and identification of flow direction (see chapter 5). Simulation of material movement and volume calculation, as well as flow direction, were performed based on the x,y,z of points or pixels values before and after a landslide. In other words, sometime we may or may not have same spatial resolution of the two different datasets of DEMs from before and after a landslide. Therefore, this study used two algorithms to model and simulate the length, width, area, and deformation. There are two possibilities of the DEMs resolutions from before and after a landslide. First, if both DEMs are in the same pixel resolution, then the pixels of both DEMs are converted into points (x,y,z) by using ArcGIS software. Further, the script recommends introducing points from before and after a landslide and running the program to determine the deformation and flow direction of the material movement. Second, if the DEMs have different pixel resolutions, then the pixels of both DEMs are re-sampled to a similar pixel resolution. This study recommends re-sampling the high to low pixel resolution for the purpose of distributing the high pixel resolution of a DEM to the low pixel resolution of a DEM. Then the pixels of both DEMs are converted into points (x,y,z) by using ArcGIS software. Similar to the first option, the script recommends introducing points from before and after a landslide and running the program to determine the deformation and flow

direction of the material movement. It is important to know that the model is based on the assumption of nAfter ≥ nBefore because this proposed algorithm has been designed in a way that to accept running the program when the number of points for after landslide is more than the number of points for before landslide otherwise, the output result map will be incorrect. In addition to above, often the high-resolution LiDAR-derived DEMs are not available for before a landslide. In other words, the number of points/pixels in a DEM (i.e. after a landslide) is more than the number of points/pixels in a DEM before a landslide. Because the assumption is nAfter ≥ nBefore and if the analyst considers number of points or grids for after a landslide less than number of points/grids before a landslide (i.e., nAfter<nBefore or nAfter=nBefore) the code cannot be processed in the MATLAB. The reason that this study has considered this assumption is because in real-practical life, the high resolution of DEMs from LiDAR are not normally available for landslides due to its costs. In addition to the above, no one knows when landslide occur in a particular area, however, it has been seen that sometime likely the LiDAR-derived DEMs with high resolution are available. For example, in Malaysia where landslides have occurred ever year because of the environmental condition, slopes, and deforestation.

The MATLAB platform was used to code and script the algorithm. This platform allowed computing landslide geometry and to simulate the deformation of a landslide and measure the volume of the material displacement as well as the flow direction of the mass movement (Figure 2.8). In other word, the proposed algorithm in MATLAB platform can run the code with many iteration of selecting maximum/minimum x and maximum/minimum y points to determine d_1 and d_2. It also runs the code and scripts to measure, detect and determine the length, width, and type of landslide and volume of material displacement as well. This algorithm and code allowed the analysis, computation, simulation, and modelling of a landslide material displacement.

Nevertheless, the following procedure describes the scripts for simulation of deformation and volume calculation.

a. Input data (points);

b. Find maximum and minimum x & y;

c. Calculate $d_1=(l_1)$ & $d_2=(w_1)$ and their slopes;

d. Determine landslide type;

e. For wide landslide, recognize top and bottom points and sort them into two separate matrices;

f. Calculate the area under top and bottom curves;

g. Identify, measure, and determine width (Alpha angle between length and width);

h. Calculate area and print output (type, length, width, and area);

i. Plot direction; and

j. Calculate volume.
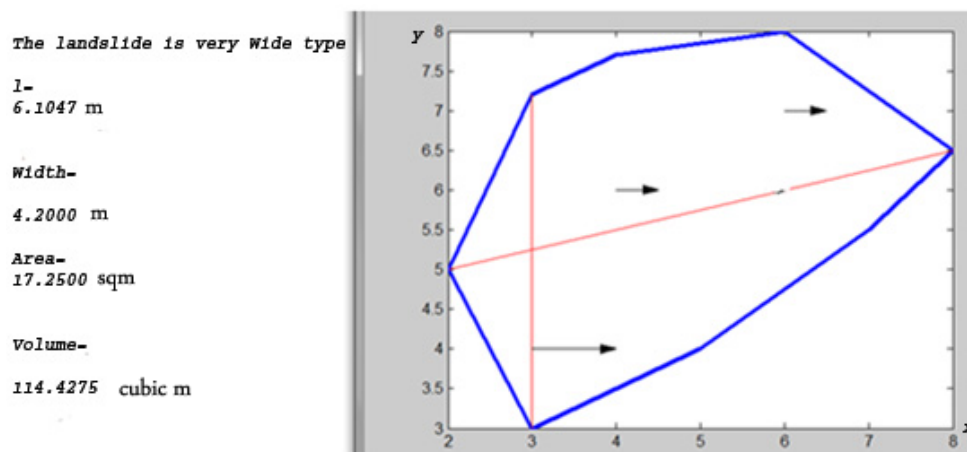
Figure 2.8: Simulated result of before and after landslides.

The detailed procedure of deformation and flow direction simulation and modelling is explained in Chapter 6.

2.9.2 Determining Landslide Type

This study (see Chapter 6) presents the utilization of LiDAR-derived DEMs and Google Earth images as well as UAV captured images of the selected landslide of the Chalus area in the Alborz Mountains. An analytical approach was attempted to develop an algorithm for the semi-automated derivation of landslide classification (i.e. type of landslide) (Figure 2.6). Similar to the landslide geometric analysis of length, width, and area, this study used the NITR method to write a code in the MATLAB. The code is scripted to be interpreted in accordance with the proposed landslide classification into a) very long, b) long, c) very wide, and d) wide. This geometric classification of landslides is based on the geographical coordinates system, slope angle (θ), length (L), and width (W) (Table 2.2).

Table 2.2: Classification of landslides.

Type of Landslide	Slope angle (θ)
Long	$90° \geq LS > 67.5°$
Very long	$67.5° \geq LS > 45°$
Wide	$45° \geq LS > 22.5°$
Very wide	$22.5° \geq LS > 0°$

This study revised and updated 95 landslides from the existing inventory dataset. The resulting performance and validation of the algorithm were conducted by field observations and tested in conjunction with the ArcGIS software (Figure 2.9). The purpose of this algorithm is to improve the performance of landslide geometry analysis and semi-automated measurements as compared to Niculiťa (2016) and typical GIS techniques in the ArcGIS.

Please note that Chapter 6 provides more detailed information about the methodology of the semi-automated extraction of the new landslide classification and mass movement volume and flow direction simulation.
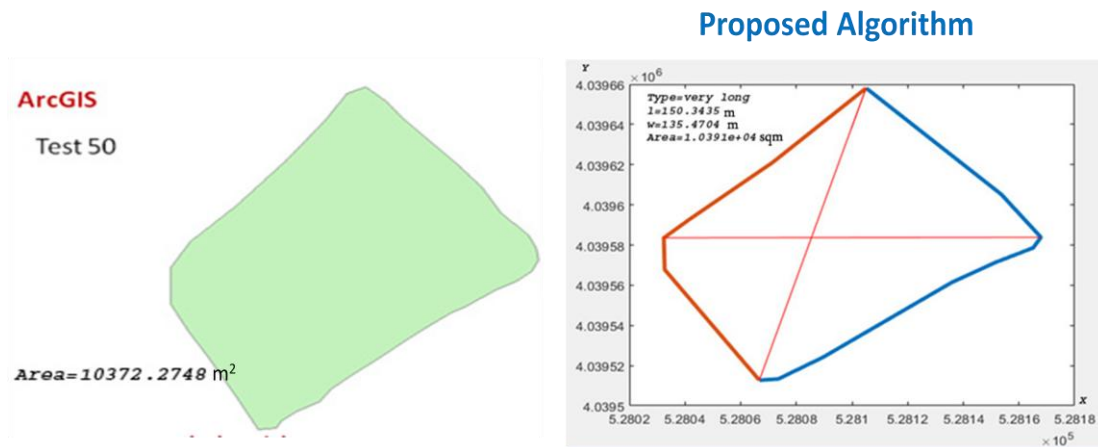
Figure 2.9: Proposed algorithm for a landslide classification vs. ArcGIS.

2.10 Chapter Summary

In this chapter, a framework of landslide investigations was identified by understanding the type of data and LiDAR remote sensing technologies, quality of data, challenges, accessibility to the study area, method flaws, and research gap. Three different approaches of landslide investigations including inside and outside of the landslide boundary were described by implementing a) tectonic geomorphology features' determination from empirical and analytical perspectives b) the PFR model for susceptibility mapping from remote sensing data, LiDAR-derived DEMs, and GIS spatial analysis; and c) development of the proposed algorithms and codes for geometric analysis and simulation of deformation. LiDAR-derived DEMs, Google Earth images, ASTER DEM, thematic geospatial maps, UAV images, GPS data, and field observations were used for landslide investigations. Flowchart steps for development of algorithms (Figure 2.6) and the proposed classification of landslides were discussed.

The proposed methods are described in detail in Chapters 3, 4, 5, and 6.

Chapter 3

Use of LiDAR-derived DEM and a Stream Length-Gradient Index Approach to Investigate Landslides in Zagros Mountains, Iran

This chapter presents an approach to stream length-gradient index analysis in the identification of tectonic signatures. The graded profile of the Dez River in Zagros Mountains, Iran, indicates that the area has been tectonically disturbed, and this triggers landslide hazards. The high-gradient index shows that a steeper gradient could be a potential signature for landslide identification. The digital surface models acquired by Airborne LiDAR were used in this study to generate the high-resolution DEM. The result showed great potential for improving landslide investigations by implementing stream length-gradient index derived from the high-resolution DEM in conjunction with the landslide inventories dataset in the GIS environment. Also, this study identified a correlation between the stream length-gradient index and the graded topographic profile with slopes and landslides. This empirical approach was verified by geospatial analysis in GIS and a landslide inventories data set in conjunction with field observations. This study recognized the locations of high-gradient indices with susceptibility to landslides.

3.1 Background and Introduction

In the Zagros Mountains, the mechanisms of landslides are complex in geological-geomorphological activities. These activities have created an immature and rugged landscape that imposes various natural hazards. A high slope can influence the stability of the region,

particularly with high tectonic activities. Also, the presence of active faults influences the occurrence of landslides. At times earthquakes trigger landslides in this region. Thus, finding a logical relationship between slopes and tectonic geomorphologic signatures such as stream length-gradient index and graded topographic profile could be effective in suggesting landslide-susceptible areas. Moreover, the high rainfall and erosion in some rock types such as marls, calcareous, and silt are major concerns of stability in the Zagros Mountains. The Zagros Mountains have experienced catastrophic landslides to low magnitude landslides in the form of rock falls, rock slides, and debris flows. Sometimes a high density of lineaments and faults control the landslides in this region. Thus, tectonic geomorphologic signatures play a significant role in landslide assessments (Burbank and Anderson, 2001; Ali et al. 2003).

Landslides are the movement of a mass of rock, debris, or earth down an unstable slope (Highland et al., 2008; Farrokhnia et al., 2011; Seefelder et al., 2016; Pirasteh and Li, 2017). Definitions of the landslide are diverse and reflect the complex nature of various disciplines such as geology and geomorphology (Ali et al., 2003a, 2003b; Ali and Pirasteh, 2004). This study considers landslides as a general term used to describe the downslope movement of soil and rock under the effects of gravity (Cruden, 1991). Landslide hazards can be investigated qualitatively or quantitatively. Many efforts have been made to investigate the causes and mechanisms of landslides using remote sensing data, GIS-driven techniques, and statistical models (Carrara et al., 1991; Montgomery and Dietrich, 1994; Zhou et al., 2003; Gomez and Kavzoglu, 2005; Yilmaz and Yildirim, 2006; Ardizzone et al., 2007; Yalkin, 2008; Abellan et al., 2010; Yilmaz, 2010; Goetz et al., 2011; Pirasteh et al., 2011a; Pirasteh et al., 2011b; Schicker and Moon, 2012; Cavalli et al., 2013; Zare et al., 2013; Guan et al., 2014; Jebur et al., 2014; Lee et al., 2014; Su et al., 2015; Yousef et al., 2015; Ciampalini et al., 2016). Very few studies have noted the role of tectonic geomorphology such as stream length-gradient index in landslide investigations (Bull,

37

2007; Hamdouni et al., 2010; Catani et al., 2013). These studies suggest that the stream length-gradient index in river segments with higher landslide frequencies is associated with the slope instability and lithology in active tectonics structures.

One remote sensing technique that has been undergoing rapid developments for landslide investigations is LiDAR point cloud processes and extraction of high-resolution LiDAR-derived DEM. LiDAR, which can provide high resolution point clouds of the topography, has demonstrated great potential for monitoring landslide or rockfall displacements (McKean and Roering, 2004; Ardizzone et al., 2007; Teza et al., 2007; Abellan et al., 2010). There has been much scholarly research in different aspects of image processing (Rau et al., 2011; Li et al., 2015a, 2015b; Pirasteh et al., 2015; Su et al., 2015) and natural hazards such as landslides (Wu and Sidle, 1995; Pack et al., 1998; McKean and Roering, 2003; McKean and Roering, 2004; Watts, 2004; Van Den Eeckhaut et al., 2005; Su and Bork, 2006; Glenn et al., 2006; Safaiee et al., 2010; Spaete et al., 2011; Schicker and Moon, 2012; Guzzetti et al., 2012; Choi et al., 2012; Solaimani et al., 2013.

An overview of the different applications of LiDAR techniques for landslide investigations is given in Jaboyedoff et al. (2012). The authors present how LiDAR-derived DEMs can be used to investigate landslide hazards, including detection and characterization of mass movements, modelling, hazard assessment, and susceptibility mapping. Nevertheless, most of the existing landslide studies of the Zagros Mountains have not been presented well due to the lack of detailed surface information about the region. Aerial photographs, satellite images, and DEM derived from topographic maps have been used by various statistical and deterministic approaches (Rajabi et al., 2011). Thus, this lack of detailed surface information has motivated the utilization of the LiDAR-derived DEMs to investigate landslides in this region.

This study has attempted to take advantage of the LiDAR-derived DEMs to support the investigation of landslide hazards by mapping stream length-gradient index anomalies and assessing graded topographic profile in the Zagros Mountains, southwest Iran (Figure 2.2). This study contributes to the visual interpretation and tectonic geomorphology of geodata analytics in the ArcGIS 10.4 version software by utilizing LiDAR-derived DEM. The objective of this research is to investigate the stream length-gradient index and graded channel profile of the Dez River in conjunction with the landslide inventory dataset and field observations. This study examines how landslides are associated with various tectonic geomorphology, faults, folds, and stream length-gradient indices. Detailed information and the lineament map were used to improve landslide investigations. Point cloud data was used to extract the DEM derivatives in the GIS environment. The Dez River profile was digitally drawn on screen using RiverTools software and the prone-area of landslide hazards was determined by visual interpretation and interpreting indicators such as stream length-gradient index anomalies and graded closely spaced step-like of the Dez River profile to address landslide-prone areas. The performance of this study was validated by the existing landslide inventory data-set and several field observations.

3.2 Geological and Tectonic Setting

Geologically, the study area consists of various lithological units ranging from Cretaceous age at the Sanandaj Sirjan Zone (SSZ) contact in the north-east (i.e. dominated by calcareous strata), and subrecent and recent age in the Zagros Structural Belt (ZSB) in the south. A generalized stratigraphic column (Figure 3.1) and a geological map (Figure 3.2) for the Zagros Simple Folded Belt show Cretaceous through Miocene strata grouped into four units according to relative resistance to erosion. Also, Figure 3.2 depicts the spatial distribution of landslides inventory on the geological map of the study area in the GIS environment. The area is mostly

39

dominated by calcareous Cretaceous dolomite, limestone, shale, and marls in the north and evaporites (such as gypsum) and highly cemented conglomerate of the Pliocene Bakhtiari Formation in the south. The closure of the Zagros Basin during the Cretaceous-Miocene period has generated diverse styles of folding and faulting.
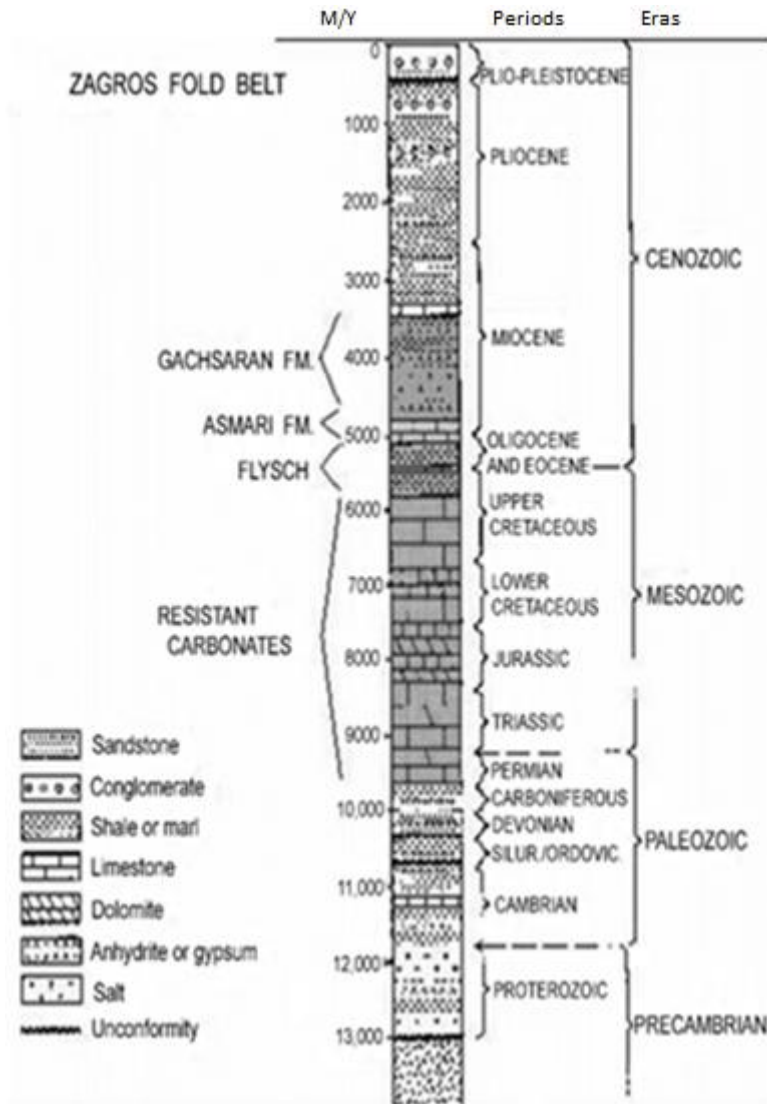
Figure 3.1: Generalized stratigraphic column of the study area (Ali et al., 2003).

These structures, especially in the ZFB, exhibit tight, NW-SE trending folds with closely-spaced fracture systems that can be interpreted as accelerating the potential of landslide hazards occurrence. These types of geological settings have facilitated severe erosion (Figure 4.3), the

formation of rugged and immature topography, and a closed drainage system. In southwest Iran, the movement of the Arabian plate has been approximately NNE and has resulted in the closure and subduction of the Neo-Tethys beneath the Iranian plate from approximately the Late Cretaceous onwards. Also, the movement has formed roughly NW-SE trending Zagros fold mountains from approximately the Miocene onwards.
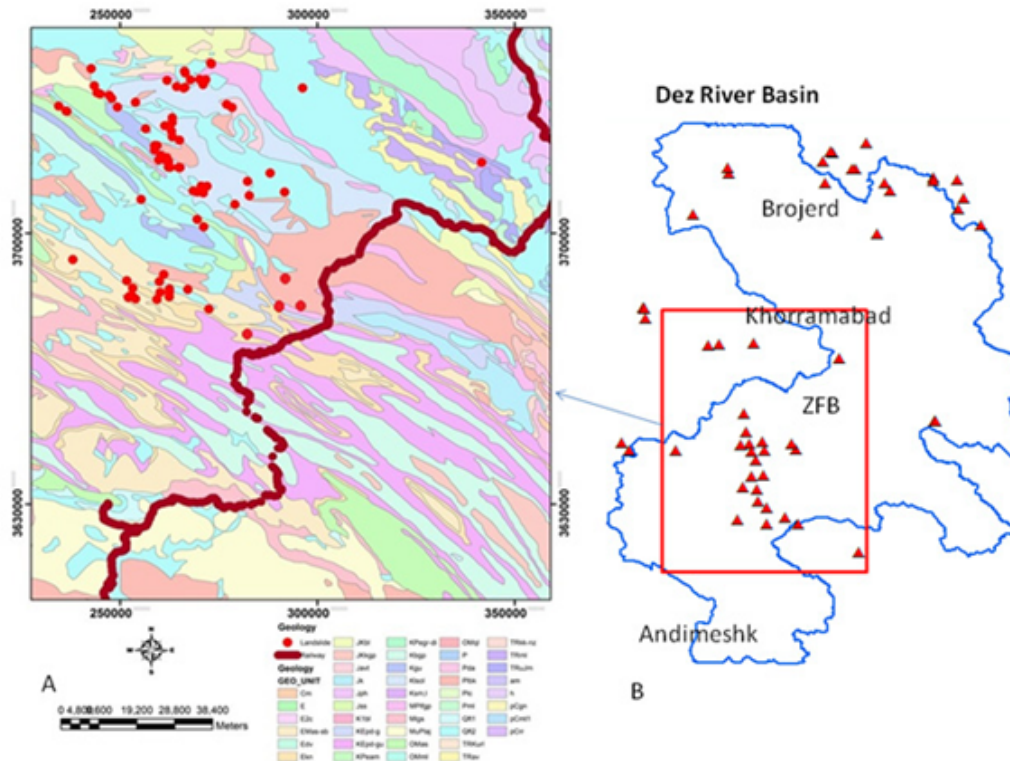
Figure 3.2: (a) New landslides identified in ZSB by red dots. (b) Landslide inventory data-set overlaid on the Dez River Basin represented by red triangle.

However, the details of the collision are complex and have been accounted for by various diverse models. While the details of the sub-surface structural geology such as folds and faults may be unresolved, the scenario at the surface using a DEM (Figure 3.4) and structural lineaments forming field checks (Figure 3.5) are relatively clear in this research. In the study area once fold growth has ceased, the landscape remains subject to uniform uplifting at a rate of 1 mm/yr due to crustal thickening at depth (Berberian, 1995). Uplifting and folding are the two

most important factors that accelerate landslides over time. As the uplifting continues, the drainage networks are adjusted and controlled by the structure and lithology. Thus, the drainage network influences landslides in some parts of the area where the lineament density and slope are high.

Figure 3.3: Field photo shows landslides due to erosion in the Zagros Mountains.

Tectonic force is a spontaneous event that occurs at the beginning of the geomorphic cycle and further influences landslides. Subsequently, geomorphic processes attack and degrade the topography and susceptibility of the landslide hazards. Since tectonic activities in the area first started during the Triassic and Late Cretaceous periods, the oldest geomorphic features have formed in the Zagros Mountains and resulted in the rugged topography. The effects of tectonic activities in the Zagros Mountains are more than those of sedimentation and the rate of erosion. Therefore, erosion may not have a significant contribution to changes in topography, landscape uplifting, and landslides. The zone of rapid rock uplift has a steeper gradient, higher relief, and

higher gradient indices than the gentle topography zone (Burbank and Anderson, 2001; Kirby and Whipple, 2012).

(a)   (b)
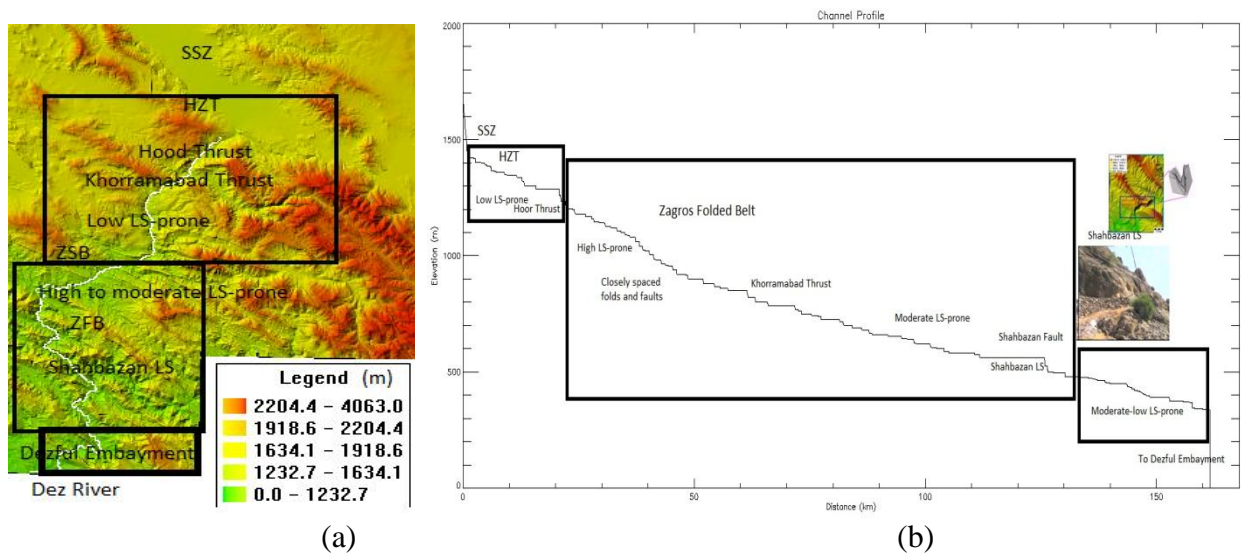
Figure 3.4: (a) Dez River on DEM with three landslide-prone areas, (b) The Dez River

topographic profile and closely spaced step-like of folding and faulting of study area.
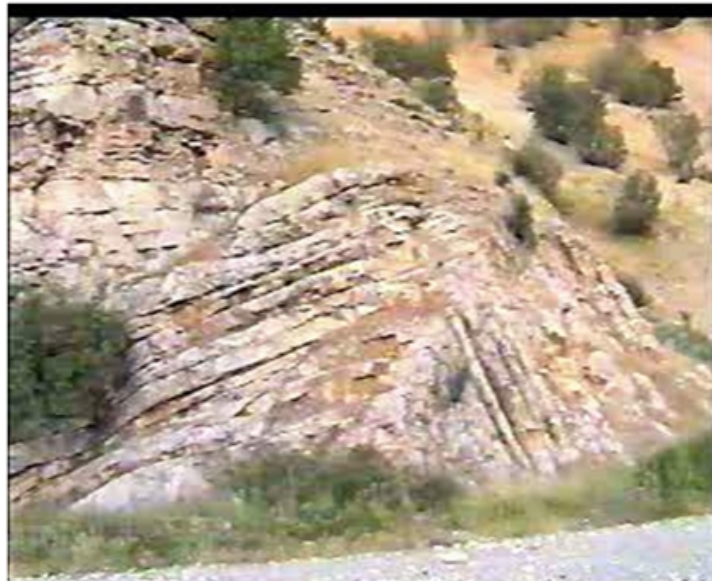
Figure 3.5: Development of folds and faults in Poledokhtar area.

To emphasize the stream length-gradient index as one of the tectonic geomorphologic

signatures on landslide hazards recognition, the lineament density map that was developed by Ali

and Pirasteh (2004) has been compiled with the stream gradients of the Dez River profile derived from the DEMs (Figure 3.4). Nevertheless, a visual interpretation and stream length-gradient index analysis on the LiDAR-derived DEMs have contributed considerably to the investigation of landslides, and it seems that the proposed method can deliver a reasonable support for landslide susceptibility mapping. It is to applying analytic techniques to data which has a geographical or spatial aspect. In this research, for tectonic geomorphology analysis the author employed RiverTools software that is capable of rendering maps processing spatial data, and applying LiDAR data or geographical datasets, including the use of ArcGIS. Therefore, information about geographic locations of each stream length-gradient index and anomalies are stored in a format with location-based that can be used in a geographic information system (GIS). This study has interpreted the anomalies and the results and data output can be stored in a GIS database as a shapefile, raster image, or even a dbf table or Microsoft Excel spreadsheet where anyone can use it in the future studies (Burbank and Anderson, 2001, Farrokhnia et al. 2011). In other word, the geospatial analysis was carried out in the GIS platform and the drainage network stream length-gradient index value was analysed to determine the behaviour of drainages. The behaviour of stream length-gradient index was interpreted based on Burbank and Anderson (2001) statement. Normally, value near to 1 or above 1 is considered as a tectonic active region.

The following section describes the methodology of how DEMs are processed and stream-gradient index is determined.

3.3 Methodology for Landslide Investigations

3.3.1 Data Characteristics, Acquisition and LiDAR-derived DEM

In spatial analysis measurements, the DEM, slope, stream profile, and river network of the ZSB were considered. The DEM of the ZSB is the most useful representation of terrain in the GIS for

spatial analysis. A DEM is the raster representation in which each grid cell records the elevation of the Earth's surface and reflects a view of terrain as a field of elevation values.

In this study, the acquisition of point cloud data over the ZSB was completed using a Leica ALS80-UP airborne LiDAR system in July, 2015. The data are in digital form with x, y, and z. The airborne LiDAR dataset consists of first pulse returns. The fly altitude was 4,200 m above ground with a laser scanning swath width of 5000 m. The laser scan's Field of View (FOV) was set up for max 75°. This was up to 70 Hz (FOV dependent) scan rate and 24-25 kHz laser pulse rate, and 3 at 45 kHz laser returns for less than 30 cm RMSE absolute positional accuracy. airborne LiDAR specifications are depicted in Table 3.1.

The Iranian Survey Organization (ISO) had used the Hierarchy Robust Filter (HRF) on LiDAR data and applied four processing steps including (1) thinning out, (2) filtering, (3) interpolating, and (4) sorting out (Pfeifer et al., 1998). After HRF was completed by the ISO, the pre-processed LAS data were collected to create DEMs of the study area. The LAS data were used in ArcGIS 10.2 and the DEM was derived from the current data set by interpolation approach and using LAS to raster function in ArcGIS software. Also, the LAS data were converted to txt format in x,y,z coordinates and the DEMs were generated in RiverTools software 3.0. Therefore, the DEM (5m) is ready to use in the GIS environment for tectonic geomorphology analysis and visual interpretation to identify susceptible landslide-prone areas. This landslide assessment was done based on the empirical approach in conjunction with the updated landslide inventory dataset and field observations.

Table 3.1: Airborne LiDAR system specifications.

Measuring frequency	24-25 kH
Flight height	800 m
Scanning frequency	70 Hz
Scanning angle	75° max

3.3.2 Determining Stream Length-gradient Index in GIS

Tectonic activities have formed different geomorphic features on the Earth's surface. These features are signatures and insights which guide an understanding of the tectonic activities of the Zagros Mountains. Sometimes landslides are influenced by tectonic activities and triggered by earthquakes. These signatures have shown that they can be good indicators to recognize landslides in an active tectonic region. Various factors such as slope and lithology can cause a landslide. A high stream length-gradient index and a step-like graded profile can be found in high slopes and scarps with low resistance rock types such as sandstone, limestone and marls of Aghajari Formation, and evaporites of the Pliocene Bakhtiari Formation (i.e. ZFB). The resistance rock type are such as schist, igneous and slate in SSZ. Thus, this study could possibly establish a logical interpretation of the correlation between stream length-gradient index and topographic graded profile with the slope and resistance of rock type for landslide recognition.

The DEM was used in the RiverTools 3.0 to extract the river profiles, networks, and stream length-gradient index for landslide investigations. Also, the stream length-gradient index and topographic graded profile of the ZFB were extracted. The Dez River profile (Figure 3.6) was extracted from the DEM to represent the relationships between topography, slope, and tectonic geomorphic features on the landslide assessments. This process was conducted by utilizing the channel profile function from the Tools menu in the shaded relief windows of the RiverTools. Then the stream length-gradient index (SL) was calculated automatically (Figure 3.7). The three classes of potential prone landslide areas are determined based on the density of the landslide locations correlated with tectonic signatures such as stream length-gradient index anomaly and closely spaced step-like lineaments, folds, and faults (Safari et al. 2009). They are considered as tools to map landslides.
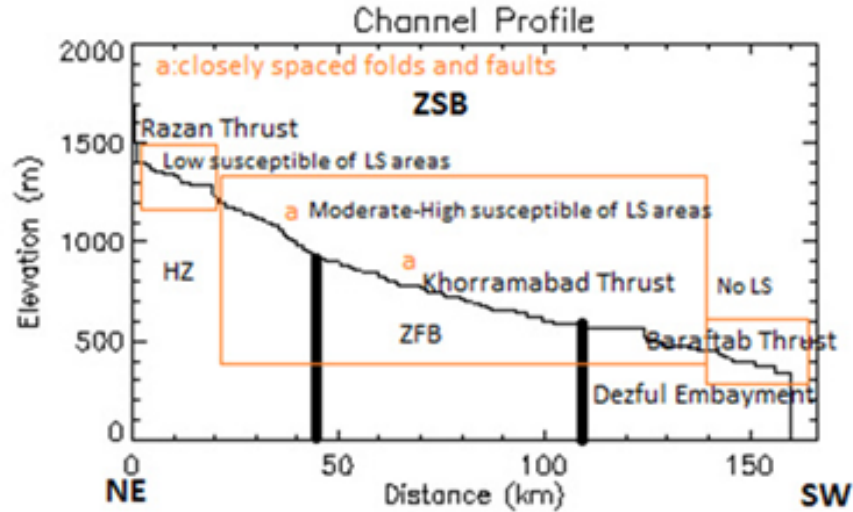
Figure 3.6: The Dez River step-like graded profile with landslide susceptible areas.

The stream length-gradient index is a signature that is sensitive enough to analyze the reach scale variability of tectonic function, rock resistance, and topography associated with the landslide process (Burbank and Anderson, 2001). It is because the stream length-gradient describes the morphology of the stream network using distribution of the topographic gradient along rivers or streams. Also, in the study area direction of streams are followed by lithology, tectonic, resistance of rock, and structural features. These features and parameters could be considered as predisposing factors to determine a landslide in conjunction with the stream length-gradient anomalies mapping that possibly supports identification of landslide and it seems to be a promising tool. The Dez River, which flows over the rocks and soils in the Zagros Mountains, tends to attain equilibrium with distinct longitudinal profiles and hydraulic geometries (Bull, 2007). By employing visual interpretation techniques, the study estimated the relative tectonic activity in a river basin that influences potential landslide phenomena (Burbank and Anderson, 2001; Dar et al., 2014).

The stream length-gradient index (SL) is approximated by

$$SL = \Delta H/\Delta L \times L \qquad\qquad (3.1)$$

47

where *L* is the total river length from the midpoint of the chosen reach whose index is calculated to the highest point on the channel. $\Delta H/\Delta L$ is the channel slope or gradient of the reach, in which ΔH is a change in elevation for a particular channel of the reach with respect to ΔL which represents the length of the reach (Figure 3.7). To calculate the stream length-gradient, I used the Dez River profile from Chalanchoolan police station close to Brojerd City which is in contact with the Sanandaj-Sirjan Zone (SSZ), High Zagros (HZ), and Zagros Fold Belt (ZFB). Figure 3.6 shows the Dez River step-like graded profile with a total stream length of approximately 165 km. The profile shows closely spaced step-like and knickpoints that are indicators of high tectonic activity and landslide-prone areas. In geomorphology, knickpoint is part of a river or channel where there is a sharp change in channel slope such as water fall and scarpment. The HZ topographic profile almost does not appear of closely spaced folds and faults density whereas in the ZFB, due to the high tectonic activity, this area has experienced moderate to high potential for landslide susceptible areas.
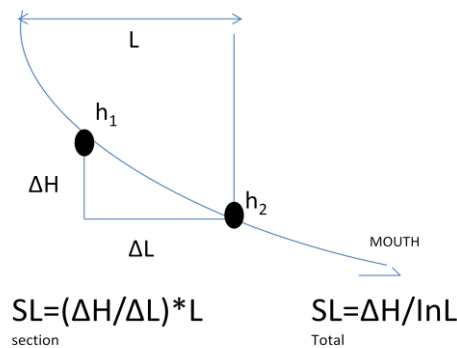
Figure 3.7: Concept to calculate stream length-gradient index.

In the next step, the literature of tectonics and the structural features of the study area including the structural map and the lineament density map have been compiled and overlaid on the LiDAR-derived DEM in GIS (James and Wynd, 1965; Alavi, 1994; Pirasteh et al., 2009; Safari et al., 2009). Ground observation in conjunction with the landslide inventory dataset and

image interpretation techniques of the DEM (5m), enhanced the expression of the stream length-gradient index anomalies to recognize tectonic signatures for investigation of landslides in UTM system. The precision of the map is based on the DEM (5m) in which the stream length-gradient index anomalies is depicted in Figure 3.8.

The final stage of the process was extracting the Dez River network. This was accomplished by using the river network function in the RiverTools 3.0 software. The morphometric parameters such as stream length, stream length-gradient were converted to the ArcGIS format, in which the stream length-gradient index map was generated (see Figure 3.8). The step-like river profile of the study area has been predicted by field observations to approach a graded profile. This study indicates that the area has been tectonically disturbed and is therefore associated with a high probability of landslides. The stream length-gradient index was deduced in each part of the profile (Figure 3.6). The stream length-gradient index map of the study area shows the tectonic zones in the ZSB and landslide-prone areas (see Figure 3.6) to pinpoint the areas prone to landslide). The high-gradient index anomalies on the map indicate the areas prone to landslide.

However, the susceptible or landslide-prone areas are detected based on the (a) stream length-gradient index value, and (b) the Dez River topographic profile indicators such as graded step-like that most likely show knickpoints, scarps, and high slopes. Landslide-prone areas on the map are determined by high value of stream length-gradient index. As it goes near to 1 or more than 1, it means the area is more prone to tectonic activities and possibly prone to landslides. Overlaying the inventory landslide map on the stream length-gradient index map shows the agreement between my result and the training landslides occurred in the past. Therefore, the boundary of landslide-prone areas were drawn manually on the map associated with the support of ground truth observations.
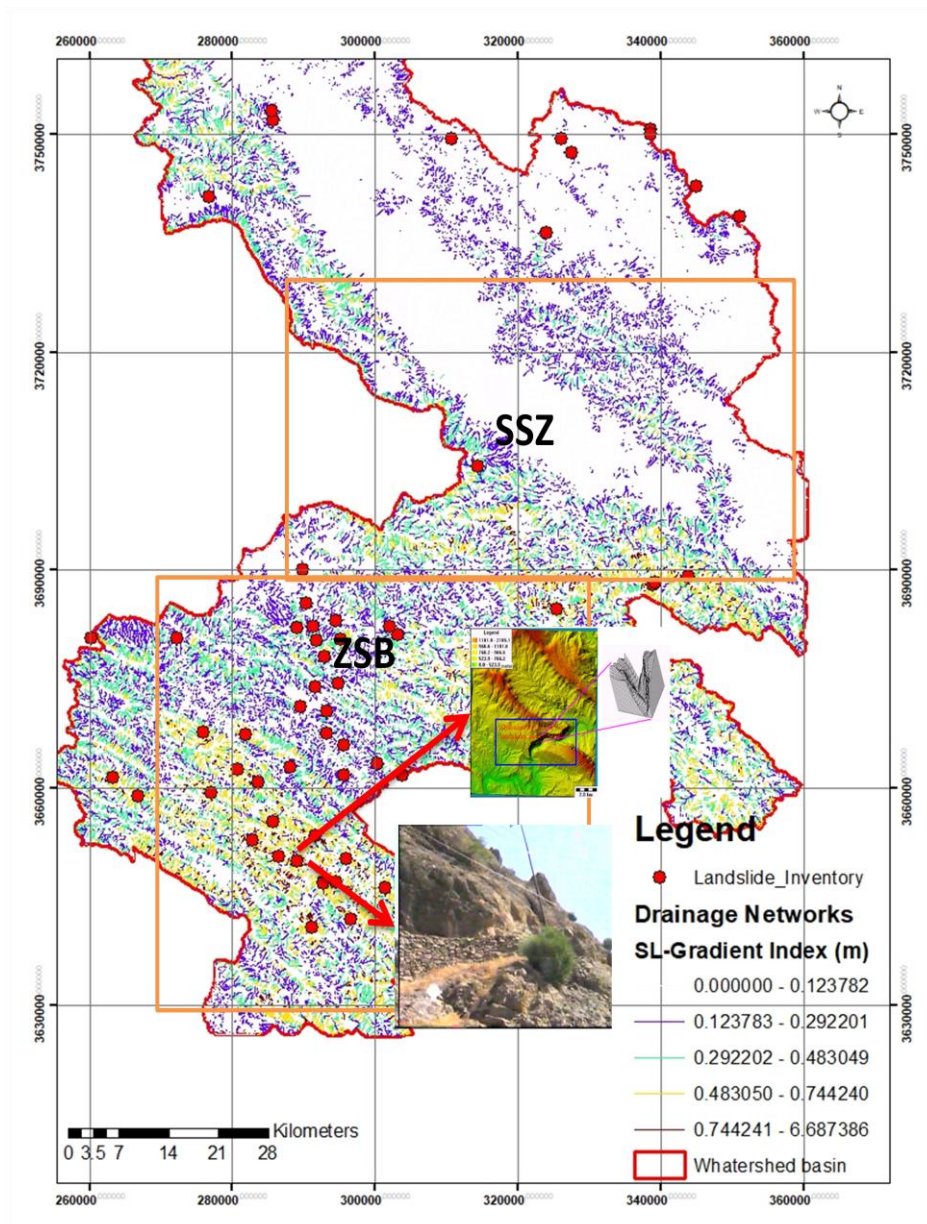
Figure 3.8: The stream length-gradient index map (see Figure 3.6 to pinpoint areas susceptible to landslide.

3.3.3 Performance Assessment

One fundamental step in the proposed approach to the landslide recognition process is validation. In this study, a reliable process was applied to ensure the reliability of the previous landslides inventory map and model used by the Geological Survey of Iran and the National Geoscience

50

Database of Iran (Safaiee et al., 2010; Rajabi et al. 2011). The validation of thematic GIS layers was obtained through ground truth observations and surveys. This method determined the performance of the output information derived from the stream length-gradient index and the visual interpretation of the LiDAR-derived DEMs. The proposed approach was assessed as one of the supporting tectonic geomorphology tools and methods of landslide investigations to incorporate it with further study of landslide susceptibility mapping in Chapter 4, if required. Moreover, the performance of detected landslide-prone areas (Figures 3.6 and 3.8) were validated based on the existing landslide inventory maps and a field observations. An example of Shahbazan's landslide-prone area visualization is pinpointed on the map shown in Figure 3.8.

3.4 Results

Although this study has not explored or discussed in detail the influential factors of landslides, it shows that the LiDAR-derived DEMs for stream length-gradient index anomalies mapping are probably good tools for landslide investigations in the Zagros Mountains. The LiDAR-derived DEMs of the study area obtained using the Hierarchy Robust Filtering (HRF) algorithm and RiverTools 3.0 software have shown considerable improvement in landslide investigations compared to other filtering such as adaptive TIN (ATIN) and Maximum Local Slope (MLS) because this HRF could deliver a reasonable result in a high and rugged topographic area such as Zagros Mountains (Yang and Li, 2013; Korzeniowska et al. 2014; Pirasteh and Li, 2016). Moreover, this method enhanced the landslide features that are in harmony with the stream length-gradient index and tectonic geomorphic signatures.

Based on the field observations and the stream length-gradient index anomaly map associated with the river topographic profile and lineament map, this study has indicated possibly, a direct relationship between slope instability, graded Dez River topographic profile,

51

and active tectonics in the Zagros Mountains as expressed by anomalous stream length-gradient index values on the map (Figure 3.8). In other word, it is interpreted that where stream length-gradient index is near to 1 or greater than 1, the more tectonic activities, the more graded profile with closely space step-like shape and high lineament density are seen; therefore, possibly it addresses areas with more potential to landslide-prone (Burbank and Anderson, 2001). The analysis of the stream length-gradient index in the Dez River with the landslide inventory dataset and high landslide frequency reveals that slope instability is associated with stream length-gradient index anomalies. This result corresponds to active tectonics structures in the Zagros Mountains with active faults and the presence of earthquakes. However, there are exceptions for debris flows and rock falls in conglomerates of Bakhtiyari Formation. This proposed approach is intended mainly for tectonic active regions such as Zagros Mountains which have complex landslides and rock falls that are mainly associated with not only upper fault blocks (where slope angles are increasing) but also with scarps and high angle slopes (approximately 90°).

The stream length-gradient index could possibly be applied as an indicator to determine areas prone to landslides, thus it may be considered as one of the predisposing factors to support the landslide susceptibility mapping for the future studies. The stream length-gradient index (SL), which shows anomalies of the stream geomorphic parameter, has proven to be possibly a suitable tool for detecting stream-profiles related to active tectonics and surface processes such as landslides.

Second derivatives of the DEM such as slope, stream profile, and drainage network resulted in improving the visual interpretational method and processing data to map the spatial distribution of the SL index in the ArcGIS environment. This method uses stream length-gradient index as a tool to identify landslide prone areas. Figure 3.8 shows the landslide prone areas around the stream segments where the extreme index values occur.

An increase in stream length-gradient index values signifies elevated tectonic activity and accelerates the potential for landslides (Burbank and Anderson, 2001). The study demonstrated the existence of active deformation associated with landslides in the ZSB as an indicator by steeper gradients in the zone of rapid rock uplift (Berberian, 1995; Safari et al., 2009). High index values are supported by ground truth observations and it shows that the steeper gradient and high tectonic activities associated with landslides in some areas mainly consist of thrusting and faulting, such as the Main Zagros Thrust, Hoor Thrust, Chamsangar fault, Shahbazan strike-slip fault (Figure 3.8), and Baraftab fault (Figure 3.4). The Dez River profile indicates that the most active tectonic zone and landslide prone areas fall within the Folded Zagros (Figure 3.6). The reduction in the gradient values towards the Dezful Embayment is interpreted as low tectonic activities and landslide probability.

The different formations dominating various types of rocks like limestone and evaporates of the Gachsaran Formation, shale of the Aghajari Formation, marls of the Kashkan Formation, and Cretaceous calcareous (i.e. contact of the Imbricate Zone and the Zagros Fold Belt with the Sanandaj-Sirjan Zone) may also approach the graded profile of the Dez River and be associated with landslides. Therefore, this study has mapped new landslides based on the stream length-gradient index anomalies, the Dez River graded topographic profile evidenced by the ground truth observations (Figure 3.8). This study emphasized that the ZSB has formed and developed landslides as compared to the existing inventory dataset not only because of the tectonic processes, but also because of rugged and immature topography (Farrokhnia et al. 2011; Safari et al., 2009). A river profile of the study area is predicted to exhibit a graded profile, indicating that the area has been tectonically disturbed slowly rather than rapidly and that most occurrences of landslides depend upon high tectonic activities.

The systematic stream-gradient map of the ZSB in the GIS environment shows the correlation between tectonic and landslides. From the map (Figure 3.8), it is evident that the Sanandaj-Sirjan Zone exhibiting 0 to 0.483 (i.e. SL slope) has low tectonic activity with no landslide visibility. This map also reveals that the stream length-gradient index in the Zagros Fold Belt exhibits up to 6.687m. In other words, the area has a moderate to high tectonic activity and significant potential for landslides. This study revealed that a low gradient index is less prone to landslides in comparison to a high-gradient index (Figure 3.8) (Burbank and Anderson, 2001). However, these tectonic activities in the Zagros Mountains have generated terraces and different types of landslides such as rock fall, flow debris, and complex geomorphic structures.

3.5 Discussion

LiDAR systems have been reviewed and discussed in Wehr and Lohr (1999). A clear reference to an updated discussion is commented on in Shan and Toth's (2008) book. A brief review of LiDAR and other remote sensing techniques utilized in landslide studies is found in Prokop and Panholzer (2009). The DEM of the study area allowed for the detection of more informative landslide features than the coarse-resolution (e.g. 20 m or 30 m) DEMs derived from traditional techniques such as aerial photographs, topographic maps, and other remote sensing techniques (Farrokhnia et al. 2011; Pirasteh and Li, 2016).

However, obtaining flight permission from the Iranian authorities remains a challenge, and using airborne LiDAR for studying landslides and monitoring natural hazards from time to time is not wise. Moreover, the cost is high. Airborne LiDAR cannot be used on a regular basis to monitor a landslide before and after the event. Thus, when considering the future direction of landslide investigations in Iran, it is not possible to study landslides before and after their occurrence nor expect to practice an early warning system using LiDAR techniques. The study

area is a dense vegetation area which may obscure the morphology of landslides both in the field and in remotely sensed data. LiDAR data is processed to reveal the topography beneath vegetation (James et al., 2006). It has proven to be useful in identifying tectonic fault scarps and folds, and in generating high quality DEM derivatives such as river networks, previously unmapped landslides, and other geomorphic landforms (Haugerud and Harding, 2001; Haugerud et al., 2003; Sherrod et al., 2004).

The strength of using airborne LiDAR-derived DEMs in comparison to other techniques lies in the generation of high-resolution DEMs. Still, it is a challenge for users to develop a software tool to detect landslides using LiDAR-derived DEM automatically. The experience of this research shows the particular challenge of obtaining clear shots in certain areas (e.g. the ZSB) with very steep terrain and cliffs (Pirasteh and Li, 2016). Also, geological features such as bedding and layering can sometimes be mistaken for instability. Therefore field verification is always an essential component of the process.

3.6 Conclusions and Recommendations

Steep hillslopes and graded river profiles are mostly susceptible to landslide processes, but they are also affected by lithology and structure. Identification of streams in hillslopes with DEM is a difficult task. Therefore, it is recommended that researchers fit certain analytical models with the help of existing landslide inventory dataset and stream gradient. These models will differ in different geological areas. Thus, the stream gradient alone cannot identify the landslide prone areas.

This study concludes that the zone of rapid rock uplift in the ZFB has steeper gradient and higher gradient indices than the SSZ in north of the map (Figure 3.8), and likely has highly susceptible zones to landslides. This study found that the LiDAR-derived DEM provided

55

detailed information about the stream-profile metrics and thereby may improve the landslide investigations as compared to the previous studies used 20m resolution DEMs developed by photogrammetric techniques (Safaiee et al. 2010; Farrokhnia et al. 2011). Possibly, this improvement may be because of the extracted more information of the streams behavior and changes in the Dez River profile. The stream profile and stream length-gradient index map could possibly provide insights with high potential to support landslide-prone areas assessment with limited resources in a very short time when no data such as land use, vegetation, precipitation and other influencing factors are available (see Chapter 4). In particular, the method of this study has shown a very promising approach to identify landslides in the Zagros Mountains. This proposed method has also shown potential to detect landslides that directly reach the streambeds as well as landslides whose magnitude and activity are high enough to generate stream perturbations in the Zagros Mountains.

3.7 Chapter Summary

This study identified features that can provide insights for landslide assessments. The high stream length-gradient indices in the study areas are determined in conjunction with field observations and an available dataset of landslide inventories. Remote sensing data such as LiDAR-derived DEM sometimes may be a better choice as compared to the DEMs that are generated from topographic maps or sensors such as ASTER (Pirasteh et al. 2011a; Burden and Faires 2011; Caimpalini et al., 2016) for extraction of the stream length-gradient index to assess landslides. This study used an empirical approach with spatial analysis of drainages in the GIS environment to estimate landslide-prone areas. This chapter delivered an empirical approach in conjunction with the GIS analysis for landslide investigations from LiDAR-derived DEMs.

Finally, this study contributed by: a) Expanding upon previous efforts to present a tectonic geomorphology approach of localizing landslide-prone areas; b) Suggesting stream length-gradient index and topography river profile for landslide investigation when we have only a DEM, and do not access to related data; and c) Updating the landslide inventory map of the study area.

Chapter 4

Probabilistic Frequency Ratio Model for Landslide

Susceptibility Mapping from LiDAR-derived DEMs

This chapter presents a quantitative approach to terrain analysis. LiDAR point clouds were utilized to evaluate both spatial and temporal factors contributing to landslides in the Alborz Mountains, Iran. The probabilistic frequency ratio (PFR) model was used to possibly improve the quality of landslide susceptibility evaluation. The PFR model was applied to consider the effect of landslide-related factors associated with Google Earth's high-resolution images and field observations. The LiDAR point cloud data and GIS-based analysis have allowed in landslide hazard assessments to be performed using inventory dataset as compared to previous studies. This chapter contributes a revised and updated landslide inventory map of the Mazandaran Province. Image elements interpretation was applied on the available 30 m ASTER Digital Elevation Model (DEM), LiDAR-derived DEM (5 m), and Google Earth high spatial resolution images (0.5m-1m) in conjunction with field observations. In this study, factors such as geology, geomorphology, land use, soil, slope, and distance from roads and drainage were evaluated to represent, manipulate, and analyze landslide susceptibility. Also, the performance success of the rate curve of landslide susceptibility was evaluated. Results led to an improved landslide susceptibility map from LiDAR-derived DEM by implementing the PFR model with 92.59% accuracy performance in comparison to the existing data and previous studies in the same region (Safaiee et al. 2010; Farrokhnia et al., 2011). Furthermore, this study revealed that all factors have relatively positive effects on landslide susceptibility mapping in the study area.

However, the most effective predisposing factor for landslide occurrence is lithology with 13.7%.

4.1 Introduction

Landslides are one of the most common deformation scenarios in the real-world environment. Almost every year catastrophic landslides cause loss of life and result in billions of dollars in property damage around the world. Landslide-prone areas reconnaissance is playing a major role in motivating decision-makers to prepare a loss reduction plan. Identification and spatial distribution of landslides require knowledge of not only geologic and geomorphic processes, but also techniques including GIS. Moreover, LiDAR and UAV techniques have become excellent tools for improving landslide recognition processes in mapping (Haugerud et al., 2003; Eeckhaut and Van, 2007).

Significant research on landslide hazards has been conducted in an effort to study slope instability hazards mapping (Carrara et al., 1991; Carrara et al., 1999; Guzzetti et al., 2005; Roering et al., 2009; Pirasteh et al., 2011; Su et al., 2015). Also, some researchers have applied deterministic models for landslide susceptibility mapping and modelling (Binaghi et al., 1996; Zhou et al., 2003; Watts, 2004; Sarkar and Kanungo, 2004; Lee et al., 2004; Lee and Dan, 2005; Westen et al., 2008; Jebur et al., 2014). Moreover, researchers have applied the logistic regression model to landslide hazard mapping (Choi et al., 2012). Recently, landslide hazard evaluation has been carried out by using fuzzy logic and artificial neural network models (Lee et al., 2004; Yilmaz, 2010; Lee et al., 2014). During the last decade, landslide susceptibility and deformation measurement has been performed extensively, particularly for landslide assessment (Luzi et al., 2000; Su and Bork, 2006; Streutker and Glenn, 2006; Schulz, 2007). For example, McKean and Roering (2003) studied low-density DEM to determine the potential of

differentiating components within a landslide morphologically (Lee and Dan, 2005; Glen et al., 2006; Yilmaz, 2008; Niculitˇa, 2016). Also, McKean and Roering (2003) explored how to provide insight into the material type and activity of the slide. As a result of this exploration, the literature review indicated that these techniques and low pixel resolutions of DEM and satellite imageries could not provide sufficient accuracy to visualize the objects extracting an informative description of the landslide locations, nor could they predict the probability of landslide occurrence.

In this study, a 5 m resolution LiDAR-derived DEM was used. Google Earth images were used in conjunction with existing landslide inventory maps (1:25,000 scale, Natural Resources of Iran) to apply the PFR model. This approach could potentially contribute the PFRmethod for research scholars by improving landslide evaluation and possibly the quality of susceptibility mapping prediction. Therefore, the existing inventory spatial distribution of landslide data, Google Earth images, LiDAR point clouds, and ASTER data were collected to study landslide probability prediction in Iran's Alborz Mountains.

The Iranian plateau has potential for earthquakes and various types of landslides (Ali and Pirasteh, 2004) due to its high tectonic activity, rugged topography, geological setting, and climatologic variety. Most landslides occur within the following mountain ranges: a) Alborz range with NE-NW trend; and b) Zagros range with NW-SE trend. Landslide risk in Alborz range, particularly in Central Alborz, is higher risk than it is in other regions. Often, the study area has experienced landslides in Central Alborz, for example Hajiabad-Oshan Road in 2003, Fasham-Meygon road in 2006, and Atashgah-e-Karaj in 2008. Moreover, several landslides and rock falls occurred on Chalus-Tehran Road that were induced by the Baladeh-Kojour earthquake on May 28th, 2004. These catastrophic landslides have proven that an improved method such as LiDAR-derived DEMs associated with the PFR approach is required for landslide susceptibility

mapping. Therefore, the Marzan Abad area of Central Alborz has been selected for this study due to its high population and susceptibility to landslides-particularly those which are triggered by earthquakes.

The objectives of this study are: a) To use the LiDAR-derived DEMs in association with contributing factors; and b) To improve the quality performance of the PFR model in assessing and predicting landslide susceptible areas in Central Alborz by evaluating LiDAR-derived DEMs and other impacting factors. Nevertheless, this study contributes high resolution of LiDAR-derived DEMs for landslide susceptible assessments, and by increasing the quality of PFR model outcomes. To satisfy the above objectives, landslide susceptibility analysis techniques have been applied and verified in the study area by using previous research outcomes and the existing landslide inventory map in conjunction with some ground truth data. Landslide-related factors in GIS software (ArcGIS 10.4) were assessed by implementing the analysis tools for spatial management and data manipulation. Finally, satisfactory accuracy of landslide hazards prediction was achieved by applying the PFR model and using a LiDAR-derived DEM.

4.2 Materials and Method

4.2.1 Data Collection

Data collection and preparation are the first fundamental and essential steps to landslide hazard analysis. In this study, the GIS database was composed of five parts: 1) Generation of a 5 m resolution LiDAR-derived DEM and a 30 m resolution of the ASTER DEM; 2) Google Earth images; 3) Landslide inventory map shows landslides specification such as location, soil type, lithology, cause, type, length, width, area for 1990-2010; 4) Landslide predisposing factor maps and topographic maps; and 5) Collection of data by GPS from field observations.

The existing landslide inventory spatial distribution of the area (Figure 4.1) provided insights into the recognition of landslide prone areas. The study area is bounded by latitudes

61

4015000m N-4047000m N and longitudes 52300m E-54500m E in UTM. In this study, landslides have been extracted from LiDAR-derived DEMs and ASTER DEM in conjunction with field observations (Figure 4.2). The visual image interpretation of the DEMs and Google Earth images (dated from 2009 to 2016, all in December) were used in conjunction with field observations. The ENVI 4.2 software allowed for the operation of digital image processing (DIP) such as geometric correction, enhancement, and filtering on Google Earth images.
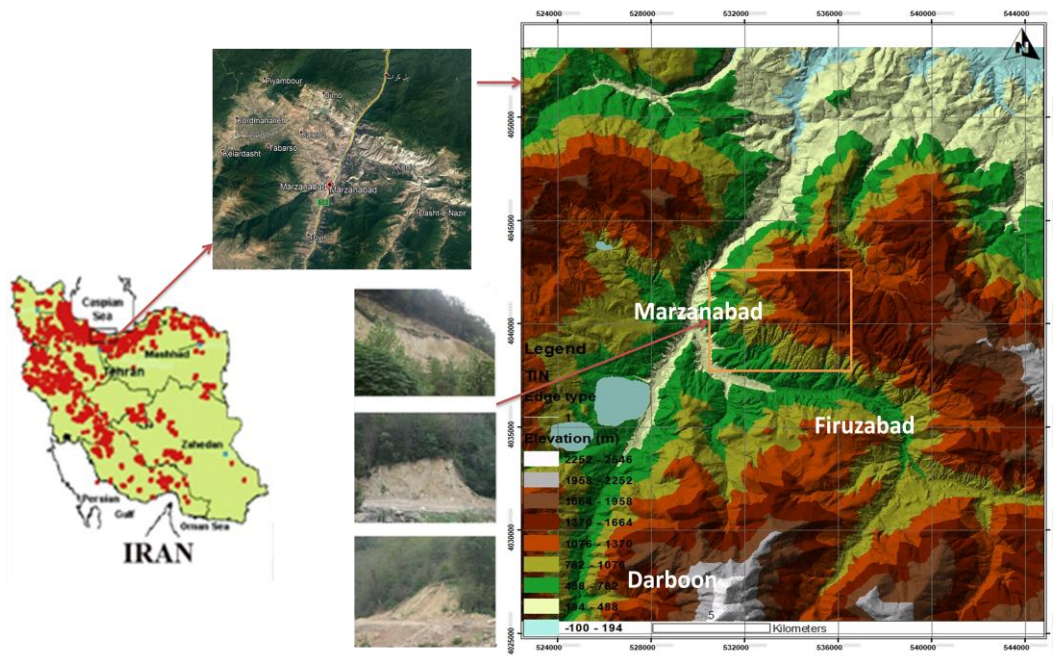
Figure 4.1: Study area of the Central Alborz Mountains and inventory landslide of geographical distribution in Iran.

Figure 4.2: Landslides in Imamzadeh Ali, Marzan Abad, Central Alborz Mountains.

Landslide susceptibility evaluation requires knowledge of factors leading to landslide analyses. This study determined the factors influencing landslides. The literature review and field investigations identified the most influential factors in the study area as topography, lithology, soil, geomorphology, steepness of slopes, land use, and distance from road networks and drainage (Varnes, 1978; Anbalagan, 1992; Brunsden, 1996; Donati and Turrini, 2002; Zhou et al., 2002; Nichol and Wong, 2005; Metternicht et al., 2005; Jebur et al., 2014; Anbalagan et al., 2015). Each category was subdivided into different classes based on its value or feature. All influential factors, which have been obtained or created in the form of maps, represent large quantities of spatial data. The preparation of hazard and susceptibility mapping involves manipulating, analyzing, and presenting data in the GIS.

This study prepared the digital geology map of the study area based on a combination of two analog geological sheet maps at 1:100,000 scale, namely Marzan Abad and Chalus (Geology Survey of Iran, 2001) and Google Earth image interpretation. The scale of the map was changed based on the spatial resolution of the satellite images as well as the existing maps. On screen digitization in ArcGIS was applied on the analog geological maps, and spatial analysis was carried out for all lithological units. The manual processing system in ArcGIS was applied to name each litho-unit type as attribute input data in a table. The image elements such as photographic and geotechnical element (i.e. texture, shape, vegetation, slope) were used to map the geology of the area. The geomorphology map was created based on the geology and topography map in 1:25000 scale associated with the LiDAR-derived DEM (5m). It was done by on screen digitization in ArcGIS in conjunction with field observations. A slope thematic map was extracted from the LiDAR-derived DEM of the area with a spatial resolution of 5 m.
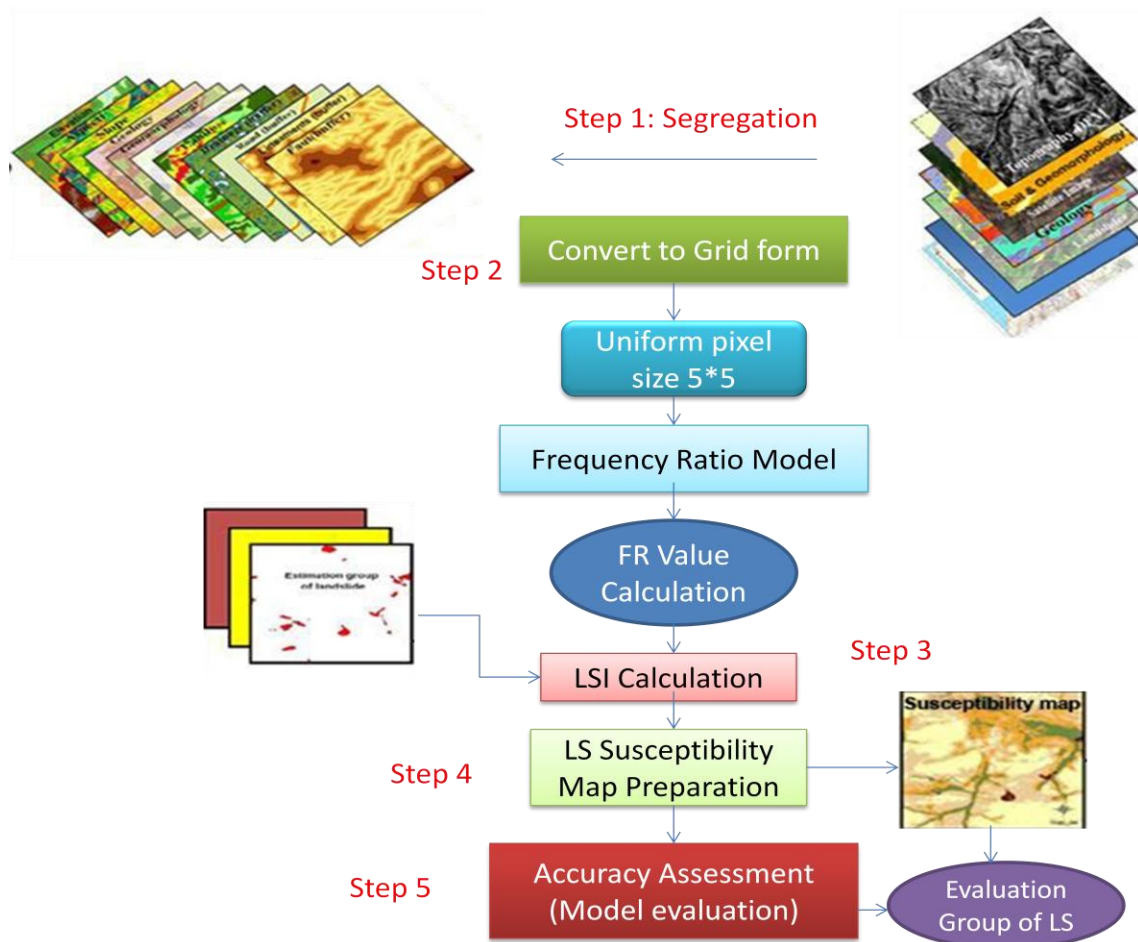
Figure 4.3: Flowchart of the method.

The soil map (1:25000 scale) was collected from the Ministry of Natural Resources of Iran. A field survey verified the given digital soil map. Road and drainage maps were extracted from the topography map of the study area (National Cartographic Center organization, 2015) at 1:25000 scale. The land use map and the Normalized Difference Vegetation Index (NDVI) of the study area were provided by Natural Resources of Mazandaran. The land use map was modified by a field check. However, the following figure (Figure 4.3) depicts the flowchart of the method. Also, Table 4.1 depicts a summary of data layer information.

Table 4.1: Predisposing factors for landslide occurrence and GIS data in the study area.

Classification	Sub-Classification		GIS Data Type	Scale or Resolution
Geological Hazard	Landslide inventory		Point, polygon coverage	1:25,000
Basic maps	LiDAR-derived DEM	Slope	GRID	5m
	ASTER DEM		GRID	30m
	Topographic map	roads and drainage	Poly line coverage	1:25,000
	Geology		Polygon coverage	1:100,000
	Soil		Polygon coverage	1:25,000
	Land use		GRID	30m
	NDVI		GRID	30m
	Geomorphology		Polygon coverage	1:25,000

4.2.2 Processing of LiDAR Point Cloud Data and DEM Generation

In spatial analysis measurements, high resolution DEM and its derivatives such as slope have been considered for landslide hazard prediction and susceptibility mapping. The high-resolution DEM of Central Alborz is the most useful representation of terrain in the GIS for spatial analysis. A high-resolution DEM is the raster representation, in which each grid cell records the elevation of the Earth's surface and reflects a view of terrain as a field of elevation values. In this study, a resolution of 5m in the pixel was applied for grids to generate the high-resolution DEM.

LiDAR point cloud data in LAS format were collected for the Marzan Abad of the Central Alborz Mountain from ISO. LAS data were used to generate a DEM in ArcGIS software. To process the data, a semi-automated method was used to remove the noise and classify the objects (Evans et al., 2009). This semi-automated method allowed for the detection and

interpretation of particular objects in the study area. The pre-processing technique was applied to the point cloud data to achieve a certain level of quality data before being used for landslide hazard prediction and susceptibility mapping. The bare-earth was extracted by applying SCOP++ software (i.e. segregating objects such as trees from the surface and extracting the earth's surface). This process has a direct impact on the quality of the DEM and landslide investigations.

During the last two decades, various solutions and algorithms for the classification of the LiDAR data have been published (Glenn et al., 2006; Derron and Jaboyedoff, 2010; Su et al., 2015). The method was based on the surface interpolation and the DEM was generated based on the x,y,z points of the entire study area (Pfeifer et al., 1998). In other word, the Hierarchical Robust Filtering (HRF) method and ArcGIS 10.4 software were used to develop the high-resolution DEM of the study area. The HRF method was originally designed for laser data in vegetated and rugged topography areas such as Central Alborz Mountains. To determine the relationship and influence of each individual grid of factors such as land use within the whole DEM of the study area in the GIS, the whole DEM and individual factors must be considered to identify the number of pixel/grids contributing to a landslide.

This HRF algorithm is embedded in the SCOP++. After HRF was completed by the ISO, the pre-processed LAS data were collected to create DEMs of the study area. The LAS data were used in ArcGIS 10.2 and the DEM was derived from the current data set by interpolation approach and using LAS to raster function in ArcGIS software.

4.2.3 ASTER DEM

This study imported ASTER images by using Ortho-Engine software as part of the PCI Gemomatica 9.1. The DEMs were generated automatically by using the DEM extraction tool from the PCI Gemomatica 9.1 (Figure 4.4). A detailed description of the procedure of generating

ASTER DEMs has been provided by Al-Rousan et al. (1997). The quality of the ASTER DEM was satisfactory after applying re-sampling (Al-Rousan et al., 1997). The satisfaction is determined by how it is acceptable, but maybe not great in creating a 3D model when to visualize a 3D surface view in ENVI platform and to see objects. Also, this satisfaction is achieved by field observations and consultation with the Natural Resources of Iran.
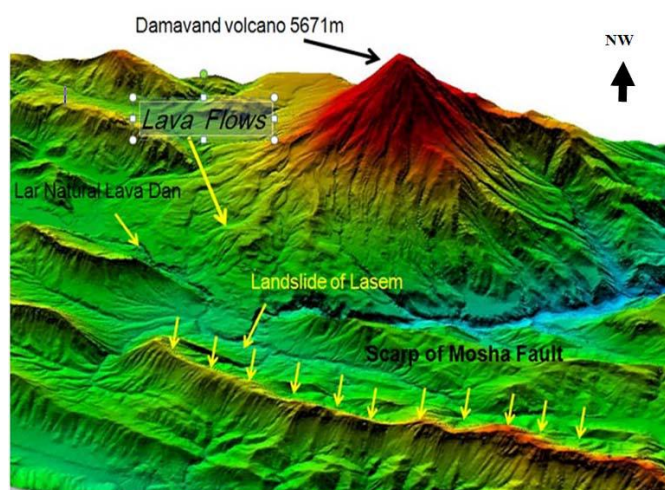
Figure 4.4: 3D surface view of ASTER DEM 30 m.

4.2.4 Probability Frequency Ratio (PFR) Model Approach

This study assumed that future landslides would occur under similar circumstances to those of previous landslides. This study applied the PFR model based on the given assumption. This model is used because the author assumed that the accuracy of map could be increased. Also, this is because to compare it to other existing models' accuracy and quality such as logistic regression; and finally to improve the quality of the proposed susceptibility landslide map (Table 4.6). Frequency ratio approach is based on the observed relationships between the distribution of landslides and each landslide-related factor to reveal the correlation between landslide locations and factors in the study area (Lee and Pradhan, 2006). Frequency ratio (FR) describes how often

something happen divided by all outcomes. The PFR is a statistical relationships between historical target location (inventory data) and its conditioning factors. A bivariate statistical analysis method is based on spatial distribution of dependent and conditioning factors such as slope. To apply the PFR model, a spatial database of landslide-related factors was constructed in the GIS platform. All data layers (Table 3.1) were converted to the GIS format and geo-referenced into the Universal Transverse Mercator (UTM) coordinate system. Maps represent each factor in the GIS environment (Figure 4.5).

This research constructed maps of various factors in different classes. A fine grid was overlaid over the study area with each grid cell representing a small unit area (rasterization). The data layers obtained a square-grid matrix with 3,400 lines by 2,982 columns. Each pixel of LiDAR-derived DEM represents 5×5 m area on the ground (Figure 4.5). By utilizing the overlay of training subsets of landslides, geospatial distribution map, and predisposing factor ranges such as topography, the spatial relationship between landslide locations and each factor's range was extracted. The number of landslide occurrence pixels in each class were evaluated, and then the Frequency Ratio (FR) value for each factor's range was calculated. This allowed for the division of the occurrence landslide ratio by the area ratio. Landslide frequency ratio was calculated by the ratio of percent domain of a factor class and percent landslide in that class. Next, the frequency ratio (FR) method was implemented to evaluate the rank of correlation between the selected factor's ranges (i.e. slope, land use, soil, lithology, distance from drainage, and distance from the road network) and landslide locations in the study area. The value of 1 for FR value is an average value.

This study defined the greater ratio above the unity as meaning that the stronger correlation is between the selected factors and landslide geographical distribution. Likewise, the lower ratio than unity means a lower correlation between landslide occurrence and the given factors

attribute. Therefore, based on the calculated FR values, the relation of each category's factor with landslide occurrences have been evaluated. After the FR values calculation, this study calculated the Landslide Susceptibility Index (LSI) for each pixel of the study area. This method considers point x with m (number of layers) pixel values $(x_1,\ldots, x_m)$ in the study area. In pixel x, LSI can be calculated by summation pixel values $(x_1,\ldots, x_m)$, as indicated by the following equation (4.1):

$$LSI = \sum FR = FR_1 + FR_2 + FR_3 + \ldots + FR_m \qquad (4.1)$$
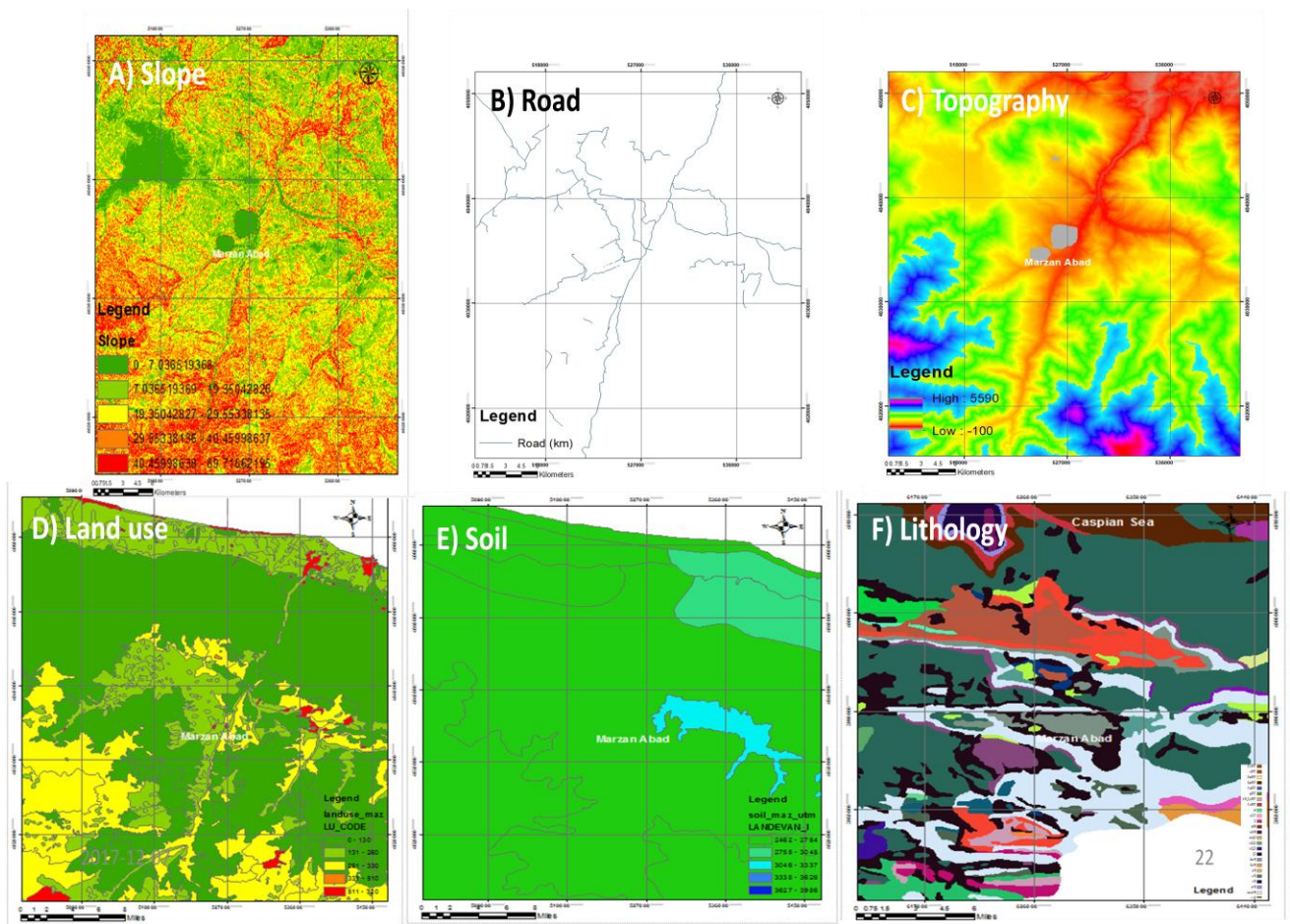
Figure 4.5: Predisposing factors and maps in the GIS environment. a) Slope map, b) Road map, c) DEM, d) Land use map, e) Soil map, and f) Lithology map of Marzan Abad and study area.

69

Where FR is the rating of each factor's range (Frequency ratio value) and Landslide Susceptibility Index (LSI) represents the relative susceptibility to landslide occurrence in unit of area.

4.2.5 Contribution of the PFR and the High Resolution DEM to the High Accuracy Relative to Other Methods

The FR method was produced using the weights for each class of each conditioning factor. The PFR model was applied in order to evaluate the landslide susceptibility of the area based on the observed spatial relationship between landslide occurrences and conditioning factors. In general, the landslides that will occur in the future have the same condition as past landslides. The FR is the ratio of the probability of the presence to the absence of landslide occurrence (Yilmaz, 2009). The advantages of this model are that it can be simply implemented and its result is completely easy to comprehend (Yalcin et al. 2008). The spatial relationship between each related conditioning factor and all landslides were derived utilizing the frequency ratio.

Though the resolution of DEM is playing a role in landslide susceptibility mapping and hazard assessment, a finer resolution is not always necessarily result in a higher accuracy of landslide susceptibility mapping. For example, Tian et al. (2008) studied the effects of raster resolution on landslide susceptibility mapping in Shenzhen of China and they selected eight factors to calculate landslide susceptibility with eleven groups of different resolutions (5m to 190 m). They found that 90m resolution has the best accuracy and the 150m resolution has the worst one. It is basically because when we use a different type of predisposing factors and a model that has its precision. That is why the difference sometimes is caused by the method and the kind of data we use.

Sometimes, the spatial resolution is essential, especially when we study small landslides and the dimensions of slope failures vary. If the spatial resolution is relevant to the surface

features found in the landslide morphology, it will help improve the extraction, identification, and mapping of landslide surface features. For example, Mora et al. (2014) studied the effect of spatial resolution on small landslide susceptibility mapping, and they concluded that the spatial resolution affects the accuracy and surface features extracted for small landslide susceptibility mapping, as the performance is dependent on the scale of the landslide morphology.

Also, the resolutions may be variable due to the size of the study area. In this study, the prediction capability of the performed PFR model is considered for predisposing factors for landslide susceptibility mapping. That is why, this study with the LiDAR-derived DEM probably impacts the PFR model outcomes and increases the precision and quality of susceptibility hazards mapping in comparison to the DEM with lower resolution used in previous research than 5m used (Figure 4.11, Table 4.5) (Guns and Vanacker 2012; Chen et al. 2014; Rui et al. 2017). However, in all methods, the DEM is the base for deriving the slope and other predisposing factors such as drainages and aspect. Normally, by any methods we use, the grid size of predisposing factors including slope-derived from DEM may not also be a similar size.

Gholami et al. (2017) studied FR, Fuzzy Gamma (FG) and Landslide Index method (LIM) with 20m DEM resolution. This study determined landslide prone areas in Sari-Kiasar watershed, Mazandaran Province of Iran. The DEM was derived from aerial photographs in the 1:25,000 scale of topographic maps and extensive field observations. Some of similar predisposing factors were considered, and spatial relationships among them in the GIS allowed to evaluate the predictability of landslide hazards. The 20m resolution DEMs and predisposing factors such as geomorphology, rock type, vegetation, and distance to road employed to the three above methods. This study revealed that the most important factors in landslide occurrence were rainfall, slope, and vegetation. The performance of the prediction capability of the models was evaluated by using Receiver Operating Curve (ROC) and the Area Under Curve (AUC). It

revealed that PFR has a better accuracy than FG and LIM regardless the spatial resolution of the DEMs.

Nevertheless, in the present research, the slope-derived from DEM with 5m resolution was calculated to identify FR and the percentage of its contribution to landslide susceptibility mapping. The prediction capability of the performed model is compared with the previous research (Guns and Vanacker 2012; Chen et al. 2014; Gholami et al. 207; Rui et al. 2017) with almost similar predisposing factors for landslide susceptibility mapping (see Figure 4.11, Table 4.5). Perhaps, the 5m resolution DEM affects the accuracy of the surface features extracted for landslide susceptibility mapping because it depends on the scale of the landslide morphology. The lithology has more influence to the landslide susceptibility mapping.

4.2.6 Performance of the Effect Analysis

One of the most fundamental steps in the FR approach and the landslide hazard prediction and susceptibility mapping process is validation. The authentic process was applied to determine the reliability of the previous data and parameters involved in the present study. For this study, the data were obtained from the Geological Survey of Iran and the National Geoscience Database of Iran. This study verified the performance of the result by relative operating characteristic (ROC) curve method of comparing the existing landslide inventory geospatial distribution map with the landslide susceptibility map (a cross-validation technique) (Chung and Fabbri, 2003; Paolo et al., 2010; Wen et al., 2017). In other words, the ROC curve was used to validate the accuracy of the PFR model Eq. (4.1). Previous studies have used "success rate" to evaluate model performance (Dietrich et al., 1995; Duan and Grant, 2000; Lee and Dan, 2005; Liu et al., 2012; Jebur et al., 2014). The success rate is defined as a ratio of how many actual landslide sites are successfully predicted. This allows researchers to estimate the goodness of the fit of the predictive models

with actual landslide sites.

In this study, the results of the landslide susceptibility analysis and the prepared landslide prediction map have been verified by using the test subset of landslides for the same study areas. Test subset includes unconsidered landslide locations (20% of all) and some newly mapped landslides through image interpretation and ground truth observations with the help of the Global Positioning System (GPS) (Figure 4.6). Intersections between the prediction images and total landslide locations allowed for the computation of the number of occurred landslides in each LSI value. The method could determine the performance of the output information. Overall, the approach has positively improved the method of landslide evaluation for susceptibility mapping by utilizing the LiDAR-derived DEM and PFR model (see Table 4.5). However, the effectiveness of DEMs has not been studied to identify whether the LiDAR-derived DEM (5m) compared to DEMs with lower resolution might possibly achieve the improved landslide susceptibility or not (Safaiee et al. 2010; Rajabi et al. 2011; Jebur et al. 2014).

Figure 4.6: Field observations and newly mapped landslides.

Nevertheless, a far less conventional procedure in conjunction with technologies such as LiDAR high resolution data and PFR method results in a much more satisfying outcome for all

concerned. The calculated index values of cells were sorted in descending order to obtain the success rate of the curve. This study divided the ordered cell values into one hundred classes and accumulated 1% intervals to present the percentage of landslides in the study area. Also, some landslide occurrences in each index value are represented as a percentage of total landslides cumulatively. Effect analysis studies associated with the high resolution of DEM and landslide influential factors have possibly indicated how a solution could change when the input factors are changed. In this study, the effect analyses were conducted by the exclusion of each factor in turn during the summation stage using Eq. (4.1). However, the effect of each contributing factor evaluated the related success rate by using the area under the curve calculation.

4.3 Results and Discussion

4.3.1 PFR Model and Factors Analysis

LiDAR-derived DEMs and ASTER DEM were used to identify new landslides from an existing inventory dataset in conjunction with field observations. The high resolution of LiDAR-derived DEM exhibits better performance in identifying new landslides in comparison to ASTER DEM. As well, implementing the PFR model from LiDAR DEM demonstrates acceptance precision and quality of susceptibility mapping. The study shows that geology plays a major role in controlling factors for landslides in Central Alborz, since the geology of this area is very complex. Lithologically, the study area is comprised of several formations as depicted in Table 4.2. The FR calculations (Table 4.3) indicate that the highest FR values are the most susceptible groups for landslide occurrences. The calculation of FR is belong to areas with some geological layer outcrops such as Q_1, K_{11}, P_n, K_{M2}, and K_{1M2} (FR: 39.5, 9.0, 3.3, 1.5, and 1.5, respectively).

These groups primarily include marl, marl limestone, limestone, shale associated with old landslides, and rock stream traces which are mostly fissile, soluble, and easily weathered

materials. The lowest FR values (FR=0) belong to geological groups including J_1, TR_3J_s, P_d, E_d, E1, O_1, P_{1q}, and PE_e. FR values show a very low correlation with landslide occurrence (Table 4.3). Thus, we predict a very low susceptibility of landslide occurrence in these classes. The strata mostly contain dolomite, cherty dolomite sandstone, siltstone, and quartzite. These strata were identified as being among the resistance and hard fracturing litho units in the study area.

Table 4.2: Different formations and litho-units in the study area.

Era	Period	Formation	Code	Lithology	Area covered (KM^2)	%
Paleozoic	Up-Pre. Cambrian	KAHAR	PE_K	Salty shale, sandstone, minor dolomite, quartzite	148.33	14.64
	Cambrian	SOLTANIEH	PEe	Thick bedded to massive light-coloured dolomite, locally with chert bands	53.64	5.30
		BARUT	E_b	Micaceous variegated siltstone and shale, cherty dolomite intercalations	8.8	0.87
		LALUN	E_1	Red arkosic sandstone	19.77	1.95
	Ordovician	MILA	O_1	Sandstone, shale, limestone, marl phosphatic layers	2.08	0.21
	Carboniferous	MOBARAKL	C_M	Black limestone, dolomitic limestone, marl intercalations	80.38	7.94
	Permian	DORUD	P_d	Sandstone, shale, limestone intercalations, quartzite, siltstone	26.93	2.66
			P_V	Basic flows, pyroclastics, sandstone	0.99	0.10
		RUTEH	P_r	Fusulina limestone, dolomitic limestone	43.97	4.34
		NESEN	P_n	Cherty limestone, marly limestone, marl and sandy shale	3.88	0.38
Mesozoic	Triassic	ELIKA	TR_{em}	Thin-bedded limestone, calcareous shale, quartzitic sandstone	2.77	0.27
			TR_{dc}	Massive dolomite	36.04	3.56
	Jurassic	SHEMSHAK	TR_3J_S	Shale, sandstone, siltstone, claystone, quartzite, conglomerate, local limestone intercalations: coal seams and lenses	179.45	15.28

		LAR	J_1	Limestone, local dolomitic limestone	8.35	0.82
	Cretaceous	TIZ_KUH	K_1	Orbitolina limestone (Apian - Cenomanian)	31.09	3.06
		CHALUS	K_{11}	Limestone (Berriasian - Valanginian)	2.04	0.20
			K_{v21}	Alkali basalt, spilitic basalt conglomerate, tuff braccia, tuff	71.05	6.07
			K_{V22}	Trachyandesitic basalt, tuff breccia, pyroclastics, tuffite	41.58	4.10
			K_{12}	Globotruncana limestone, marl limestone	69.77	6.89
			K_{M2}	Marl, calcareous marl, marly limestone	51.11	5.05
			K_{1M2}	Alternations of limestone and marl	33.06	3.26
Cenozoic	Tertiary		P1Q	Conglomerate, sandstone, siltstone, siltymarl	28.28	2.74
	Quaternary		Q	Undifferentiated young and old alluvial fans, traces, colluvium, residual soils, fill valley sediments lake deposits	90.81	8.90
			Q1	Landslide and rock stream	11.48	1.13
			river and lake	Water body, terraces, colluvium, residual soil	2.80	0.27
			total		1048.45	100.00

Table 4.3: Frequency Ratio (FR) of factors to landslide occurrence.

Factor	Class	Total number of pixels		Landslide occurrence pixels		Frequency ratio
		Number[a]	%	Number[b]	%	
Soil	Weathered	85091	0.84	0	0.00	0.00
	Medium soil from alluvial	804145	7.94	0	0.00	0.00
	Thin soil over rock	658226	6.50	15979	7.80	1.20
	Medium soil over rock	2185002	21.57	80	0.04	0.00
	Medium soil over colluvial	1746851	17.24	60913	29.72	1.72
	Deep soil from alluvial	111793	10.32	5300	2.59	2.34
	Fine alluvial soils	1045712	3.45	45430	22.17	2.15
	Thin sandy soils	349206	31.04	1939	0.95	0.27

Factor	Class	Total number of pixels		Landslide occurrence pixels		Class
		Number[a]	%	Number[b]	%	
	Rocks	3145180	1.10	75275	36.73	1.18
Distance from drainage (m)	100	4424123	43.67	76569	37.36	0.86
	200	2464779	24.33	59288	28.93	1.19
	400	2222416	21.94	53917	26.31	1.20
	800	987245	9.75	15042	7.34	0.75
	>800	40237	0.40	100	0.05	0.12
Slope (degree)	0-5	490045	4.83	3442	1.68	0.35
	5-10	669427	6.60	12333	6.02	0.91
	10-20	2746384	27.09	67408	32.89	1.21
	20-30	3200304	31.56	67151	32.77	1.05
	30-40	2530305	24.96	47358	23.11	0.94
	40-50	453592	4.47	6937	3.38	0.76
	>50	48743	0.48	310	0.15	0.31
Lithology	TRem	27679	0.27	785	0.36	1.33
	PEE	536418	5.30	2	0.00	0.00
	Pn	38776	0.38	2735	1.27	3.31
	Pr	439706	4.34	5295	2.45	0.56
	PV	9875	0.10	39	0.02	0.19
	Q	901467	8.90	10859	5.02	0.56
	Q1	114961	1.13	96880	44.81	39.49
	TR3JS	1547999	15.28	654	0.30	0.02
	K1M2	330740	3.26	10652	4.93	1.51
	KM2	511173	5.05	16768	7.76	1.54
	KV22	415791	4.10	12040	5.57	1.36
	P1Q	277810	2.74	0	0.00	0.00
	Pd	269380	2.66	42	0.02	0.01
	TRdc	360447	3.56	764	0.35	0.10
	CM	804135	7.94	11461	5.30	0.67
	O1	20800	0.21	0	0.00	0.00
Lithology	E1	197786	1.95	0	0.00	0.00
	Eb	87995	0.87	1	0.00	0.00
	PEK	1483288	14.64	6760	3.13	0.21
	J1	83479	0.82	147	0.07	0.08
	K1	309512	3.06	1364	0.63	0.21
	K11	20444	0.20	3925	1.82	9.00
	K12	697915	6.89	10374	4.80	0.70
	kv21	614502	6.07	13330	6.17	1.02
	river	25575	0.25	0	0.00	0.00
	lake	2424	0.02	64	0.03	1.24
Land use	Agricultural land	1467497	14.49	78969	38.53	2.66
	Settlement	407629	4.02	9869	4.82	1.20
	Open Vegetation	2914371	28.77	49777	24.29	0.84

	Lake	2101	0.02	163	0.08	3.84
	Grassland	1395207	13.77	36045	17.59	1.28
	Dense vegetation	3385573	33.42	30078	14.68	0.44
	Bad land	558122	5.51	38	0.02	0.00
Distance from road(m)	50	226534	2.23	15779	7.70	3.45
	100	223772	2.21	14477	7.06	3.20
	200	428101	4.22	20930	10.21	2.42
	400	784725	7.74	30603	14.93	1.93
	800	1344647	13.26	31178	15.21	1.15
	>800	7131021	70.33	91972	44.88	0.64
Geomorphology	Debris land	255864	2.53	15629	7.23	2.86
	Deep valley	670098	6.61	45181	20.90	3.16
	Limestone Relief	1373183	13.56	3040	1.41	0.10
	Moderate Relief	2238436	22.10	58355	26.99	1.22
	Alluvial Fan	263711	2.60	0	0.00	0.00
	Alluvial Plain	385201	3.80	0	0.00	0.00
	Alluvial Terrace	311277	3.07	10000	4.63	1.51
	Volcano Relief	4632287	45.73	72711	33.64	0.74

a: Total number of pixels in the study area: 10,138,800 pixels.

b: Total number of landslide occurrence pixels: 204,939 pixels (Estimation group).

The land use map has indicated that the most hazardous classes are in the lake area (coastal landslides), agricultural lands, and grasslands (FR value 3.8, 2.6, and 1.3, respectively). This is due to geological characteristics (K_{1M2} and Q_1) and water influences in the coastal area. Thus, higher FR values are expected in these areas in comparison to that of other locations. In the study area, the results pertaining to the agricultural lands are controversial bbecause the land use and land cover situation of Marzan Abad area at the time of failure is unknown. Moreover, it is not possible to know whether the presence of agricultural lands was a cause of failure or consequence. In fact, it is possible that the changes in steepness are due to the evolution of the scarps that may have favoured agricultural lands. This study shows that deep soils from alluvial and fine alluvial soils are the most susceptible groups for landslide occurrence with FR>2. Geomorphologically, deep valleys and debris lands are the most susceptible classes with FR>2. Unexpectedly, alluvial fan and alluvial plain areas have the lowest susceptibility of landslide occurrence with FR=0.

The relationships between landslide occurrences and slope show that gentle slopes have a low frequency of landslides because they have a lower shear stress. This study found that at a slope of 10° or less, the frequency ratio is below 1. This result indicates a low probability of landslide occurrence. However, slopes above 11° have a ratio of >1. This result shows a higher likelihood of landslide occurrence. The areas with slope steepness of more than 40° covering less than 4% of the area are mostly covered by bedrocks (i.e. volcanic rocks). However, this part of the study area with slope steepness of more than 40° has a lower probability of landslide.

This study revealed that road networks have a strong relationship with landslide occurrence because of cut-slope creations through road construction. It was found that the closer the distance to the road, the greater the chance of a landslide occurring. Areas with a distance of <100m from the road are the most susceptible class with FR>3, and areas with a distance of >800m from the road network show a minor relationship with landslide occurrence (FR<1).

4.3.2 Landslide Susceptibility Map

Landslide Susceptibility Index (LSI) calculation shows that the LSI has a minimum range value of susceptibility class of 2.3, a maximum range value of susceptibility class of 55.7, an average value of 6.95, and a standard deviation of 5.02 (Table 4.4). This study prepared the geospatial distribution of the updated landslide inventory dataset which is illustrated on the Landsat TM. This revised and updated inventory dataset includes recent landslides, minor-medium and human casualty landslides (Figure 4.7). The final landslide susceptibility map in five susceptibility prediction class is based on the LSI values (Figure 4.8).

Figure 4.9 shows that the evaluated success rate curve is very steep in the first part of the curve. This indicates an excellent predictive capability. This study found that more than 50% of the landslides are located in 3% of the area where the landslide hazards index has a higher rank.

79

Approximately 22% of the study area has been predicted to be the most hazardous, and it was found that 90% of landslides are in these regions.

Table 4.4: Statistics of the LSI value for all classes.

	Min. value	Max. value	Mean value	Std.	AUC ratio
Except drainage	1.50	53.87	5.95	5.01	0.92
Except soil	1.80	53.34	5.95	4.85	0.91
Except slope	1.52	53.86	5.95	5.01	0.92
Except road	1.66	52.05	5.95	4.87	0.90
Except land use	1.85	52.41	5.95	4.83	0.92
Except geology	2.21	13.83	5.95	1.93	0.78
Except geomorphology	1.56	51.91	6.0	4.81	0.92
Total factors	**2.30**	**55.07**	**6.95**	**5.02**	**0.92**

The area under the curve (AUC) (Figure 4.10) assesses the prediction accuracy, and the total area=1 denotes a perfect prediction. In this study area, the ratio is approximately 0.926. The study indicates 92.6% agreement between the prepared hazards map and landslide locations from the existing landslide inventory geospatial distribution map and the field observations. Based on this promising result, the quality of the landslide susceptibility and hazards prediction mapping was improved by using the LiDAR-derived high resolution DEM associated with the PFR model (Table 4.5) compared to logistic regression, fuzzy, and AHP methods (Chen et al. ,2014; Guns and Vanacker, 2012;Gholami et al., 2017; Rui et al. 2017).

The ROC curve method was used to validate the accuracy of the PFR model (Deng et al. 2017; Wen et al., 2017; Kreyszig et al., 2011). The validation of the results proves the relationship between the susceptibility map and the landslide location data, as the prediction accuracy is 91.45%. Furthermore, the result showed a satisfactory prediction rate of 92.6% in comparison to the existing landslide location data in this study.
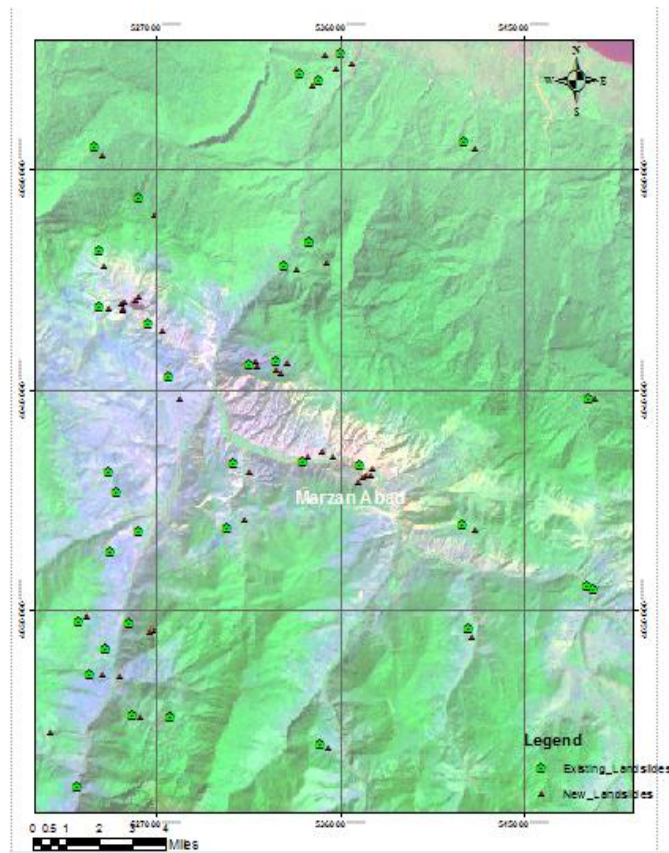
Figure 4.7: Geospatial distribution of landslides inventory.
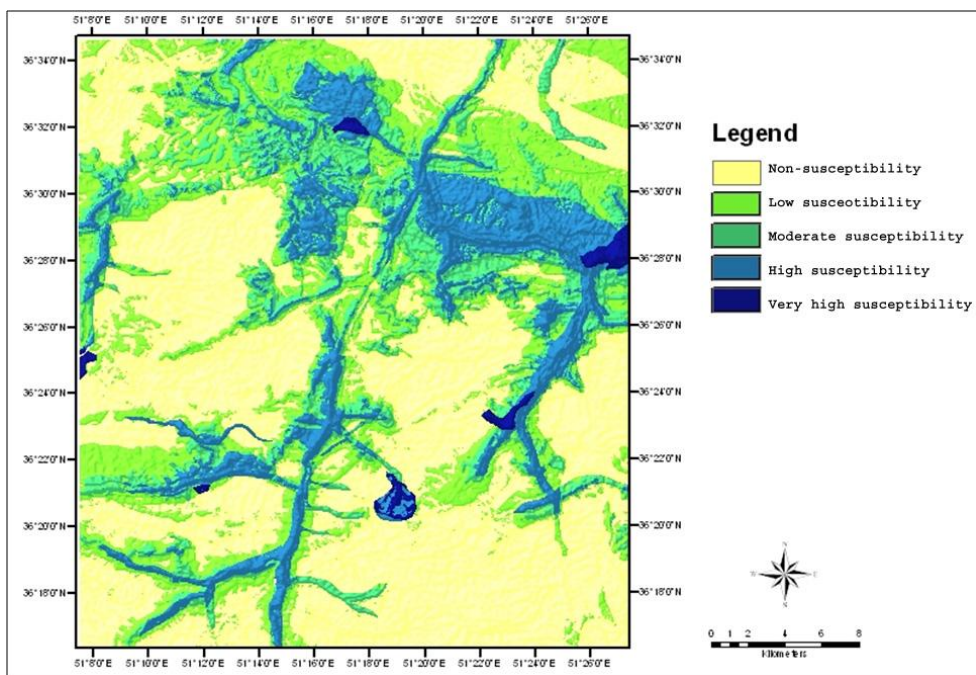
Figure 4.8: Landslide susceptibility map of Marzan Abad area, Central Alborz Mountains.
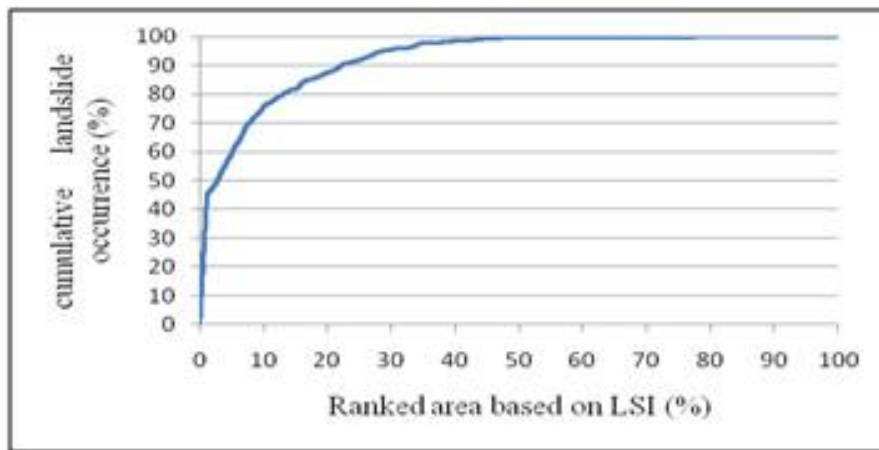
Figure 4.9: Success rate of the curve.
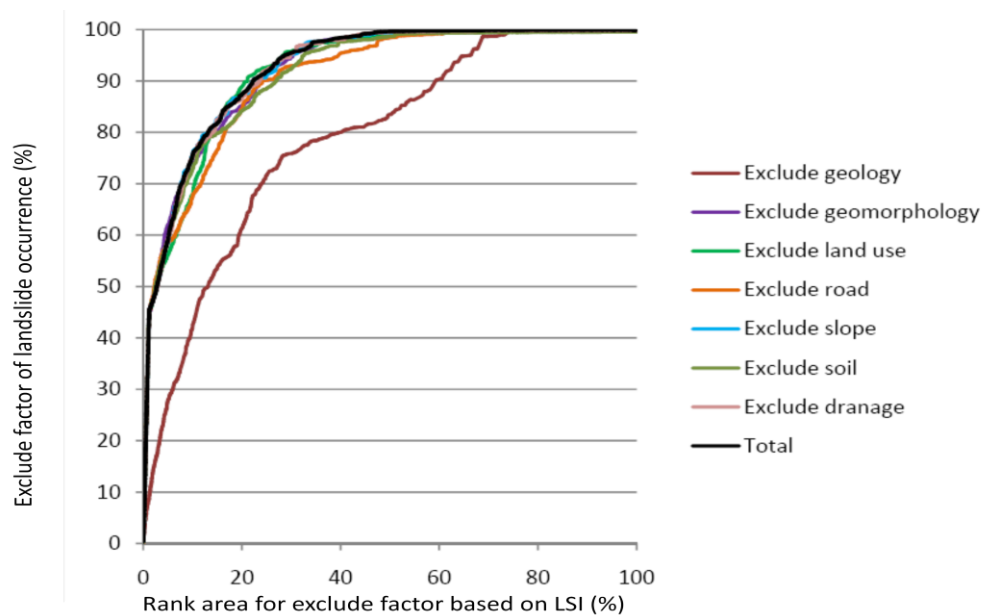
Figure 4.10: Prepared success rates by the exclusion of each factor's values.

Figure 4.10 shows seven success rates prepared by the exclusion of each factor's values from the original susceptibility map. Also, Table 4.4 depicts the statistics of the LSI value for all cases.

This study reveals that by using the effect analysis, we can qualitatively know the influence of factors on the landslide susceptibility map. However, the selection of positive factors associated with the PFR and possibly a high-resolution DEM and its derivatives can

improve the prediction accuracy of the landslide susceptibility map. Table 4.4 shows that the geology of the area is the most important and effective factor of landslide analysis (AUC ratio=0.79) in the Marzan Abad area. In addition to geology, the roads network (AUC ratio=0.91) and soil (AUC ratio=0.92) are influential factors related to the evaluation of landslide susceptibility mapping. Aside from the factors mentioned above, all other effective factors show a relatively small positive effect on landslide analysis (AUC ratio<0.93). It can be concluded that all selected factors exert some positive influence on landslide hazard analysis and improved landslide prediction.

4.4 Conclusions and Suggestion

The results of this study could motivate the Iranian Government to capture the LiDAR point cloud data for development of big data and geodata analytics for the landslide inventory of Iran. This study concluded that probably the LiDAR-derived DEM impacts the PFR model outcomes and increases the precision and quality of susceptibility hazards mapping in comparison to the DEM with lower resolution used in previous research than 5m used (Figure 4.11, Table 4.5) (Guns and Vanacker 2012; Chen et al. 2014; Rui et al. 2017). As an advanced technique, LiDAR could provide a good set of three-dimensional data with x, y, and z axis of Marzan Abad area. The PFR model applies the high-resolution DEM, and its derivatives such as slope have provided an improved quality of outcomes of landslide susceptibility mapping in conjunction with the ASTER DEM and Google Earth images. This study provides detailed colour, geologic, and geomorphic information using LiDAR data to generate an improved quality of DEM's derivatives to assess and predict landslides.

Table 4.5: Comparative models for percentage accuracy.

Author/Year	DEM Res (m)	AHP Accuracy (AUC)%	LIM Accuracy (AUC) %	Fuzzy Accuracy (AUC) %	LR Accuracy (AUC) %	ANN Accuracy (AUC) %	PFR Accuracy (AUC) %
Gholami et al. (2017)	20	N/A	73.61	81.08	N/A	N/A	82.04
Rui et al. (2017)	30	N/A	N/A	N/A	83	85.9%	N/A
Pirasteh et al. (2017)	5	N/A	N/A	N/A	N/A	N/A	**92.59**
Chen et al. (2014)	30	**75.97**	N/A	N/A	N/A	N/A	N/A
Guns and Vanacker (2012)	20	N/A	N/A	N/A	81.1	N/A	N/A

ANN-Artificial Neural Network.
LR-Logistic Regressions.
AHP- Analytic Hierarchy Process.
LIM-Landslide Index Model.
PFR-Probabilistic Frequency Ratio.

This study concludes that movements and landslide predisposing factors such as topography are similar to those that have been verified by landslides in the past. This study constructs acceptable relationships between improved landslide inventory spatial distribution and influential factors for landslide susceptibility mapping by utilizing PFR model and LiDAR approach to extract a high-resolution DEM. The PFR was applied to study the influence of different earth surface factors upon landslide occurrence and to evaluate the landslide susceptibility of hazards prediction. This model is advantageous in its simplicity; moreover, inputs, outputs, and calculation processes are understandable. Also, a large amount of data can be quickly and easily processed in the GIS environment. Based on qualitative studies, influential factors on the landslide susceptibility map were evaluated to select positive factors and to improve the prediction accuracy of the landslide susceptibility map. Thus, the selection of factors is significant to landslide susceptibility mapping. This study emphasizes that the most significant causative factors for landslide susceptibility are geology, soil, and road networks. Additionally, this study identified that other factors such as lithology and land use have positive influences on

landslide susceptibility analysis.
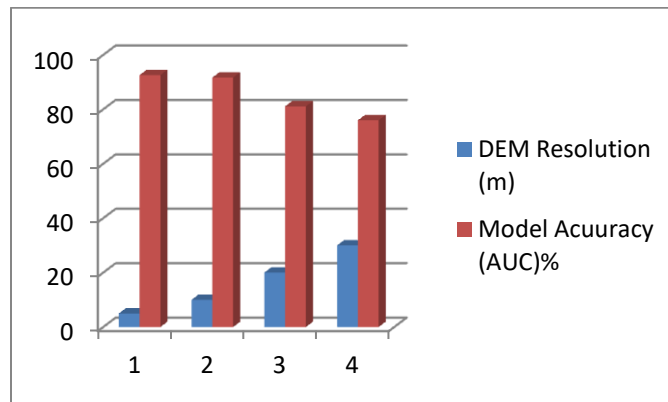
Figure 4.11: Model accuracy vs. DEM resolution. Comparison of the previous research used DEMs with the accuracy of the model given in the table 4.5.

Nevertheless, this study concludes that the most sensitive classes of landslides in the Central Alborz are: (a) Quaternary deposits, (b) Chalus Formation, and (c) Nesen Formation. In addition, this study confirmed that areas located less than 100m from the roads with more than 10° slope have potential for landslides. The results of this study are valuable to decision-makers because the most landslide-susceptible areas are in deep alluvial soils, deep valleys, debris lands, and areas near water. This study prepared an improved landslide susceptibility and hazards prediction map which shows recent landslides. This map may be used by decision-makers for future operations. As well, the information provided by this map can help citizens, planners, and engineers for loss reduction caused by existing and future landslides. Because high tectonic activities and earthquakes can trigger landslides, this study suggests that factors such as tectonic activities, seismicity, and vulnerability of buildings be considered for evaluating the PFR model when researchers use LiDAR point cloud data and satellite images.

4.5 Chapter Summary

This chapter identified potential susceptible areas for landslides in Marzan Abad, Central Alborz Iran. This study has improved the quality of landslide evaluation by using high-resolution DEM

to identify new landslides in the study areas. LiDAR remote sensing data are useful for landslide investigations, particularly in conjunction with high-resolution DEM. This study estimated the operational use of the LiDAR technology associated with geoanalytical approaches for landslide investigation and susceptibility mapping.

This study delivered an integration method of LiDAR data associated with the ASTER DEM and Google Earth images by applying the PFR model to evaluate landslide analysis, and to increase the quality of susceptibility mapping in Alborz Mountains.

Chapter 5

An Approach of Semi-Automated Geometric Analysis and Classification of Landslides Incorporating LiDAR-derived DEMs

This chapter presents a method of utilizing LiDAR-derived digital elevation model (DEM) to update the existing inventory landslide database for the Alborz Mountains, Iran. The method consists of the automated derivation of landslide geometry (length, width, and area) followed by classification of landslide types. The Trapezoidal Rule for Numerical Integration (TRNI) was first implemented through coding in MATLAB. The landslides were then classified into four types (very long, long, very wide, and wide) based on slope, length, and width. A total of 95 landslides were updated from the existing inventory database. The proposed method was verified and evaluated by field observations and fourteen samples tested in conjunction with ArcGIS using the relative error method (Kreyszig et al., 2011). The results demonstrate that the mean percentage relative error is 0.496% in length and width and 0.008% in area, respectively, as compared to that from ArcGIS.

5.1 Introduction

Landslides, a natural hazards phenomenon, are common deformation scenarios on the Earth's surface. This geomorphic process is significant in developing the geometry of landslides and can be used to determine landslide typology (Hattanji and Moriwaki, 2009; Niculiță, 2016). Characterization of topography and morphology and classification of landslides requires knowledge of not only geologic and geomorphic processes, but also technologies such as

LiDAR. In the last two decades, researchers have applied the high-resolution DEM derived from LiDAR point clouds to improve landslide delineation (Ali et al., 2003b; Su and Bork, 2006; Ardizzone et al., 2007; Teza et al., 2007; Travelletti et al., 2008; Jaboyedoff et al., 2012; Pirasteh et al., 2017). LiDAR-derived DEMs allow for the detailed exploration of morphology and geometry of landslides that could possibly be used for updating of landslide inventory (McKean and Roering, 2003; Schulz, 2007).

Landslide inventory contains a collection of polygon shapes, types, lengths, widths, areas, locations, and other information related to landslides. With such information, landslides can be represented digitally in the GIS environment either manually of semi-automatically (Freeman, 1991; Ali et al., 2003a; Malamud et al., 2004; Martha et al., 2010; Lyons et al., 2014). Landslide inventory and spatial analysis have played a significant role for decision-makers in preparing a loss-reduction plan as well as in establishing an early warning system. However, few studies have focused on the development of semi-automated algorithms for geometry characterization and landslide classification (Ardizzone et al., 2002; Malamud et al., 2004; Mondini et al., 2011; Lyons et al., 2014; Niculiţă, 2016). Characterization of landslide geometry depends upon various factors. For this reason, classification of landslides has been based on different discriminating factors and is therefore at times very subjective (Varnes, 1978; Hutchinson, 1988; Cruden and Varnes, 1996; Dikau et al., 1996). However, some researchers have abstracted the shapes of the landslide to a rectangle to define the long side (i.e. length) and short side (width), instead of the factual shape of a landslide. The length of a landslide is defined as the length of the line from the crest to the end of the toe in the failure direction of a landslide area. The landslides are then classified based as either a long or a wide type upon the geometry (length and width) of the defined rectangle that covers the landslide (Niculiţă, 2016). Moreover, most researchers have considered the failure direction as the length of a landslide with respect to engineering geology

and have dealt with vector system, three-dimension, and dynamic system. Therefore, the failure

direction is defining the length of a landslide. Although Taylor and Malamud (2012) assumed

that all landslide shapes can be abstracted to a rectangle to define the long side (i.e. length [L])

and short side (width [W]) (Figure 5.1), previous researchers developed semi- semi-automated

tools (Ardizzone et al., 2002; Malamud et al., 2004; Mondini et al., 2011; Lyons et al., 2014;

Niculitˇa, 2016) to measure the length and width of landslide polygons.
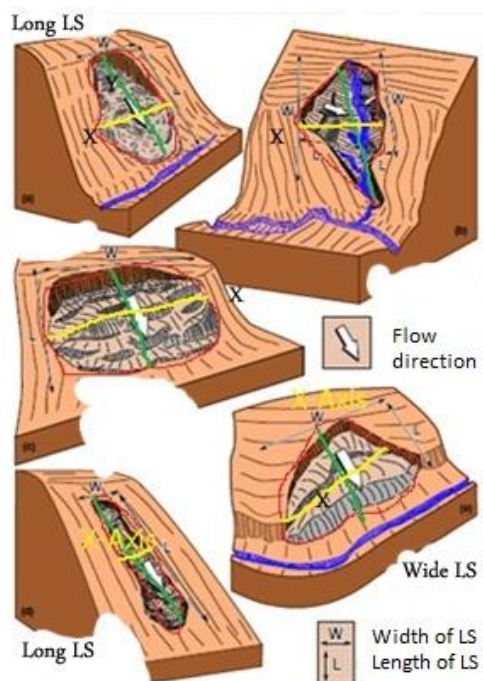
Figure 5.1: Schematic drawings of long and wide cases of landslides with X-Axis and Y-Axis:

(a) Rotational slide – long type, (b) Gully bank slides – long type, (c) Translational slide –

wide type, (d) Flow – long type, and (e) River bank slide – wide type. (Source: Niculitˇa,

2016).

In contrast, this study uses the Numerical Integral Trapezoidal Rule (NITR) (Burden and

Faires, 2011) to develop an algorithm for semi-automated landslide geometric analysis and

classification. The proposed approach includes determination and measurement of the length,

width, and area; as well as the identification of the landslide type. The 2D scalar system for

characterization of the landslide geometry is applied regardless of the failure direction, type of materials, and speed of movement and type of materials.

This chapter presents the proposed approach to semi-automated landslide detection through determining the length, width, area, and type of landslide in a 2D, scalar, and static-based polygon covering the factual shape of the landslide. The approach is utilized to update the landslide inventory in the Alborz Mountains, Iran, where typical geomorphologic features and various shapes of landslides exist. The 2D scalar static system is based on the projected geographic coordinates system for representing the slope angle, length, and width of landslide polygons. The slope angle, which is the angle of the segment with respect to X-axis, is not a topographic slope. The LiDAR-derived DEMs along with field observations and remotely-sensed images are used to support on screen manual digitization of landslide polygon in GIS environment and to update the landslide inventory.

5.2 Data Process and Method

The landslide inventory archives of the Alborz Mountains, Mazandaran Province (Figure 5.2) and Google Earth images (dated in December of 2009, 2010, 2011, 2012, 2013, 2014, 2015, and 2016) were used together with the 5 m resolution LiDAR-derived DEMs. The Real Time Kinematic (RTK) Global Positioning System (GPS) SmartNet was also used during field observations to enable digital drawing of landslide polygons in ArcGIS using ArcBruTile tool. There are complex landslides and a single event in the inventory database of the study area. This landslide inventory contains 173 points and polygons representing landslides small to large in length, width, and area. To update the landslide inventory and to test the performance of the proposed algorithm, 20 cm resolution unmanned aerial vehicle (UAV) images covering the Chalus District in the study area were also used and; integrated with the airborne LiDAR point

clouds with point spacing of 20 cm (Figure 5.3) in order to support on screen manual digitization of landslide polygon in GIS environment. A total of 95 landslides were selected from the landslide inventory database to convert points into polygons based on screen manual digitization of the landslide polygon in GIS environment by using visual image interpretation techniques of high-resolution of UAV, Google Earth images as well as LiDAR-derived DEM; fourteen samples were used to test the proposed algorithm.
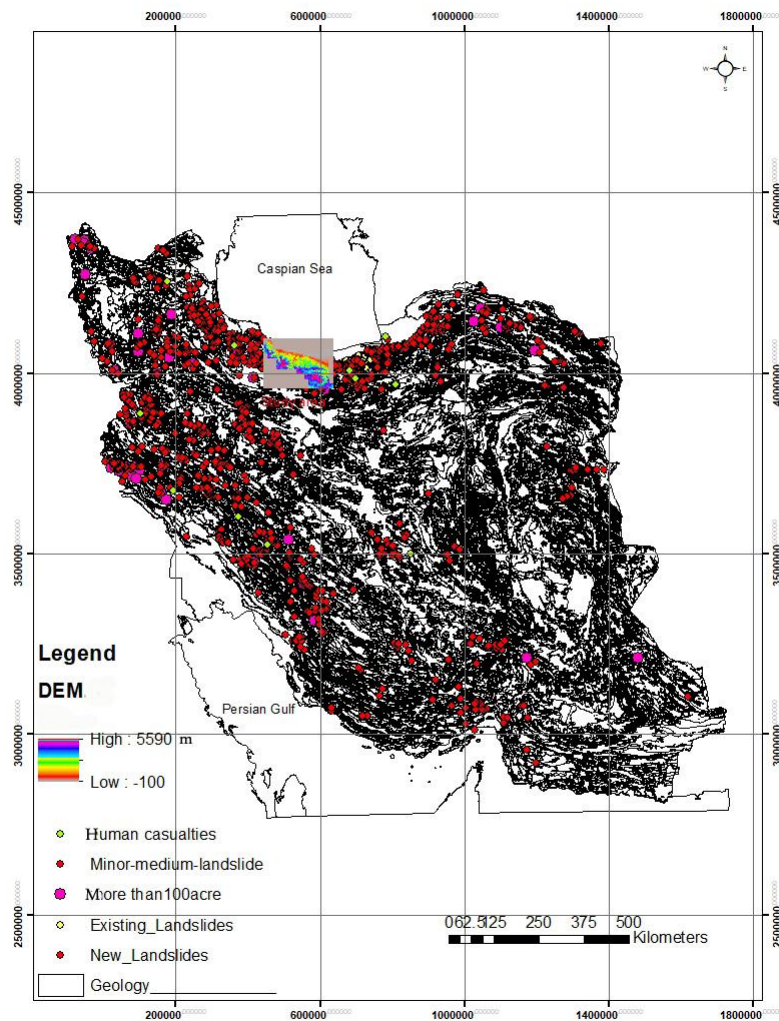
Figure 5.2: Landslide inventory of geographical distribution in Iran.

91
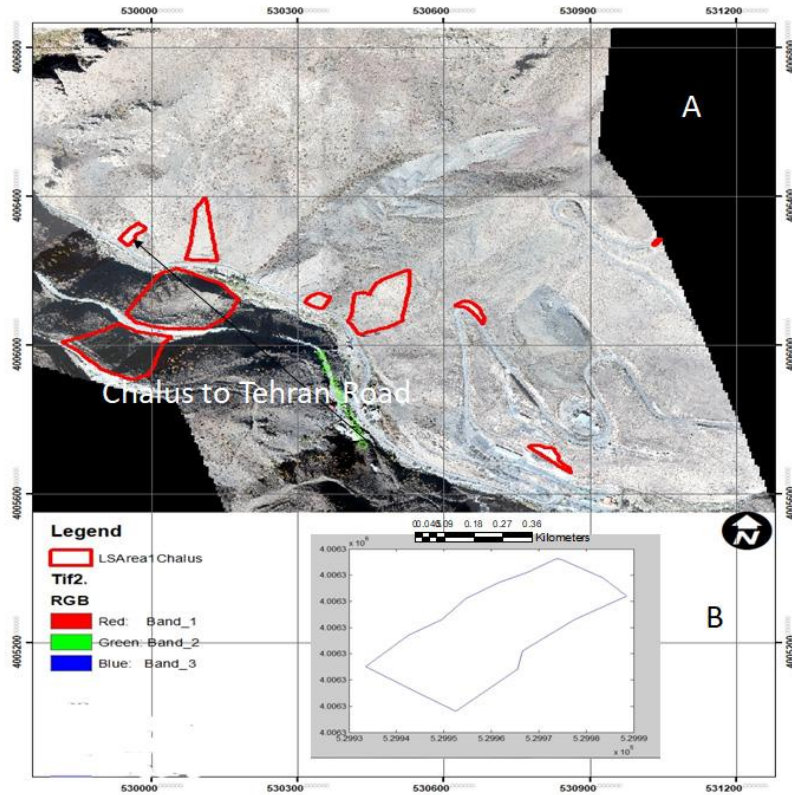
Figure 5.3: a) Landslide polygons and UAV images, b) Selected landslide polygon in the proposed software package. Location: Chalus District.

Materials move towards downslope, and the distance of the mass displacement in a landslide is greater than the width of the displaced material. This occurs especially for flows, but also for the majority of slides, and it means that the length is greater than the width (L>W) (Figure 5.1). In some landslides, this phenomenon does not happen and we might have a smaller length than width (L<W). In the proposed method, the maximum distance of two points (i.e., the longest segment) in either X-axis or Y-axis in the 2D scalar system is taken into account to discern the length and width of a landslide and to define the landslide type. The following section details the proposed methodology.

In engineering geology, the length of a landslide is defined as the length of the line from the crest to the end of the toe in the failure direction of a landslide area. However, the proposed

92

approach assumes that a landslide polygon can be represented in a 2D static scalar system, instead of considering the failure direction as the length of the landslide to be represented in a 3D dynamic vector system. As such, landslide length, width, area, and type can be applied for determining the landslide geometry regardless of the failure direction, speed of materials movement, type of materials, and type of materials movement.

5.2.1 Numerical Integral Trapezoidal Rule

In this study, the trapezoidal rule was used to analyze landslide geometry and to classify landslides. The trapezoidal rule is a numerical analysis method that has been applied to approximate the value of a definite integral (Burden and Faires, 2011). The integral is approximated by using n trapezoids formed by straight line segments between the points $(x_i - 1, y_i - 1)$ and (x_i, y_i), for $1 \leq i \leq$ n, as shown in Figure 5.4. Each trapezoid in a landslide polygon is calculated by:

$$\int_a^b f(x)\, dx \approx \frac{\Delta x}{2}(y_0 + 2y_1 + 2y_2 + \cdots + 2y_{n-1} + y_n) \qquad (5.1)$$
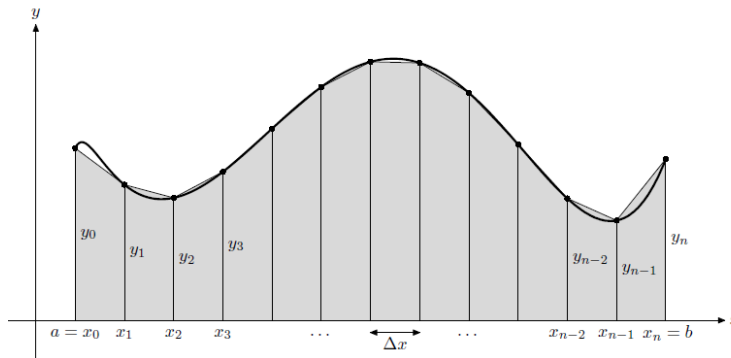
Figure 5.4: Each trapezoid is shown in a landslide polygon.

The numerical integral trapezoidal rule (NITR) method was coded by matrix-based MATLAB language in several lines to run the computational process of a landslide and to determine the length, width, area, and type of landslide. The script code is available at www.widm.ca upon request.

In this study, RTK SmartNet with 14-20 cm accuracy was used in ground truthing to collect ground control points (GCPs) for simulating landslide polygons. Then the polygons were created both in ArcGIS by using the measurement tools (Figure 5.5) and in the proposed software to calculate the length, width, and area and to identify the landslide of the polygons. This study used ArcGIS 10.4 version to determine the boundary' points of a landslide polygon by moving curser manually on the screen visualization to identify the coordinates of each point on the polygon. The coordinates of each selected point was recorded in Excel that is to be used further in the proposed algorithm and MATLAB software. Later, the points in Excel with geographical coordinate system (x,y) were introduced to ArcGIS and the proposed software to draw the polygon and to calculate the geometry of the polygon.

The proposed algorithm was tested and verified by ArcGIS and field observations. However, ArcGIS and other software package are possibly not available to determine the length and width of a landslide automatically, and to classify landslide types automatically as well. In contrast, the proposed software package performs these functions automatically. The following figure describes the procedures of automated computation of the landslide geometry and classification.
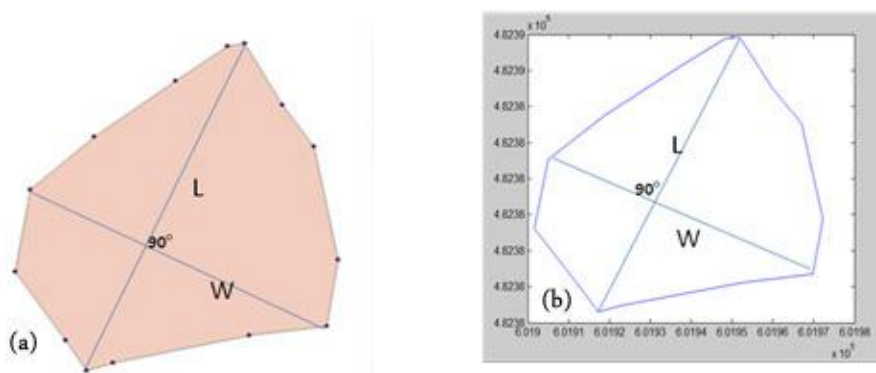
Figure 5.5: (a) A polygon in ArcGIS. (b) The same polygon in the proposed software package.

94

5.2.2 Geometric Analysis and Rules of Classification

In the Alborz Mountains, variable shapes of landslides cause uncertainty in determining the length, width, area, and landslide type of a polygon. Instead of using the existing methods, this study develops semi-automated computing approach to landslide geometry by taking advantage of LiDAR-derived DEMs, Google Earth images, and UAV images for analyzing available landslides in the study area. The boundary of a landslide was determined by visual on screen digitization on the Google Earth and UAV images using image element techniques that are supported by field observations and inventory data.

In order to perform the semi-automated calculation of segments in landslide polygons in this study, the rectangular coordinate system has the X-axis coincide with the east-west direction and the Y-axis coincide with the north-south direction, in which the x-coordinates are referred to as latitude/northing and the y-coordinates are referred to as longitude/easting in the UTM with unit of meters (see Figure 5.6). Polygons were converted to points in ArcGIS to measure the length and width. These points were then introduced to the proposed software as attributing data in a table containing x- and y-coordinates. The following steps describe the procedure of computing length, width, and area by the proposed algorithm.

Step 1: To determine the X_{max} (A) and X_{min} (B) as well as Y_{max} (C) and Y_{min} (D) (Figure 5.6) in scalar system. Points $A(X_{max}, Y_{Xmax})$, $B(X_{min}, Y_{Xmin})$, $C(X_{Ymax}, Y_{max})$, and $D(X_{Ymin}, Y_{min})$ are in the geographical coordinates system. The segment between points A and B is "d_1" and the segment between points C and D is "d_2". The d_1 is always in the favour of the X-axis and is considered to be x-coordinate or Latitude/Northing (m).

Step 2: To calculate $AB(d_1)$ and CD (d_2) using the following equations:

$$AB = d_1 = \sqrt{(X_{max} - X_{min})^2 + (Y_{Xmax} - Y_{Xmin})^2} \qquad (5.2)$$

$$CD=d_2=\sqrt{(X_{Ymax}-X_{Ymin})^2+(Y_{max}-Y_{min})^2} \quad (5.3)$$

Step 3: To compare d_1 *and* d_2 and to determine which landslides are classified into long types or wide types. The following section describes the next step and explains how this study classifies landslides based on the geometric features.
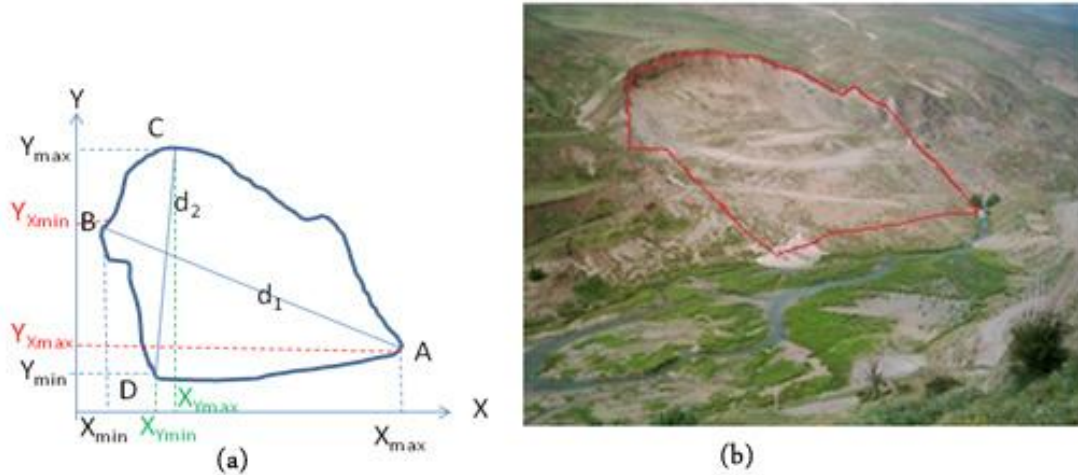
Figure 5.6: (a) A landslide polygon in the x-y coordinate system. (b) Photo taken during the field observation in the study area.

Furthermore, the semi-automated classification of landslides was carried out in this study. Landslides were classified upon the d_1 and d_2 values with respect to the x- and y-coordinates as well as the slope angle (θ). Geometrically, the maximum distance between the two points can define the type of landslide aligning along either the X-axis or the Y-axis. If d_1 is larger than d_2, then the landslide polygon will be classified as the wide type and d_1 will be the "length" of the landslide polygon. If d_1 is smaller than d_2, then the landslide polygon will be classified as the long type. Figure 5.7 depicts the conceptual flowchart of the proposed landslide classification algorithm. This algorithm calculates both the maximum and minimum x-coordinates and y-coordinates of the landslide polygon. The *maximum segment distance* along the X-axis is

96

determined the long side of the polygon, while the *maximum segment distance* along the Y-axis is determined the short side of the polygon. The algorithm also compares these two distances. In other words, the algorithm computes the maximum and minimum Latitude/Northing (m) coordinates of points (x,y) from the landslide polygon in favour of the X-axis to estimate the "*maximum horizontal segment distance*". It also computes the maximum and minimum Longitude/Easting (m) coordinates of points coinciding with the Y-axis from the landslide polygon to estimate the "*maximum vertical segment distance*". The algorithm compares the maximum horizontal and vertical segments distance.
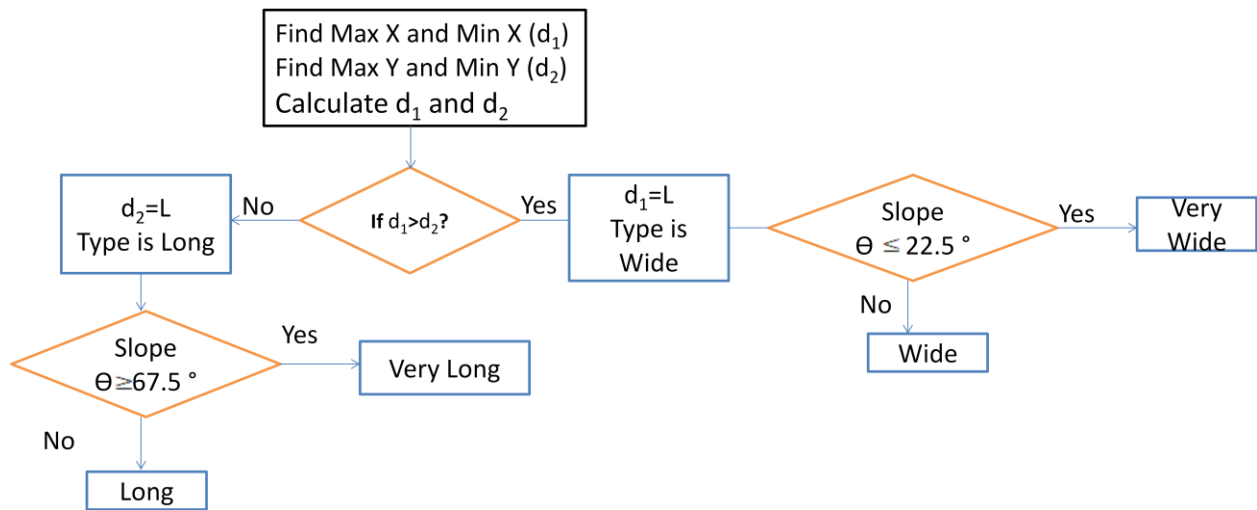
Figure 5.7: Flowchart of the proposed landslide classification method.

Following the previous steps, the fourth stage considers the amount of the slope angle (θ) in order to sub-classify landslides (Table 5.1).

To classify a landslide based on the proposed algorithm, this study has considered long segment (d1) length, angle of slope with respect to x-axis, and failure direction. The side which is close to horizontal is considered to be very wide and as it gets close to vertical is very long. The selection of degrees in angle is based on bisector angle (i.e. equal angle) and of division in angle between $0°$ to $90°$.

Table 5.1: Classification of landslides by the proposed method.

Type of Landslide	Slope angle (θ)
Long	90°≥LS>67.5°
Very long	67.5°≥LS>45°
Wide	45°≥LS>22.5°
Very wide	22.5°≥LS>0°

The slope angles can be calculated by:

$$Slope\ L = \frac{(Y_{X_{max}} - Y_{X_{min}})}{(X_{max} - X_{min})} \qquad (5.4)$$

$$Slope\ W = \frac{(Y_{max} - Y_{min})}{(X_{Y_{max}} - X_{Y_{min}})} \qquad (5.5)$$

where L is the length and W is the width of a landslide polygon (see lines 38 and 39 of the code). The slope is always defined as Δy/Δx. Slope L describes the drawn segment slope between X_{max} and X_{min} in scalar 2D static system and slope W describes the slope of a drawn segment between two points that are with maximum y and minimum y.

Step 4: This step aims to determine the slope angle (θ) in order to sub-classify landslides (Table 5.1). The slope angle (θ), which is the angle of the segment with respect to X-axis, is not a topographical slope. If the slope angle (θ) is below 45°, then the landslide is classified as the wide type. If the slope angle (θ) is above or equal to 45°, then the landslide is classified as the long type (Table 5.1). For wide type landslides, there are two possibilities: (1) If the slope angle (θ) is below or equal to 22.5°, then the proposed algorithm identifies the landslide as the very wide type; or (2) If the slope angle (θ) is above 22.5° but below or equal to 45°, then the landslide is classified as the wide type. For long type landslides, there are two possibilities: (1) If the slope angle (θ) is above 45° but below or equal to 67.5°, then the landslide is classified as the long type; or (2) If the slope angle (θ) is above 67.5° but below or equal to 90°, then the landslide

is classified as the very long type. The upper and lower limits of the slope angle depend on the x- and y-coordinates (Figure 5.8). In this study, the classification of landslides into the very wide type (0°-22.5°), very long type (67.5°-90°), wide type (22.5°-45°), and long type (45°-67.5°) was dependent on the angle indicating the inclination of a landslide to either X-axis or Y-axis. In other words, the upper and lower limits of slope angle for the landslide classification rely on each section of the 2D space. xoy (Figure 5.8) has an angle of 90° between each axis. Because the bisector in each region is 45°, the criterion of this angle is the middle limit of 45° and it is evaluated by the proposed algorithm. Notably, this study implemented the scalar system to run the process. However, it is not important which region of the Cartesian coordinate system a landslide polygon falls in. Also, in classification of "very wide (0°-22.5°) or long (67.5°-90°)" and "wide (22.5°-45°) or long (45°-67.5°)", the criteria was the angle between the bisector to x-axis/y-axis because this angle defines the closeness to the x-axis or y-axis which indicates the inclination of a landslide to either the x-axis or the y-axis (see code lines 38 and 39).
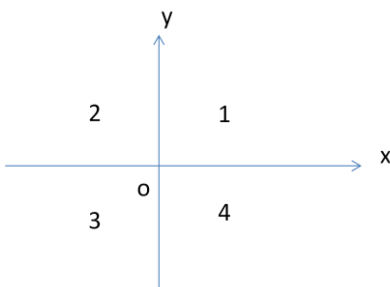
Figure 5.8: Each section of the 2D space of xoy.

The final stage calculates the width and identifies the length of the landslide. Therefore, to determining d_1, d_2, the semi-automated calculation of length and width was created. In this study, the landslide geometry was determined in the 2D scalar system where the maximum distance between points (i.e., longest length of a segment) in a landslide polygon was considered. The proposed algorithm calculates and compares d_1 and d_2. The d_1 is the length of the landslide if

99

$d_1 > d_2$, or the width of the landslide if $d_1 < d_2$. The algorithm can determine the longest segment when d_1 is perpendicular to d_2 (Figure 5.9).

Y_{pmax} = The maximum Y-coordinates point of the longest perpendicular segment to the AB
Y_{pmin} = The minimum Y-coordinates point of the longest perpendicular segment to the AB
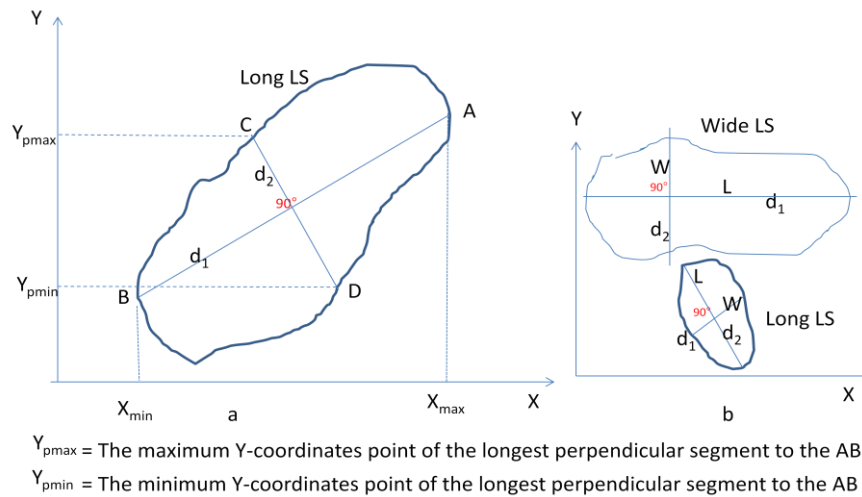
Figure 5.9: (a) The longest segment of the landslide polygon. (b) Wide type and long type of landslides.

5.2.3 Use of LiDAR-derived DEMs and Inventory Dataset

In this study, 5 m resolution LiDAR-derived DEM was generated and represented in ArcGIS (Figure 5.10). This figure shows geographical distributions and locations of landslides in the study area. Those generated DEM derivatives were used to assist landslide classification along with field observations, UAV images, and Google Earth images.

The raw LiDAR point clouds were first converted into the LAS format. LiDAR-derived DEM was used in ArcGIS to be integrated with the existing inventory datasets, while Google Earth images were used for better visual interpretation of landslides. In addition, 20 cm resolution UAV images covering Chalus District were used together with some field observations (Figure 5.11) to identify new landslides, test the proposed algorithm, and update the landslide inventory map of the study area (Figure 5.3). Only some landslide polygons from the inventory database containing a total of 173 landslides were selected to test the proposed method. These polygons were converted into the points with x- and y-coordinates. These x- and

y-coordinates were used to measure the long and short sides of the landslide polygon as well as to determine the landslide length, width, area, and type.

5.2.4 Validation

The performance of the algorithm was verified in ArcGIS using field observations in conjunction with the inventory dataset. Fifty eight landslide polygons were selected from the study area. Fourteen actual and simulated polygons were selected to test the proposed algorithm. for A polygon was selected and calculated in ArcGIS and in the developed software, respectively. Other landslide polygons were also calculated in ArcGIS, ground truth, and in the developed software, respectively, for the algorithm performance and relative error analysis. The proposed method was verified using field observations, measurement tools, and the Real Time Kinematic (RTK) SmartNet system in ground truth. Basically, the RTK technique is used to collect points with x,y,z and to measure the length and width of the segment on the ground truth for further geometric analysis in ArcGIS as well as the proposed software. RTK satellite navigation is a technique that has been used in this study to enhance the precision of landslide position data during ground truth measurement for simulation of the model. This RTK has derived from satellite-based positioning systems (global navigation satellite systems, GNSS) such as GPS. The percentage relative error was calculated by Ken et al. (2007), Irigaray et al. (2007), and Kreyszig et al. (2011).

$$\text{Relative Error \%} = [\, |L_{\text{ArcGIS or ground measurement}} - L_{\text{proposed software}}| \,/\, A_{\text{ArcGIS}} \,] \times 100$$

$$(5.6)$$

$$\text{Relative Error \%} = [\, |W_{\text{ArcGIS or ground measurement}} - W_{\text{proposed software}}| \,/\, A_{\text{ArcGIS}} \,] \times 100$$

$$(5.7)$$
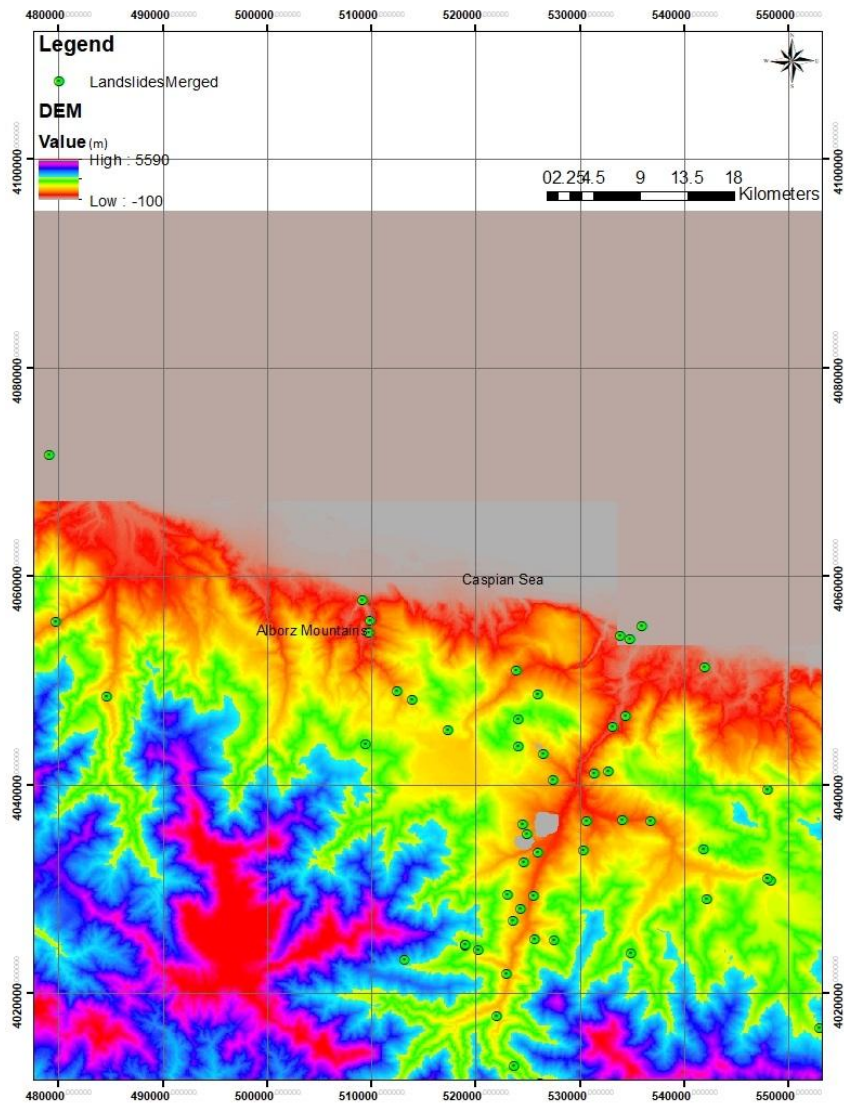
Figure 5.10: Landslide inventories on the DEM of the study area.

Figure 5.11: Field photo of a long type landslide in Haraz District, Mazandaran Province.

5.3 Results and Discussion

The results of this study form a response to the previous studies attempted by Taylor and Malamud (2012) and Niculita (2016). This study presented a semi-automatic landslide length and width extraction based on the NITR geometric processing of the landslide polygon and the geomorphometric analysis of LiDAR-derived DEMs.

The results of this study demonstrated that the proposed algorithm was able to automatically determine the landslide length, width, and type which probably shows a promising approach in contrast to the existing GIS software and algorithm delivered by Booth et al. (2009) and Niculia (2016). Both the long side and the short side of the landslide polygon can be measured automatically and the type of the landslide can be classified with the proposed method at an acceptable level. This investigation classified landslides into a) long, b) very long, c) wide, and d) very wide.

Table 5.2 depicts the comparative measurement and relative percentage error with ArcGIS and the proposed algorithm. The dimensions of one of the selected polygon samples are 83.74 m in length and 69.30 m in width in ArcGIS, in comparison with 83.75 m in length and 69.31 m in width in the proposed software, respectively. The calculated area of the selected polygon in ArcGIS is 3606.7 m^2, in comparison with 3606.4 m^2 in the proposed software, respectively. The percentage relative errors obtained were 0.496% in length and width, and 0.008% in area when using the proposed software as compared to ArcGIS software (Table 5.2a). Also, Table 5.2b depicts another example of the comparative measurement and relative percentage error with ArcGIS and the proposed algorithm.

Table 5.2: Comparative measurement and relative percentage error of ArcGIS and the proposed algorithm.

(a)

Geometry	ArcGIS	Proposed Algorithm	Relative Error (%)
Length (m)	83.74	83.75	0.01
Width (m)	69.30	69.31	0.01
Area (m^2)	3606.7	3606.4	0.008

(b)

Geometry	ArcGIS	Proposed Algorithm	Relative Error (%)
Length (m)	113.12	113.40	0.30
Width (m)	101.34	99.64	1.67
Area (m^2)	6976.91	6988.20	0.16

Also, the relative error of measurement of a tested landslide length and width of the polygon is 0.01% and 0.01%, respectively (i.e. the proposed algorithm in MATLAB vs. ArcGIS) (Figure 5.12). Also, a ground truth sample polygon (Figure 5.13) was simulated and measured by using RTK technique. The relative mean error percentage of measurement for the landslide polygon tested in area is 0.49% (i.e. the proposed algorithm in MATLAB vs. ground truth measurement) and 0.43 (i.e. ArcGIS vs. ground truth measurement). These results showed that the developed algorithm can calculate the length, width, and area of landslide polygons .

Moreover, this study indicated that the LiDAR-derived DEM plays an important role to support enhancing landslide on screen visualization to determine a landslide polygon boundary and to revise landslide inventory. This method also helps in determining the length, the width, and particularly the area of landslide polygons when integrating such DEM with the UAV and Google Earth high-resolution images. To support the output results, this study has compared the selected landslide to inventory data and the ground truth observations (Figure 5.13). However,

this study has not attempted a quantitative research on accuracy performance of the output results. It would be suggested for the future works to compare a quantitative study on the output result by the proposed software and available inventory data.

Finally, the proposed method can semi-automatically determine and classify the landslide type from the landslide inventory database.
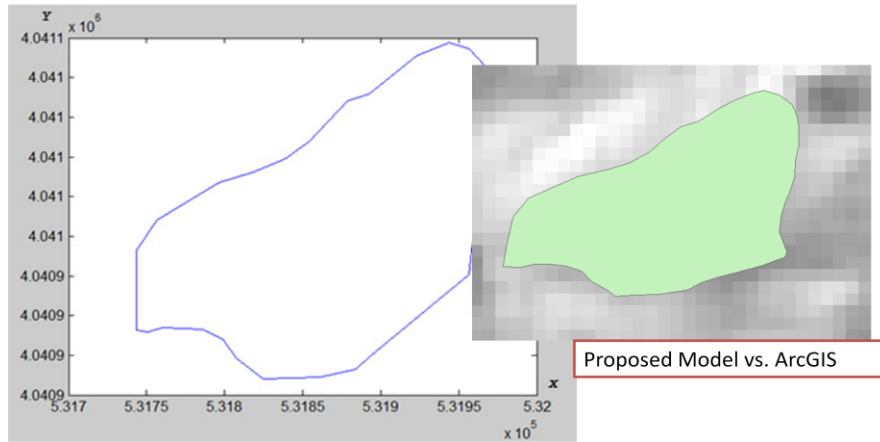

Figure 5.12: Landslide polygon by the proposed software vs. ArcGIS.
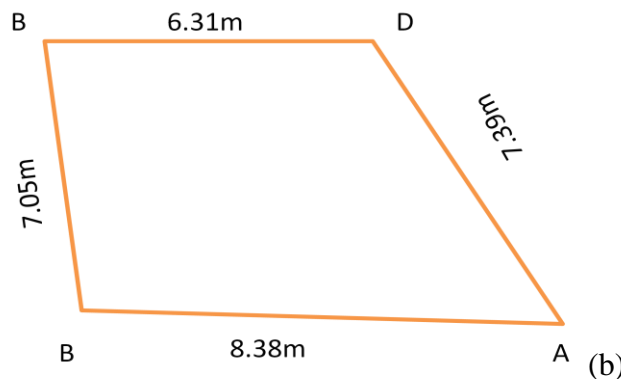
Figure 5.13: (a) Ground truth measurement using RTK system, (b) schematic of a simulated polygon on the ground.

5.4 Concluding Remarks

This chapter has presented a method to define the landslide polygon in a 2D scalar Cartesian coordinate system. The landslides can be classified based on geographic coordinates (x, y), long side or maximum distance of the segment in a landslide polygon, and slope angle (θ). This study has implemented geometric calculation and landslide classification through NITR-based MATLAB coding. The results showed that the proposed method can discern the length and width of a landslide at a satisfactory level for any landslide polygon shapes. In general, there are regular and irregular shapes. Regular shapes are such rectangle, triangle, and square. Regular shapes have sides that are all equal and interior (inside) angles that are all equal. Irregular shapes have sides and angles with any length and size. Landslides are in various shapes in nature. That is why, this study presumed they can be in regular shape such as rectangle or they can be irregular shape (Figure 5.12, Figure 5.13).

This study concluded that use of the LiDAR-derived DEM together with UAV images and Google Earth images can possibly not only improve visual interpretation and recognition of landslides, but also increase the performance in measurements of landslide geometry when integrated with field observations. Therefore, this approach can be used to revise and update the landslide inventory in the study area. This study also identified that the majority of landslides in the study area are rhombic or hexagonal, trapezoid, and oriented to the downslope direction of the hillslope. Also, this study found that the round-shaped landslides are associated with highly dense vegetation. The field observation showed that in a few cases, the material movement and displacement are towards the bed and strata dip direction of the rocks.

The findings of this study suggest that the flow direction or aspect value of mass displacement should be considered for determining landslide type in future studies. Also, the failure direction and slope direction in the 3D vector system and dynamic environment (before

and after a landslide) should be considered when determining the deformation, materials displacement, and flow direction. Given the fact that the algorithm developed in this study was not able to accurately identify the right direction or aspect value, a logic relationship should be defined. Further development is required for computing the volume of material displacement using a high-resolution LiDAR-derived DEM and UAV images obtained before and after landslides.

However, the results of this research could possibly motivate researchers to begin a new driving point in developing algorithms for automatic geomorphometric analysis of landslides in the GIS environment toward this future direction delivered by the UN-GGIM (http://ggim.un.org/).

5.5 Chapter Summary

This chapter identified the geometric process to determine landslide length, width, area, and type by developing the proposed algorithm. Remote sensing data such as LiDAR are useful to improve the enhancement of determining landslide boundary polygons, geometric analysis, particularly when a high-resolution DEM is acquired. The contribution of this study is on semi-automated geometric and classification of landslides. This contribution allows to do the necessaries action for emergency response and disaster planning and management after a landslide occurrence because we can do geometry calculation immediately by implementing DEMs of before and after a landslide associated with high-resolution of UAV and satellite images. This study aimed to introduce an approach to landslide geometry analysis and classification for future GIS techniques. This study perhaps predict that future geodata analytical and numerical approaches will be explored more in-depth for geometric analysis using UAV for

landslide studies. This study delivered a geoanalytical and numerical method to landslide analysis and classification.

Chapter 6

Landslide Deformation Modelling-Simulation and Flow Direction Using LiDAR-derived DEMs and UAV

A modelling and simulation procedure for landslide deformation including calculating landslide displacement and flow direction are presented in this chapter. The proposed algorithm is coded in MATLAB based on the DEMs of before and after a landslide. The proposed method calculates: (a) the volume of the material displacement, (b) the potential displacements of the slide mass after the onset of failure, and c) the flow direction of the material movement. The proposed algorithm is used to model, simulate, and calculate the displacements of landslides in the Zagros and Alborz Mountains of Iran and potentially other locations in the world. An example of modelling the landslides of Guizhou Province in China was used to test and validate the proposed algorithm for deformation pattern and volume calculation as well as failure flow direction of material displacement. However, more ground truth validations in other geographical locations are required to implement the algorithm and to confirm the proposed model for calculating displacements which are compared favourably with field measurements.

6.1 Introduction

One of the most important phenomenon in environmental science and engineering is deformation of landslide and calculation of materials' movement. Assessment of such deformation process is not only scientifically interesting, but also beneficial for hazard/risk control and prediction. This assessment may also be used for regional planning and development. This geomorphic process phenomenon, which is significant in developing the geometry of landslides, can be used in

conjunction with DEMs (before and after landslide) to determine landslide typology as well as deformation pattern and flow direction (Hattanji and Moriwaki, 2009; Niculitˇa, 2016).

Assessing topography and morphology of landslide for geometric analysis, deformation, and flow direction of materials' movement requires knowledge of not only geologic and geomorphic processes and computing techniques, but also of technologies including remote sensing and GIS. In the last decades, researchers have identified considerable improvements in landslide delineation by using the high resolution of DEM derived from LiDAR techniques (Wehr and Lohr, 1999; Su and Stohr, 2000; Ali et al., 2003b; Tarchi et al., 2003; Su and Bork, 2006; Ardizzone et al., 2007; Teza et al., 2007; Travelletti et al., 2008; Roering et al., 2009; Pirasteh et al., 2011; Liu et al., 2012; Jaboyedoff et al., 2012; Ren et al., 2014; Pirasteh and Li, 2016). GIS, remote sensing techniques, and LiDAR-derived DEMs allow for an extensive and detailed exploration of geomorphology, geometry, and deformation assessment of landslides with an acceptable level of certainty. These methods have also helped in improving and updating landslide inventories. Every landslide inventory contains a collection of information such as polygon shape, type, length, width, area, location, and other related information including volume of mass displacement. These landslides can be drawn digitally in the GIS environment using manual and semi-automated methods (Freeman and Shapira, 1975; Freeman, 1991; Ali et al., 2003a; Malamud et al., 2004; Martha et al., 2010; Mondini et al., 2011; Lyons et al., 2014). Landslide inventories and geospatial data analytics are certainly playing a significant role in decision-makers' preparation of a loss reduction plan as well as in challenging the established infrastructure of an early warning system.

However, very few researchers have studied the development of semi-automated algorithms for geometric analysis and deformation pattern of landslides (Ardizzone et al., 2002; Malamud et al., 2004; Booth et al., 2009; Mondini et al., 2011; Taylor and Malmud, 2012; Lyons

110

et al., 2014; Niculiťa, 2016). The method proposed in this chapter presents how to measure, determine, and calculate landslide length, width, area, volume, and flow direction. This semi-automated algorithm has been implemented for the landslide inventory dataset in the Alborz Mountains, Iran because this area is composed of typical geomorphologic features and a variety of landslide shapes. A landslide at the coal mine of Madaling in Guizhou Province, China was used to implement the proposed algorithm based on the LiDAR-derived DEMs of before and after the landslide for validation and algorithm performance. This semi-automated geometry extraction and deformation of landslides in the 2D scalar system (see Chapter 5) are further expanded in the dynamic 3D vector system. LiDAR-derived DEMs in conjunction with field observations, UAV images, and Google Earth images assist in updating the available inventory dataset.

6.2 Expanding Algorithm and Computing

Based on the built database and designed architecture in the previous chapter, the same data are used to process the landslide modelling and simulation deformation by implementing the proposed model and software package. Semi-automated calculation of segments in landslide polygons, semi-automated classification of landslide, and determining d_1, d_2 for semi-automated calculation of length and width have been described in Chapter 5. Further, to develop logic corresponding to the previous chapter and to develop an algorithm to determine the deformation of material displacement and flow direction, it is necessary to understand how materials move.

Sometimes materials move towards the downslope, and the distance of the mass displacement in a landslide is greater than the width of the displaced material (especially for flows, but also for the majority of slides). This means that length is greater than width (L>W). In some landslides, this phenomenon does not happen and there may be a smaller length than width

(L<W) (Figure 6.1). The proposed method determined the maximum distance of mass displacement (i.e. the longest segment) with respect to failure flow direction either in X-axis or Y-axis (with respect to the geographical coordinate system) to discern landslide length and width, and to define landslide type. For this reason, a logical computing approach was expanded to determine the length, width, area, volume, and flow direction of the material movement as well as to classify landslides. Therefore, this study used the previous concept of NITR and the model that was built in the previous chapter (see Chapter 5). This allowed for the expansion of the scripts and of the code for computing, simulating, and modelling the landslide geometry including volume of material displacement deformation and flow direction. Section 6.2.2 describes how the scripts from the previous chapter have been expanded.
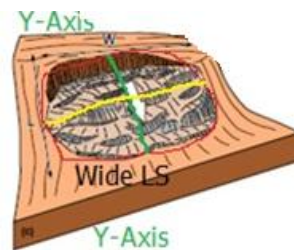
Figure 6.1: Mass displacement of downslope is smaller than the displaced materials in width.

6.2.1 Geometric Analysis and Semi-Automated Calculation of Area

To study and classify the shapes of landslide geometry is at times highly subjective. In the Alborz Mountains, landslides' shapes may be regular or irregular, which causes uncertainty in determining the length, width, area, volume, and type of landslide polygon. The geometry of landslides can be computed using different methods (Ghuffar et al., 2013; Pirasteh et al., 2015; Niculitˇa, 2016) and tools such as ArcGIS software (http://support.esri.com/technical-article/000006109). This study used geodata analytical computing and NITR to improve the precision of the measurement of landslide polygons extracted from LiDAR-derived DEMs, Google Earth images, UAV images by using visual image interpretation of photographic and

112

geotechnical elements such as texture, shape, vegetation, and slope, and the available landslide inventory dataset.

This study expanded upon semi-automated geometrical extraction of landslide deformation. Similar to the previous chapter, this study followed the 2D scalar system followed by further expansion to the 3D vector system by using two different dates of LiDAR-derived DEMs (i.e. before and after landslide) to model and simulate the deformation pattern and flow direction of material movement. This allowed for calculating the volume of mass displacement before and after landslide. In addition, failure direction was considered and expanded upon in the proposed algorithm with respect to 3D vector form.

In order to perform semi-automated calculation of area, the proposed software package computes maximum and minimum projected geographical coordinates of points (Easting and Northing) of a polygon boundary from the input data in the scalar. Next, a line (long side segment) is stretched between the maximum and minimum values of the polygon predisposed in x-coordinate. If a landslide is a "Wide" type, then a curve is drawn above the line to coincide with the X-axis. The curve above the line is called "Top Curve" (A_1). Also, the points under the line (long side segment) create another curve which is called a "Bottom Curve" (A_2). The area below the stretched line (i.e. Bottom Curve) is computed using the NITR formula. The same process is followed for the "Bottom Curve" and the area under the line is computed. Then the system begins to subtract the area of the top and bottom curves (Figure 6.2). The area of the polygon is calculated as follows:

$$A_p = A_1 - A_2 \qquad (6.1)$$
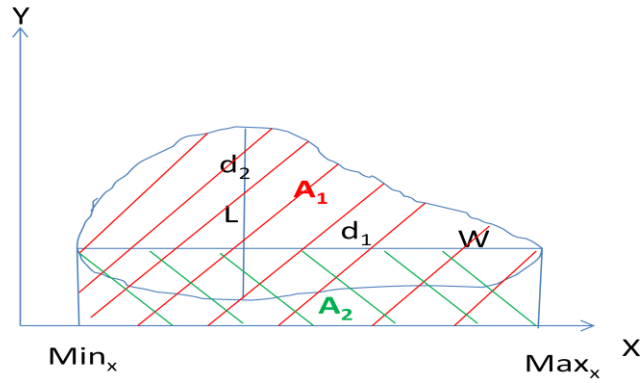
Figure 6.2: Schematic of a Wide landslide.

If a landslide is a "Long" type, then the polygon is divided into "Left Curve" and "Right Curve" coinciding with the Y-axis; and the area of "Right Curve" and "Left Curve" are computed separately. Therefore, the system begins to subtract the area of "Right Curve" and "Left Curve" (Figure 6.3), and the area of the polygon is computed.
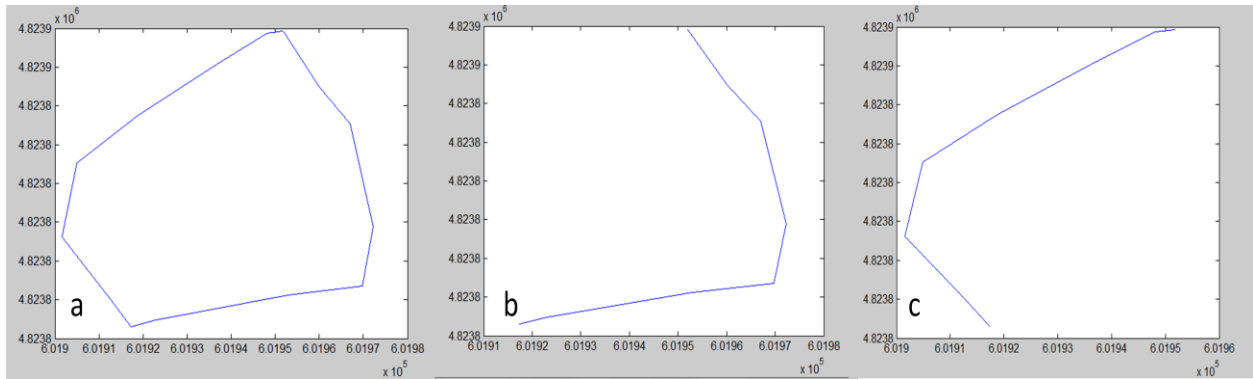
Figure 6.3: (a) A polygon sketched using proposed software model, (b) "Right Curve", (c) "Left Curve".

6.2.2 Simulation of Deformation and Flow Direction

An algorithm and a code for modelling, simulation, and semi-automated determination of a landslide deformation and flow direction of the material displacement are explored. This algorithm has performed an approach to analyzing, computing, simulating, and modelling landslide materials displacement and measurement of z value before and after a landslide. This

114

study used the MATLAB platform to code and script the algorithm. Therefore, computing machines were used as tools to simulate the deformation of a landslide, measure the volume of the material displacement, and identify the failure flow direction of the mass movement. LiDAR-derived DEMs, UAV remote sensing techniques, and Google Earth images with related field observations helped to characterize before and after landslide hazards and validate the material displacement and flow direction of a landslide in the Alborz Mountains of Iran.

In order to perform technical analysis of computing material displacement and flow direction, a simulation and modelling of landslide deformation require data in the form of points or pixels of before and after the event. This is the fundamental data and structure needed to develop an algorithm and a code to determine the volume of material displacement and flow direction. Figure 6.4 depicts the procedure of simulation and modelling of a landslide deformation and flow direction.

In this study, the two different dates of DEMs of a particular landslide before and after occurrence helped to simulate and model the deformation of a mass movement. In order to automatically and incrementally extract deformation of the landslide, a "pixel" or "point" is considered as a cell or grid value for deformation simulation and modelling. The DEMs are divided into a number of cells or grids (Figure 6.5) and the centre of each cell or grid represents a point with x, y, and z value. In other words, each cell or grid represents a point.

To build on the previous study in this thesis, the previous scripts are expanded upon in this chapter to determine the volume of the material movement and identification of flow direction. The six steps of deformation and volume calculation procedure are as follows:

i. Ask for data of points (x,y,z);

ii. Number of points for before a landslide (n_{bl}) and after landslide (n_{al}).

iii. Input points for before and after a landslide, with each point's dataset representing a matrix before landslide (M_{bl}) and a matrix after landslide (M_{al}).

iv. Resample and convert matrix (M_{al}) to a new matrix after landslide (M_{nal}), while generating the equal dimensions of both matrices. In other words, $n_{bl} = n_{nal}$, where n_{bl} is the number of points before a landslide, n_{al} is the number of points after a landslide, and n_{nal} is the number of points at the "new after landslide". The following matrices and Figure 6.6 illustrate how points are defined for each cell or grid.

v. Use previous algorithm and code developed in Chapter 5.

vi. Calculate volume.
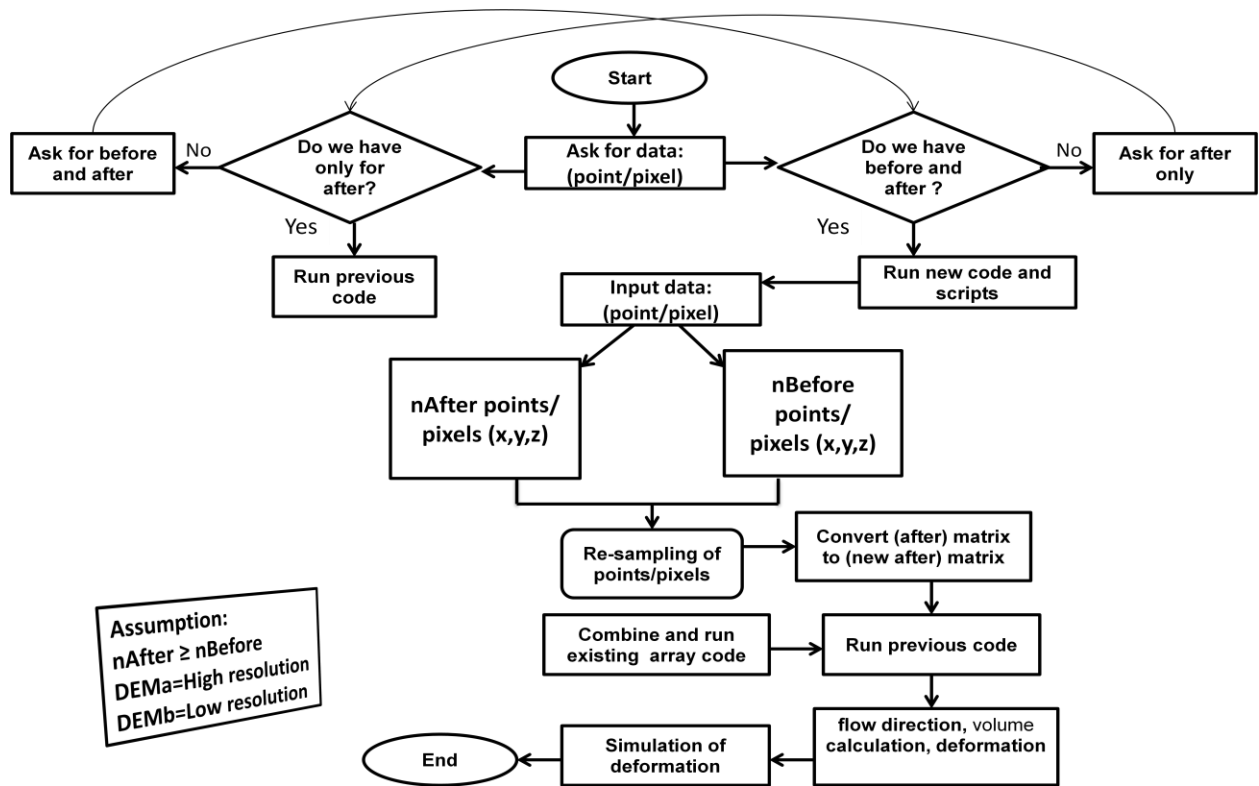
Figure 6.4: Flowchart of modeling and simulation of a landslide deformation and flow direction procedure.

$$M_{bl}=\begin{pmatrix} x_{1bl} & y_{1bl} & z_{1bl} \\ x_{2bl} & y_{2b} & z_{2bl} \\ ... & .... & .... \\ ... & ... & ... \\ x_{nbl} & y_{nbl} & z_{nbl} \end{pmatrix}$$

$$(6.2)$$

$$M_{al}=\begin{pmatrix} x_{1al} & y_{1bl} & z_{1bl} \\ x_{2al} & y_{2al} & z_{2al} \\ ... & ... & .... \\ ... & ... & ... \\ x_{nal} & y_{nal} & z_{nal} \end{pmatrix}$$

$$(6.3)$$

$$M_{nal=}\begin{pmatrix} x_{1nal} & y_{1nal} & z_{1nal} \\ x_{2nal} & y_{2na} & z_{2nal} \\ ... & ... & ... \\ ... & ... & ... \\ x_{nnal} & y_{nnal} & z_{nnal} \end{pmatrix}$$

$$(6.4)$$

117
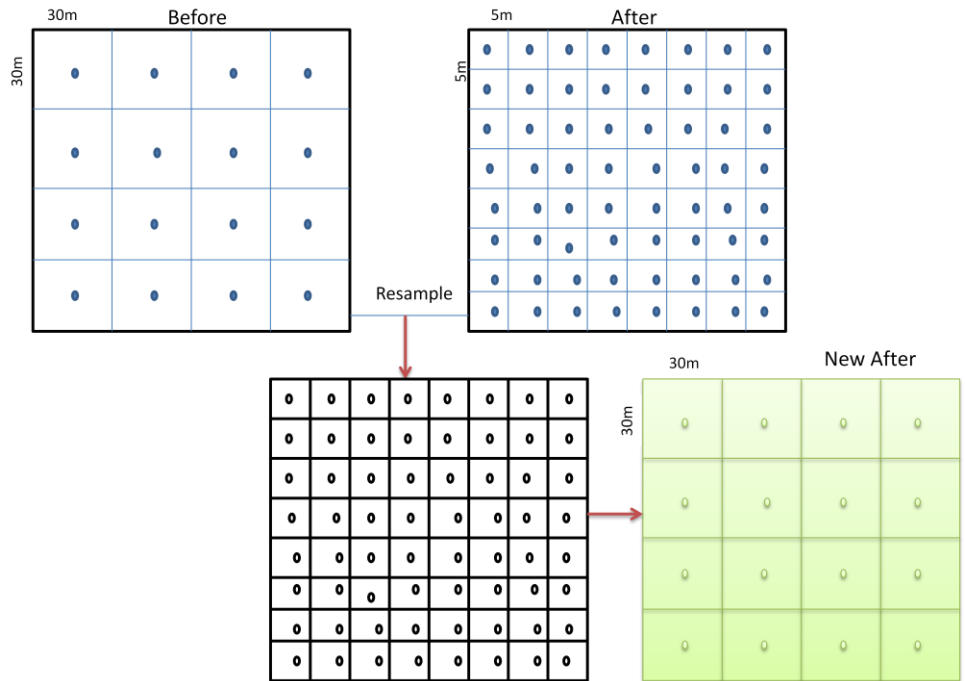
Figure: 6.5: Conversion of pixels to points and matrix conversion of points.

To calculate the volume of landslide material displacement, Figure 6.6 depicts the logic behind the volume calculation of each pixel or a grid.
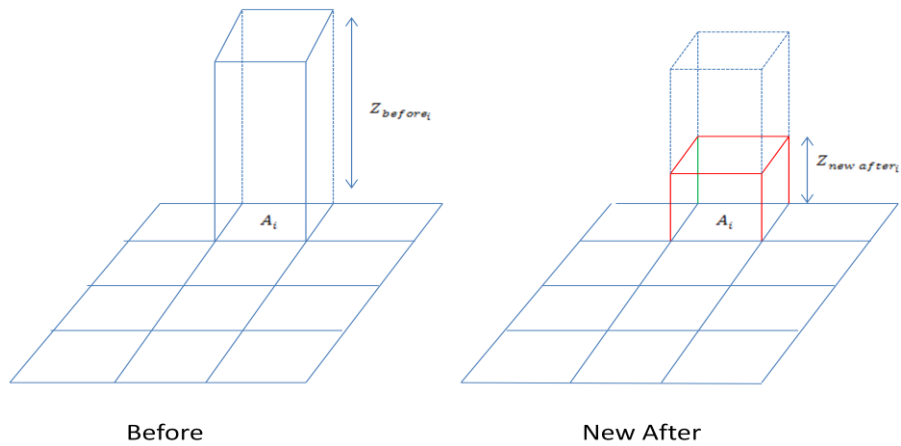
Figure 6.6: Cell or grid of DEMs before and after a landslide.

To calculate the volume of material displacement, the following equation is used:

$$V_{movement_i} = A_i(Z_{before_i} - Z_{after_i}) \qquad (6.5)$$

where $V_{movement_i}$ and A_i are the volume and area of material displacement of an arbitrary cell or a grid respectively, and Z_{before_i} and Z_{after_i} are elevations of an arbitrary cell or a grid for before and after a landslide, respectively.

To calculate the area of a cell or a grid the following equation is used:

$$A_i = A/n_{bl}, \quad (n_{bl} = n_{nal}) \tag{6.6}$$

where A is the total area of a landslide polygon.

The total volume of a landslide material displacement can be calculated by summation of the volume of the material displacement of each cell or grid from the following equation:

$$V_{total\ movement} = \sum_{i=1}^{n_{bl}=n_{nal}} V_{movement_i} \tag{6.7}$$

Simulation of material movement and volume calculation, as well as flow direction, were performed based on the coordinates x,y,z of grid values before and after a landslide. The two different datasets of DEMs from before and after a landslide with the same resolution (may or may not be) incorporated into the algorithm to simulate and model the deformation. There are two possible DEMs resolutions of before and after a landslide. First, if both DEMs are in the same pixel resolution, then the pixels of both DEMs are converted into points (x,y,z) by using ArcGIS software. Further, the script recommends introducing points of before and after a landslide and running the program to determine the deformation and flow direction of the material movement. Second, if the DEMs have different pixel resolutions, then the pixels of both DEMs are re-sampled to a similar pixel resolution (Figures 6.7 and 6.8) in 30m. This study recommends re-sampling of the high pixel resolution to the low pixel resolution in order to distribute the high pixel resolution of a DEM among the low pixel resolution of a DEM. Then the pixels of both DEMs are converted into points (x,y,z) by using ArcGIS software. Therefore, two matrices are indicated for before and after a landslide, and they are presented by point (x,y,z)

values. To develop $n_{nal} = n_{bl}$, the points of "after landslide" in the matrix were converted to a matrix that indicates "new after landslide" (Figure 6.9). Consequently, similar to the first resolution, the script recommends introducing points of before and after a landslide and running the program to determine the deformation and flow direction of the material movement.

It is important to know that the model is based on the assumption of nAfter ≥ nBefore. In other words, the number of points/pixels or grids in a DEM after a landslide is more than the number of points/pixels or grids in a DEM before a landslide. This means that DEM_a=high resolution and DEM_b=low resolution where "a" indicates "after landslide" and "b" indicates "before landslide".

The MATLAB platform was used to code and script the algorithm. It allows computing machine tools to simulate the deformation of a landslide and measure the volume of the material displacement as well as the flow direction of the mass movement (Figure 6.9). This is an algorithm and a code that allows the analysis, computation, simulation, and modelling of a landslide material displacement.
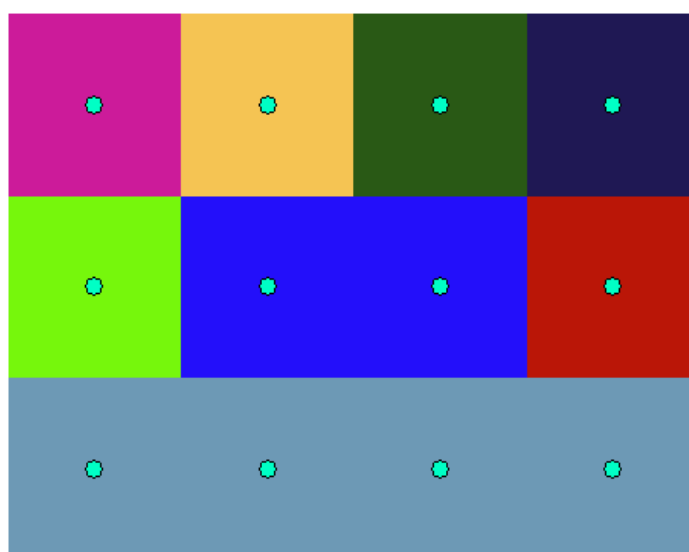
Figure 6.7: Points at centre of pixel (ASTER DEM in 30m resolution).
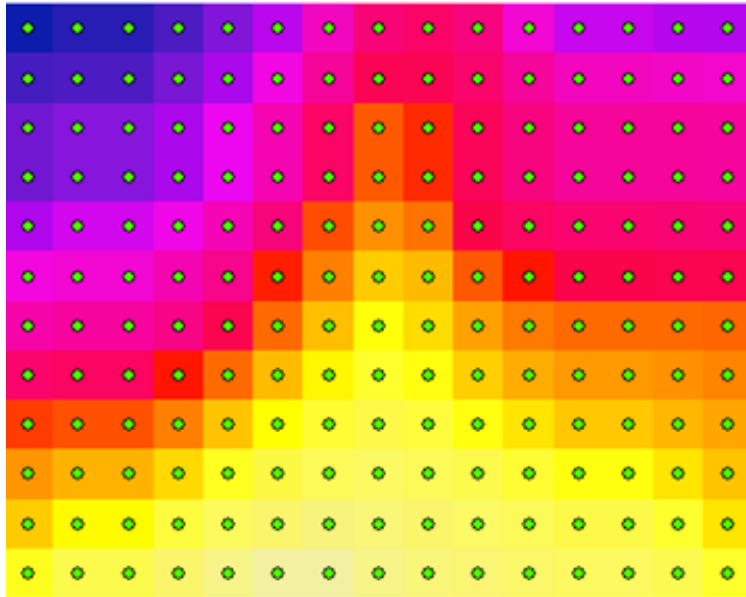
Figure 6.8: Points at centre of pixel (LiDAR-derived DEM in 5 m resolution).

The following procedure describes the scripts for simulation of deformation and volume calculation.

i.   Input data (points) and find maximum and minimum x and y;

ii.   Calculate $d_1=(l_1)$ and $d_2=(w_1)$ and their slopes;

iii.   Determine a landslide type (if required use 2D scalar system or 3D vector system with considering failure slope and flow direction);

iv.   For wide landslide: recognize top and bottom points and sort them into two separate matrices;

v.   Calculate the area under top and bottom curves;

vi.   Identify, measure, and determine width (ALPHA angle between length and width);

vii.   Calculate area and output printing (type, length, width, and area);

viii.   Plot direction; and

ix.   Calculate volume.
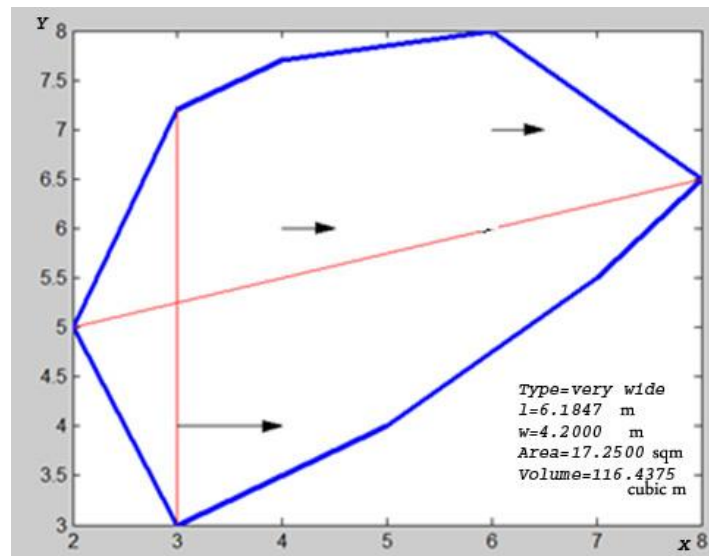
Figure 6.9: Landslide simulated for before and after a landslide.

6.2.3 Incorporating LiDAR-derived DEMs, UAV Imagery, and Inventory Dataset

The most useful representation of the Alborz Mountains terrain is the high resolution of the LiDAR-derived DEM in the GIS environment. In this study, the pixel resolution of the DEM was 5 m, and grids were envisaged to generate the high-resolution DEM derivatives of the study area (Figure 6.10) to assist landslide recognition in conjunction with field observations, UAV images, and Google Earth images.
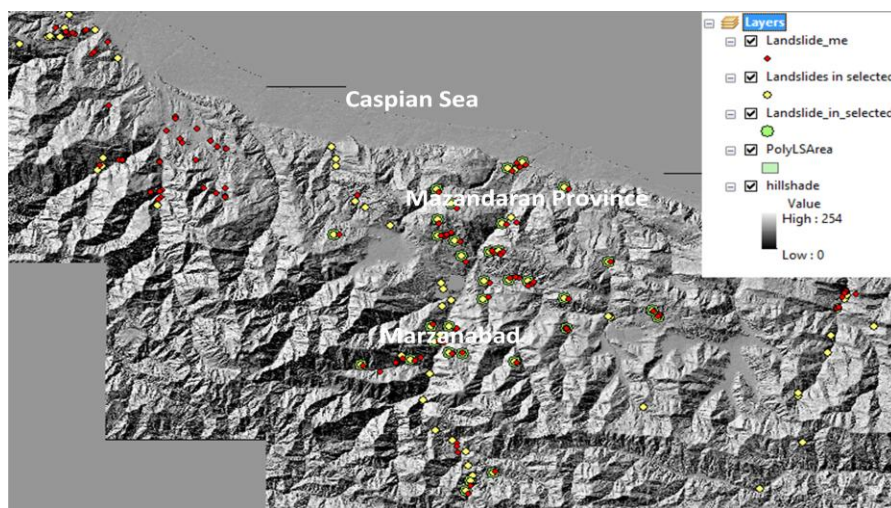
Figure 6.10: Landslide inventories on the hillshade.

The post-processed LiDAR point cloud data in the LAS format were collected and used in ArcGIS software to be incorporated with the existing inventory dataset and Google Earth images for the purpose of enriching the empirical research and visual interpretation of landslide detection. This study used UAV images with 20 cm spatial resolution for the Chalus District to identify new landslides, test the proposed algorithm with a satisfactory performance, and update the landslide inventory map of the study area. This was done in conjunction with the existing landslide inventory map and field observations. The inventory dataset of the spatial distribution of landslides was composed of points. The LiDAR-derived DEMs, UAV images, and Google Earth images were used in ArcGIS software to digitally draw the landslide polygons and to update the landslide inventory dataset. Some selected landslide polygons from the updated inventory dataset were used to test the proposed algorithm. These polygons were converted to points with x, y coordinates, and then these points were used in the proposed algorithm. The proposed software can accept the table containing x, y, and z coordinates to measure the long and short sides of the landslide polygon as well as determine the landslide length, width, area, volume, and type. The inventory map was updated manually after geometric analysis of all landslides is done. The attribute data table of landslide geometry specification is updated in ArcGIS environment.

6.2.4 Validation

The DEMs of before and after the landslide were used to compute the landslide dimensions in ArcGIS as well as in the proposed algorithm and package. Fifty eight landslide polygons were selected from this study. Fourteen landslides actual and simulated polygons were selected to test the proposed algorithm for determining and measuring the length, width, area and type of landslide; and one actual landslide polygon was tested for determining and measuring the

volume of material displacement. The algorithm was validated by the relative error method (Ken et al., 2007; Irigaray et al., 2007; Kreyszig et al., 2011; Niculitˇa, 2016) of the inventory dataset and field observations (Figure 6.11) by using ArcGIS software vs. the proposed algorithm and software package in MATLAB. A selected polygon from the coal mine of Madaling in Guizhou Province, China was used to validate the proposed algorithm based on the landslide inventory data collected from Chengdu University. To calculate the relative percentage of error of the measurement, Equation 5.6, 5.7 and the following equation (6.8) were used (Kreyszig et al., 2011).

$$\text{Relative Error \%} = [(V_{\text{Inventory}} - V_{\text{Proposed software}}) / V_{\text{Inventory}}] \times 100$$

(6.8)

where $V_{\text{Inventory}}$ is the calculated volume from the inventory dataset and the report and $V_{\text{Proposed software}}$ is the calculated volume by the proposed algorithm.

Figure 6.11: Field photo shows Lasem landslide in Mazandaran.

6.3 Results and Discussion

This study resulted in modelling and simulating the deformation pattern of the materials and flow direction of a landslide. This work is based on the NITR geometric process incorporated with the LiDAR-derived DEM, UAV images, Google Earth images, and the inventory dataset. The significance of the developed algorithm in contrast to the previous studies is the computation of the landslide polygons without selecting a boundary box outside of the landslide polygon. This method increased the precision of geometric analysis of a landslide polygon. The developed package computes the length, width, and area, and identifies the landslide type as well as the volume of the material displacement and flow direction with an acceptable result.

The results for the tested sample landslide polygons are: Example (1) The area of the selected landslide polygon in ArcGIS was 6976.92 m^2 (Figures 6.12) and the proposed software package showed 6988.20 m^2 (Figures 6.13). This means that the relative percentage of error is 0.16% (Table 5.2). Example (2) The length and width of the landslide polygon in ArcGIS were 113.12m and 101.34m, respectively; and the length and width in the proposed software package were 113.46m and 99.64m, respectively. This means that the percentage of error is 1.67% and 0.30% for length and width, respectively. Example (3) The proposed algorithm has also calculated the landslide polygon which length is 113.47m, width is 99.64, area is 69886.30 m^2, and volume of the mass displacement of the selected landslide from the coal mine of Madaling in Guizhou Province is 3479.50m^3. Therefore, it shows a close agreement achievement to the inventory data. This means that the result is acceptable (Table 6.1) as it is below ten percents of accuracy (Mousavi et al. 2011; Shirzadi et al. 2017). Based on the landslide inventory, the mass displacement volume for the same landslide was reported as 3682.35m^3. Therefore, the relative error percentage is 5.50% which promised in an acceptable agreement with the existing available data.

Table 6.1: Comparative measurement and relative error.

Geometry	ArcGIS	Proposed Algorithm	Inventory dataset	Relative Error (%)
Length (m)	113.12	113.46	N/A	0.30
Width (m)	101.34	99.64	N/A	1.67
Area (m^2)	6976.92	6988.20	N/A	0.16
Volume (m^3)	N/A	3682.35	3479.50	5.50

The results of validation of the algorithm, simulation, and modelling were followed by field observations and the ArcGIS software using relative error method (Irigaray et al., 2007; Kreyszig et al., 2011).

The comparative computing techniques of geometric analysis and classification of landslides in ArcGIS and the proposed model were attempted. This allowed for the measurement of length, width, area, and volume of the landslides as well as for the determining of failure flow direction and type of a landslide. However, it seems that there are no GIS software that can automatically determine the length, width, volume, and type of a landslide. In contrast, the proposed algorithm resolved the shortcomings of the previous study that was attempted by Niculitˇa (2016). For example, one of the shortcomings is volume calculation and material displacement where in this study the author has achieved it. This study has also not found a notably research to indicate detecting, determining, and measuring length, width, volume and the type of landslide automatically or semi-automatically. This study revealed that the suggested approach and measurement tool have resolved the flaws and can measure and determine the long and short sides (i.e. long and short segments), volume, flow direction, and type of landslide polygon.
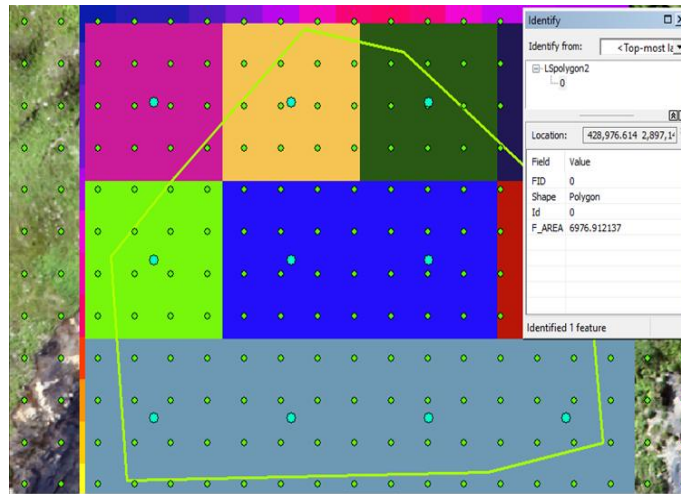
Figure 6.12: A landslide polygon overlaid on the UAV image and ASTER DEM as well as

LiDAR-derived DEM.
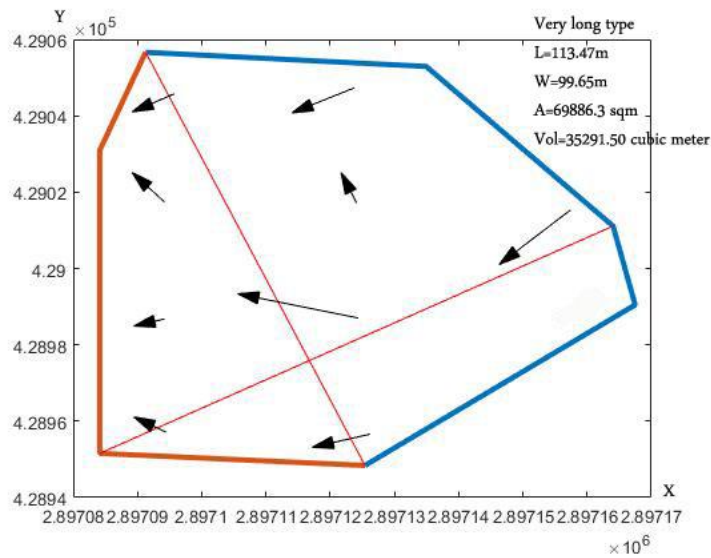
Figure 6.13: Simulation and modelling of a landslide using the proposed algorithm.

6.4 Conclusions and Recommendations

The proposed semi-automated geometric analysis algorithm and code resulted in a satisfactory performance of measurement and determination of length, width, area, volume of material displacement, flow direction, and landslide type using MATLAB (Mousavi et al. 2011; Shirazi et al. 2017). Although classifications of landslides are subjective, this study concluded that

127

geometric analysis can define a the proposed classification of landslides based on geographical coordinates (x,y), long side or maximum distance of the segment (either d_1 or d_2) in a landslide polygon, and slope angle (θ) in 2D scalar system. Further, the proposed algorithm including the failure direction has concluded classification of landslides in 3D and vector form. Also, this study concluded that employing LiDAR-derived DEM, UAV images, and Google Earth images in ArcGIS impacted enhancement of landslide boundary polygon and the visual interpretation and recognition of landslides. The proposed model might possibly revise and update the inventory dataset by measurements of landslide geometry in conjunction with field observations and high-resolution of images as well as DEMs. Therefore, this approach could review and improve the landslide inventory dataset of Mazandaran Province.

The proposed algorithm was tested and verified by ArcGIS software and field observations (Figure 6.14) with the relative error method. However, this study recommends collecting more landslide data and field observations for volume calculation and to validate the modelling and simulation of deformation as well as failure flow direction that were generated by the proposed algorithm. Also, this study recommends collecting more samples from other environmental conditions to test the developed software package.
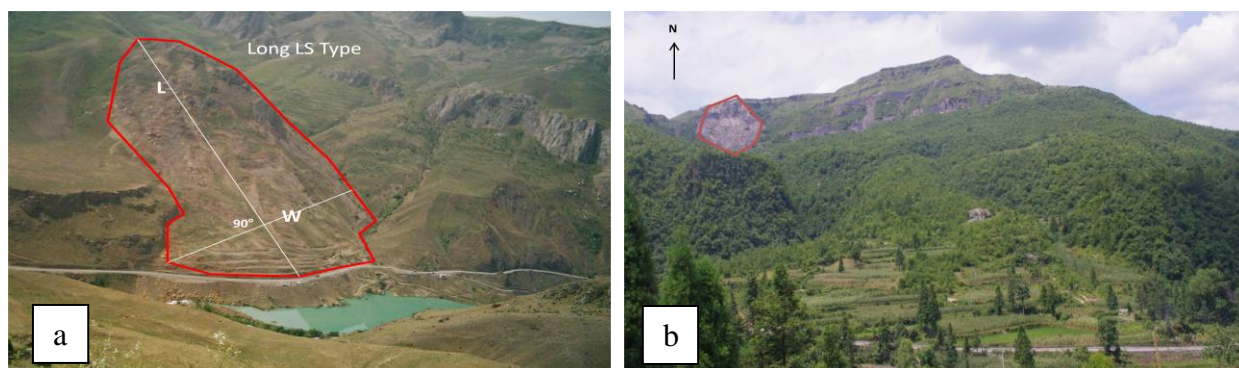
Figure 6.14: (a) Long-type landslide in Alborz Mountain, Iran (b) landslide of Madaling in Guizhou Province, China.

128

However, the review literatures (Booth et al. 2009; Niculita, 2016; Pirasteh and Li, 2016) concluded that there are not a considerable study of inside boundary of a landslide to detect, measure, and determine length, width, area, volume and type of a landslide all together at the same time. Therefore, this seems that the proposed algorithm could possibly be a reasonable approach and to be used for landslide geometric analysis. This study has not also found a notably research on automated system to determining length, width, and type of a landslide in GIS environment. Therefore, defining the angles and scripting the proposed code for geometry analysis and classification of landslide seem to be a new approach.

6.5 Chapter Summary

This study delivered geodata analytical and computing method to landslide geometric analysis and deformation assessment. Although the real challenge is to develop the proposed algorithms to better benefit from incorporating UAV images and LiDAR-derived DEMs for landslide geometric analysis, this study found that LiDAR-derived DEM and UAV images can possibly provide a considerable amount of new information which has not yet been gathered by research. While great advances have been developed by researchers in the past for geometric analysis of landslides, it seems that most of these methods remain tied to the past. Could researchers incorporate these accurate high resolution DEMs and UAV images in conjunction with inventory dataset and geometric analysis to develop better modelling of landslide mechanisms? Is it possible to integrate landslide geometric measurements with early warning systems?

Chapter 7

Conclusions and Recommendations for Future Work

This chapter presents a summary, a conclusion, and suggestions for future work that will reflect expansion of the landslide geometric analysis and deformation pattern, as well as classification.

7.1 Conclusion

Amending landslide inventories is immensely important to policy-makers and decision-makers alike. Sliding creates geometric shapes on the Earth's surface, which this study explored it in both 2D static scalar system and 3D dynamic vector system. This study presented the utilization of LiDAR-derived DEMs, Google Earth images, UAV images, and GIS techniques in Iran's Zagros and Alborz Mountains to investigate landslide assessment, revise and update susceptibility mapping, and refurbish the existing landslide inventory dataset by implementing the proposed algorithm.

Tectonic geomorphologic parameters such as stream gradient-length index and the Dez River profile assisted in the identification and localization of landslides in the Zagros Mountains. This study found that there is real potential in developing a semi-automated algorithm and codes for landslide assessment using tectonic geomorphologic features.

The PFR model improved the landslide susceptibility mapping and revised the inventory dataset in conjunction with field observations and LiDAR-derived DEMs in Mazandaran Province of Iran. However, the effectiveness of DEMs has not been studied to identify whether the LiDAR-derived DEM (5m) compared to DEMs with lower resolution than 5m may possibly achieve a desired improvement of landslide susceptibility mapping or not (Safaiee et al. 2010; Rajabi et al. 2011; Jebur et al. 2014).

This study also explored the algorithms of semi-automated geometric landslide analysis, landslide deformation, and landslide classification. A modelling and simulation procedure for landslide deformation including calculating displacement of a landslide and flow direction are presented in this thesis. The proposed algorithm is used to model, simulate, and calculate displacements of a landslide in the Zagros and Alborz Mountains of Iran and potentially other locations in the world. The deformation and flow direction codes may be improved in MATLAB to directly incorporate the pixels of a DEM into the algorithm. Pixels are converted to points and they were also used to analyze, simulate, and model a deformation of mass movement and volume material displacement.

Although, this study has not attempted a quantitative research on accuracy performance of the output results, but this study identified that there are some limitations such as availability and cost of a high-resolution LiDAR data. They include before and after a landslide, and UAV flight permission as well. The disadvantage of the proposed algorithm is conversion of pixels to point. The proposed algorithm cannot upload two or more Excel files and to calculate two or more landslide polygons geometry at the same time. In addition to the above, the proposed algorithm cannot directly process the raster (i.e., cells) without using Nearest Neighbor Assignment (NNA) re-sampling technique (i.e., converting cells to points) in ArcGIS. The flow direction arrays sometimes do not appear on the windows and it may possibly be because of the updated MATLAB version.

There are sources of error in the proposed algorithm and software package such as computational error, equipment error, and modelling error (i.e. lack of adjustment of points, pixels, and grids from before and after a landslide). However, the present package in MATLAB platform contributes by:

131

- Determining the landslide type;

- Calculating the area of a landslide polygon;

- Determining and measuring the length and width of a landslide;

- Calculating the volume of material displacement and determining mass movement (deformation); and

- Identifying the flow direction of a landslide material movement.

In addition to the above, this study introduced a taxonomy of landslides which is based on the geometry and geographical coordinates of a landslide in this Ph.D. thesis.

7.2 Recommendations for Future Work

This study recommends exploring tectonic geomorphologic features such as sinuosity of river and drainage slope for landslide investigations for the future work. In addition to explore tectonic geomorphology, this study recommends utilizing the recent Google Earth images associated with RADAR data for landslide detection and susceptibility mapping. Therefore, this study suggests determining the effectiveness of high-resolution of DEMs as compared to low-resolution DEMs on landslide susceptibility mapping performance. This study may also suggest exploring landslide susceptibility mapping using PFR at Sari-Kiasar Watershed, Northern Iran as well as the Dez River watershed, south-west of Iran with a higher resolution of LiDAR-derived DEM than 5m.

This study recommends researchers to collect more data samples from other geographical locations to implement the scripts for the future work. Because, it is to reconfirm the proposed model performances for calculating volume, material displacement, and flow direction as compared to the developed algorithms in alignment with the field measurements. Also, this study may recommend developing a code that improves re-sampling technique without giving any

assumption (i.e., nAfter ≥ nBefore) that can accept any pixel resolution of the DEMs of before and after a landslide. This study recommends researchers to compare a quantitative research on the output result by the proposed algorithm using available inventory data. This study also suggests applying the concept algorithm in developing a code by implementing ArcScript or Python languages that can be easily worked in ArcGIS.

Finally, this Ph.D. research thesis recommends that a web interface platform be created to use this algorithm and the three developed codes for geospatial location-based landslide polygons in shape file format; and to process geometric analysis, volume calculation, flow direction, and classification of a landslide automatically. This platform will allow analysts in the world to update landslide inventory datasets in real-time.

References

Abellan, A., Vilaplana, J. M., Calvet J., and Blanchard, J. (2010). Detection and spatial prediction of rockfalls by means of terrestrial laser scanning modelling. *Geomorphology*. 119:162-171.

Alavi, M. (1994). Tectonics of the Zagros Orogenic Belt of Iran: New data and interpretations. *Tectonophysics*. 229:211-238.

Ali, S.A., and Pirasteh, S. (2004). Geological applications of Landsat Enhanced Thematic Mapper (ETM) data and Geographic Information System (GIS): Mapping and structural interpretation in south-west Iran, Zagros Structural Belt. *International Journal of Remote Sensing*. 25(21):4715-4727.

Ali, S. A., Rangzan, K., and Pirasteh, S. (2003a). Remote sensing and GIS study of tectonics and net erosion rates in the Zagros Structural Belt, southwestern Iran. *Mapping Sciences and Remote Sensing*. 40(4):253-262.

Ali, S. A., Rangzan, K., and Pirasteh, S. (2003b). Use of digital elevation model for study of drainage morphometry and identification stability and saturation zones in relations to landslide assessments in parts of the Shahbazan area, SW Iran. *Cartography*. 32:71-76.

Al-Rousan, N., Cheng, P., Petrie, G., Toutin, T., and Valadan Zoej, M. J. (1997). Automated DEM extraction and orthoimage generation from SPOT level 1B imagery. *Photogrammetric Engineering and Remote Sensing*. 63:965-974.

Anbalagan, R. (1992). Landslide hazard evaluation and zonation mapping in mountainous terrain. *Engineering Geology*. 32:269-277.

Anbalagan R., Kumar R., Lakshmanan K., Parida S., and Neethu S. (2015). Landslide hazard zonation mapping using frequency ratio and fuzzy logic approach: A case study of Lachung Valley, Sikkim. *Geoenvironmental Disasters*. 2(6):20-17.

Andersen, S., and Andersen, L. (2010). Modelling of landslides with the material-point method. *Computational Geosciences*. 14:137.

Ardizzone, F., Cardinali, M., Carrara, A., Guzzetti, F., and Reichenbach, P. (2002). Impact of mapping errors on the reliability of landslide hazard maps. *Natural Hazards Earth System Science*. 2:3-14.

Ardizzone, F., Cardinali, M., Galli, M., Guzzetti, F., and Reichenbach, P. (2007). Identification and mapping of recent rainfall-induced landslides using elevation data collected by Aerial LiDAR. *Natural Hazards Earth System Science*. 7:637-650.

Berberian, M. (1995). Master blind thrust faults hidden under the Zagros folds: Active basement tectonics and surface Morpho-tectonics. *Tectonics*. 241:193-224.

Bianchini, S., Raspinia, F., Ciampalini, A., Lagomarsino, D., Bianchi, M., Bellotti, F., and Casagli, N. (2016). Mapping landslide phenomena in landlocked developing countries by means of satellite remote sensing data: The case of Dilijan (Armenia) area. *Geomatics, Natural Hazards Risk*. 7:1-17.

Binaghi, E., Brivio, P. A., Ghezzi, P., and Rampini, A. (1999). A fuzzy set-based accuracy assessment of soft classification. *Pattern Recognition Letters*. 20:935-948.

Booth, A. M., Roering, J. J., and Perron, J. T. (2009). Automated landslide mapping using spectral analysis and high-resolution topographic data: Puget Sound lowlands, Washington, and Portland Hills, Oregon. *Geomorphology*. 109:132–147.

Brunsden, D. (1996). Mass movement, the research frontier and beyond: A geomorphological approach. *Geomorphology*. 7:85-128.

Bull, W. B. (2007). Tectonic geomorphology of mountains: A new approach to Paleoseismology. *Malden*: Blackwell. Wiley.

Burbank, D. W., and Anderson, R. S. (2001). Tectonic Geomorphology. Oxford: *Blackwell Science*. John Wiley & Sons Press. USA.

Burden, R. L., and Faires, J. D. (2011). *Numerical Analysis* (9th ed.). Boston, Mass: Brooks/Cole.

Carnec, C., Massonnet, D., and King, C. (1996). Two examples of the use of SAR interferometry on displacement fields of small spatial extent. *Geophysics Research Letter*. 23:3579-3582.

Carrara, A. M., Cardinali, M., Detti, R., Guzzetti, F., Pasqui, V., and Reichenbach, P. (1991). GIS techniques and statistical models in evaluating landslide hazard. *Earth Surface Processes Landforms*. 16:427-445.

Carrara, A., Guzzetti, F., Cardinali, M., and Reichenbach, P. (1999). Use of GIS technology in the prediction and monitoring of landslide hazard. *Natural Hazards*. 20:117-135.

Catani, F., Lagomarsino, D., Segoni, S., and Tofani, V. (2013). Landslide susceptibility estimation by random forests technique: Sensitivity and scaling issues. *Natural Hazards Earth System Science*. 13:2815-2831.

Cavalli, M., Trevisani, S., Goldin, B., Mion, E., Crema, S., and Valentinotti, R. (2013). Semiautomatic derivation of channel network from a high resolution DTM: The example of an Italian alpine region. *European Journal Remote Sensing*. 46:152-174.

Chen, Y., and Medioni, G. (1992). Object modelling by registration of multiple range images. *Image Vision Computer*. 10:145-155.

Chen, W., Li, W., Hou, E., Zhao, Z., Deng, N., Danzhi, B., and Wang, H. (2014). Landslide susceptibility mapping based on GIS and information value model for the Chencang District of Baoji, China. *Arabian Geosciences Journal*. 7 (11):4499–4511.

Choi, J., Oh, H. J., Lee, H. J., Lee, C., and Lee, S. (2012). Combining landslide susceptibility maps obtained from frequency ratio, logistic regression, and artificial neural network models using ASTER images and GIS. *Engineering Geology*. 124:12-23.

Chugh, A. K., and Stark, T. D. (2005). Displacement analysis of a landslideLandslide, Senneset, Flaate, and Larsen (eds.)*: Landslides and Avalanches*.. London: Taylor & Francis.

Chung, C.-J. F., and Fabbri, A. (2003). Validation of spatial prediction models for landslide hazard mapping. *Natural Hazards*. 30:451-472.

Ciampalini, A., Raspini, F., Frodella, W., Bardi, F., Bianchini, S., and Moretti, S. (2016). The effectiveness of high-resolution LiDAR data combined with PSInSAR data in landslide study. *Landslides*. 13:399-410.

Cruden, D. M. (1991). A simple definition of a landslide. *Bulletin of the International Association of Engineering Geology*. 43(1): 27-29.

Dai, F. C., and Lee, C. F. (2002). Landslide characteristics and slope instability modeling using GIS, Lantau Island, Hong Kong. *Geomorphology*. 42:213-228.

Cruden, D. M., and Varnes, D. G. (1996). Landslide types and processes, special report, Transportation Research Board. *National Academy of Sciences*. 247:36-75

Dar, R. A., Romshoo, S. A., Chandra, R., and Ahmad, I. (2014). Tectono-geomorphic study of the Karewa Basin of Kashmir Valley. *Journal of Asian Earth Science*. 92:143-156.

Deng, X., Li, L., and Tan, Y. (2017). Validation of spatial prediction models for landslide susceptibility mapping by considering structural similarity. *International Journal of Geo-Information*. 6:103.

Dietrich, E. W., Reiss, R., Hsu, M. L., and Montgomery, D. R. (1995). A process-based model for colluvial soil depth and shallow landsliding using digital elevation data. *Hydrological Process.* 9:383-400.

Dikau, R., Brunsden, D., Schrott, L., and Ibsen, M-L. (Eds.). (1996). *Landslide recognition: Identification, movement and causes*. Wiley.

Donati, L., and Turrini, M. C. (2002). An objective method to rank the importance of the factors predisposing landslides with the GIS methodology application to an area of the Apennines (Valneria; Perugia, Italy). *Engineering Geology.* 63:277-290.

Duan, J., and Grant, G. E. (2000). Shallow landslide delineation for steep forest watersheds based on topographic attributes and probability analysis. In J. P. Wilson and J. C. Gallant (Eds.), *Terrain analysis – Principles and Applications* (pp. 311-329).

Eeckhaut, M., and Van Den, J. P. (2007). Use of LiDAR-derived images for mapping old landslides under forest. *Earth Surface Processing Landforms*. 32:754-769.

Ercanoglu, M., Kasmer, O., and Temiz, N. (2008). Adaptation and comparison of expert opinion to analytical hierarchy process for landslide susceptibility mapping. *Bulletin Engineering Geology Environment*. 67:565-578.

Evans, J. S., Hudak, A. T., Faux, R., and Smith, A. M. S. (2009). Discrete return Lidar in natural resources: Recommendations for project planning, data processing, and deliverables. *Remote Sensing*. 1:776-794.

Farrokhnia, A., Pirasteh, S., Pradhan, B., Pourkermani, M., and Arian, M. (2011). A recent scenario of mass wasting and its impact on the transportation in Alborz Mountains, Iran: Contribution from geo information technology. *Arabian Geosciences*. 4:1337-1349.

Freeman, G. T. (1991). Calculating catchment areas with divergent flow based on a regular grid. *Computer Geosciences*. 17: 413-422.

Freeman, H., and Shapira, R. (1975). Determining the minimum-area encasing rectangle for an arbitrary closed curve. *Commun. ACM*. 18:409-413.

George, B. D., Kalliopi, G. P., Ariklia, S. H. D., Dimitrios, P., and Konstantinos, C. G. (2012). Potential suitability for urban planning and industry development using natural hazard maps and geological–geomorphological parameters. *Environmental Earth Sciences*. 66:537-548.

Gholami, M., Ghachkanlu, N.E., Khosravi, K., and Pirasteh, S. (2017) Landslide Prediction Capability from Comparison of Frequency Ratio, Fuzzy Gamma and Landslide Index Method. *Environmental Earth Sciences*. In review.

Ghuffar, S., Szekely, B., Roncat, A., and Pfeifer, N. (2013). Landslide displacement monitoring using 3D range flow on airborne and terrestrial LiDAR data. *Remote Sensing*. 5:2720-2745.

Glenn, N. F., Streutker, D. R., Chadwick, D. J., Thackray, G. D., and Dorsch, S. J. (2006). Analysis of LiDAR-derived topographic information for characterizing and differentiating landslide morphology and activity. *Geomorphology*. 73:131-148.

Goetz, J. N., Guthrie, R. H., and Brenning, A. (2011). Integrating physical and empirical landslide susceptibility models using generalized additive models. *Geomorphology*. 129:376-386.

Gomez, H., and Kavzoglu, T. (2005). Assessment of shallow landslide susceptibility using artificial neural networks in Jabonosa River Basin, Venezuela. *Engineering Geology*. 78:11-27.

Guan, H., Li, J., Yu, Y., and Zhong, L. (2014). DEM generation from LiDAR data in wooded mountain areas by cross-section-plane analysis. *International Journal of Remote Sensing*. 35:927-948.

Guns, M., and Vanacker, V. (2012). Logistic regression applied to natural hazards: rare event logistic regression with replications. *Natural Hazards Earth System Science.*, 12:1937–1947.

Guzzetti, F., Carrara, A., Cardinali, M., and Reichenbach, P. (2012). Landslide hazard evaluation: A review of current techniques and their application in multi-scale study, Central Italy. *Geomorphology*. 31:181-216.

Guzzetti, F., Reichenbach, P., Cardinali, M., Galli, M., and Ardizzone, F. (2005). Probabilistic landslide hazard assessment at the basin scale. *Geomorphology*. 72:272-299.

Hamdouni, R., El Irigaray, C., Jimenez-Peralvarez, J. D., and Chacon, J. (2010). Correlations analysis between landslides and stream length-gradient (SL) index in the southern slopes of Sierra Nevada (Granada, Spain). *Geologically Active*. London: *Taylor & Francis*. pp. 141-149.

Hattanji, T., and Moriwaki, H. (2009). Morphometric analysis of relic landslides using detailed landslide distribution maps: Implications for forecasting travel distance of future landslides. *Geomorphology*. 103(3):447-454.

Haugerud, R. A., and Harding, D. J. (2001). Some algorithms for virtual deforestation (VDF) of LIDAR topographic survey data. *ISPRS Archives*, 34(3/W4): 211-217.

Haugerud, R. A., Harding, D. J., Johnson, S. Y., Harless, J. L., Weaver, C. S., and Sherrod, B. L. (2003). High-resolution LiDAR topography of the Puget Lowland, Washington. *GSA Today*. 13(6):4-10.

Highland, L. M., Bobrowsky, P., Kempthorne, D., and Myers, M. D. (2008). The landslide handbook: A guide to understanding landslides. Reston, VA: *Department of the Interior U.S. Geological Survey*.

Hodgson, M. E., and Bresnahan, P. (2004). Accuracy of airborne LiDAR-derived elevation: Empirical assessment and error budget. *Photogrammetry Engineering Remote Sensing*. 70:331-339.

Hopkinson, C., Chasmer, L., Young-Pow, C., and Treitz, P. (2004). Assessing forest metrics with a ground-based scanning LiDAR. *Canadian Journal of Forest Research*. 34:573-583.

Huabin, W., Gangjun, L., Weiya, X., and Gonghui, W. (2005). GIS-based landslide hazard assessment: An overview. *Progress in Physical Geography*. 29:548-567.

Hutchinson, J. N. (1988). Morphological and geotechnical parameters of landslides in relation to geology and hydrogeology, *Proceedings of the Fifth International Symposium on Landslides*. *Rotterdam*: Balkema.

Irigaray, C., Fernandez, T., El Hamdouni, R., and Chacón, J. (2007). Evaluation and validation of landslide-susceptibility maps obtained by a GIS matrix method: Examples from the Betic Cordillera (southern Spain). *Natural Hazards*. 41:61-79. doi:10.1007/s11069-006-9027-8.

Jaboyedoff, M., Oppikofer, T., Abellan, A., Marc-Henri, D., Loye, A., Metzger, R., and Pedrazzini, A. (2012). Use of LIDAR in landslide investigations: A review. *Natural Hazards*. 61:5-28.

James G. A., and Wynd, J. G. (1965). Stratigraphy nomenclature of the Iranian oil consortium agreement area. *AAPG Bulletin*. 49:2182-2245.

James, L. A., Watson, D. G., and Hansen, W. F. (2006). Using LiDAR data to map gullies and headwater streams under forest canopy: South Carolina, USA. *Catena*. 71:132-144.

Jebur, M. N., Pradhan, B., and Shafapour, T. M. (2014). Optimization of landslide conditioning factors using very high-resolution airborne laser scanning (LiDAR) data at catchment scale. *Remote Sensing of Environment*. 152:150-165.

Keaton, J. R., and DeGraff, J. V. (1996). Surface observation and geologic mapping. In A. K. Turner and R. L. Schuster (Eds.), *Landslide types and process* (pp. 178-230). National Academy Press; UK. p. 178-230.

Kirby, E., and Whipple, K. X. (2012). Expression of active tectonics in erosional landscapes. *Journal of Structural Geology*. 44:54-75.

Konstantinos, C., Vincenzo, G. D., Nikolaos, S., Katerina, K., George, D., George, B. D., and Hariklia, S. D. (2016). Assessment of earthquake-induced landslide hazard in Greece: From Arias intensity to spatial distribution of slope resistance demand. *Bulletin of Seismology Society America*. 106:174-188.

Korzeniowska, K., Pfeifer,N., Mandlburger, G., and Lugmayr, A. (2014). Experimental evaluation of ALS point cloud ground extraction tools over different terrain slope and land-cover types. *International Journal of Remote Sensing*. 35(13): 673-4697.

Kreyszig, E., Kreyszig, H., and Norminton, E. J. (2011). Advanced Engineering Mathematics (10th ed.). New York, NY*: Wiley.*

Lee, M. J., Park, I., and Saro, L. (2014). Forecasting and validation of landslide susceptibility using an integration of frequency ratio and neuro-fuzzy models: A case study of Seorak mountain area in Korea. *Environmental Earth Sciences*. 74:413-429 doi:10.1007/s12665-015-4048-9.

Lee, S., Chwae, U., and Min, K. (2002). Landslide susceptibility mapping by correlation between topography and geological structure: The Janghung area, Korea. *Geomorphology*. 46:149-162.

Lee, S., and Pradhan, B. (2006). Probabilistic landslide hazards and risk mapping on Penang Island, Malaysia. *Earth System Science*. 115(6):661-672.

Lee, S., Ryu, J.-H., Won, J.-S., and Park, H.-J. (2004). Determination and application of the weights for landslide susceptibility mapping using an artificial neural network. *Engineering Geology*. 71:289-302.

Lee, S., and Dan, N. T. (2005). Probabilistic landslide susceptibility mapping in the Lai Chau province of Vietnam: Focus on the relationship between tectonic fractures and landslides. *Environmental Geology*. 48:778-787.

Lee, S., Choi, J., and Min, K. (2004). Probabilistic landslide hazard mapping using GIS and remote sensing data at Boun, Korea. *International Journal of Remote Sensing*. 125(11):2037-2052.

Li, L., Liu, R., Pirasteh, S., Chen, X., He, L., and Li, J. (2017). A novel genetic algorithm for optimization of conditioning factors in shallow translational landslides and susceptibility mapping. *Arabian Geosciences Journal*.

Luzi, L., Pergalani, F., and Terlien, M. T. J. (2000). Slope vulnerability to earthquakes at subregional scale, using probabilistic techniques and geographic information systems. *Engineering Geology*. 58:313-336.

Lyons, N. J., Mitasova, H., and Wegmann, K. W. (2014). Improving masswasting inventories by incorporating debris flow topographic signatures. *Landslides*. 11:385–397.

Mahdavifar, M. R., Solaymani, S., and Jafari, M. K. (2006). Landslides triggered by the Avaj, Iran earthquake of June 22, 2002. *Engineering Geology*. 86:166-182.

Malamud, B. D., Turcotte, D. L., Guzzetti, F., and Reichenbach, P. (2004). Landslide inventories and their statistical properties. *Earth Surface Processing Land*. 29: 687-711.

Martha, T. R., Kerle, N., Jetten, V., Van Westen, C. J., and Vinod, K. K. (2010). Characterising spectral, spatial and morphometric properties of landslides for semi-automatic detection using object-oriented methods. *Geomorphology*. 116:24-36.

McKean, J., and Roering, J. (2004). Objective landslide detection and surface morphology mapping using high resolution airborne laser altimetry. *Geomorphology*. 70:339-351.

McKean, J., and Roering, J. (2003). Objective landslide detection and surface morphology mapping using high-resolution airborne laser altimetry. *Geomorphology*. 57:331-351.

Mehrdad, S., Husaini, O., Zenoddin, Y. B. M., and Vahed, G. (2010). Applying geospatial technology to landslide susceptibility assessment. *Electron Journal of Geotechnical Engineering*. 15:667-696.

Metternicht, G., Hurni, L., and Gogu, R. (2005). Remote sensing of landslides: An analysis of the potential contribution to geo-spatial systems for hazard assessment in mountainous environments. *Remote Sensing of Environment*. 98:284-303.

Mondini, A. C., Guzzetti, F., Reichenbach, P., Rossi, M., and Ardizzone, F. (2011). Semi-automatic recognition and mapping of rainfall induced shallow landslides using optical satellite images. *Remote Sensing of. Environment*. 115: 1742-1757.

Montgomery, D. R., and Dietrich, W. E. (1994). A physically based model for the topographic control on shallow landsliding. *Water Resources Research*. 30:1153-1171.

Mora, O. E., Lenzano, M. G., C. K. Toth, Grejner-Brzezinska, D. A. (2014). Analyzing the effects of spatial resolution for small landslide susceptibility and hazard mapping. The International Archives of the Photogrammetry, Remote Sensing and Spatial Information Sciences, Volume XL-1, 2014. *ISPRS Technical Commission I Symposium*, 17 – 20 November 2014, Denver, Colorado, USA.

Mousavi, S. Z. , Kavian A., Soleimani, K. , Mousavi, S.R., and Shirzadi, A. (2011). GIS-based spatial prediction of landslide susceptibility using logistic regression model. *Geomatics, Natural Hazards and Risk*. 2(1):33-50.

Nichol, J. E., and Wong, M. S. (2005). Satellite remote sensing for detailed landslide inventories using change detection and image fusion. *International Journal of Remote Sensing*. 26:1913-1926.

Niculitˇa, M. (2016). Automatic landslide length and width estimation based on the geometric processing of the bounding box and the geomorphometric analysis of DEMs. *Natural Hazards Earth System Sciences*. 16: 2021-2030. doi:10.5194/nhess-16-2021-2016.

Niethammer, U., James, M. R., Rothmund, S., Travelletti, J., and Joswig, M. (2012). UAV-based remote sensing of the Super-Sauze landslide: Evaluation and results. *Engineering Geology*. 128:2-11.

Oppikofer, T., Jaboyedoff, M., Blikra, L., and Derron, M. H. (2009). Characterization and monitoring of the A-knes rockslide using terrestrial laser scanning. *Natural Hazards Earth System Sciences*. 9:1643-1653.

Pack, R. T., Tarboton, D. G., and Goodwin, C. N. (1998). *Terrain stability mapping with SINMAP, technical description and users guide for version 1.00*. Logan, UT: Utah State University. (Report Number 4114-0).

Paolo, F., Giovanni, C., and Alberto, C. (2010). Techniques for evaluating the performance of landslide susceptibility models. *Engineering Geology*. 111:62-72.

Petley, D. (2012). Global patterns of loss of life from landslides. *Geology*. 40(10): 927-930.

Pfeifer, N., Kostli, A., and Kraus, K. (1998). Interpolation and filtering of laser scanner data-implementation and first results: *ISPRS Archives.* 32(3/1):153-159.

Pike, R. J. (1988). The geometric signature: Quantifying landslide-terrain types from Digital Elevation Models. *Mathematic Geology*. 20:491-511.

Pirasteh, S., Li, J., and Attarzadeh, I. (2015). Implementation of the damage index approach to rapid evaluation building resistance for earthquakes. *Earth Science Informatics*.

Pirasteh, S., Pradhan, B., and Rizvi, S. M. (2011a). Tectonic process analysis in Zagros Mountain with the aid of drainage networks and topography maps dated 1950-2001 in GIS. *Arabian Journal Geosciences*. 4:171-180.

Pirasteh, S., Pradhan, B., and Safari, H. (2011b). Coupling of DEM and remote sensing based approaches for semi-automated detection of regional geo-structural features in Zagros Mountain, Iran. *Arabian Journal Geosciences*. 6:91-99.

Pirasteh, S., Safari, H. O., Pradhan, B., and Attarzadeh, I. (2010). Lithomorphotectonics analysis using Landsat ETM data and GIS techniques: Zagros Fold Belt (ZFB), SW Iran. *International Geoinformatics Research and Development*. 1:28-36.

Pirasteh, S., Woodbridge, K., and Rizvi, S. M. (2009). Geo-information technology (GiT) and tectonic signatures: The River Karun and Dez, Zagros Orogen in south-west Iran. *International Journal of Remote Sensing*. 30:389-404.

Pirasteh, S., and Li, J. (2016). Landslides investigations from geo-informatics perspective: Quality, challenges, and recommendations. *Geomatics, Natural Hazards and Risk*. 8(2): 448-465.

Pirasteh, S., and Li, J. (2017). *Global Changes and Natural Disaster Management: Geo-information Technologies*. Berlin: Springer. ISBN 978-3-319-51843-5.

Pirasteh, S., Li, J., and Chapman, M. (2017). Use of LiDAR-derived DEM and a stream length-gradient index approach to investigation of landslides in Zagros Mountains, Iran. *Geocarto Journal*.

Pirasteh, S., and Li, J. (2017). Probabilistic Frequency Ratio (PFR) model for quality improvement of landslides susceptibility mapping from LiDAR point clouds. *Geoenvironmental Disaster Journal*. 4:19.

Pirasteh, S., Rizvi, S. M. A., Ayazi, M. H., and Mahmoodzadeh, A. (2010). Using microwave remote sensing for flood study in Bhuj Taluk, Kuchch District Gujarat, India. *International Geoinformatics Research and Development Journal*. 1(1):13-24.

Poiraud A.(2014). Landslide susceptibility–certainty mapping by a multi-method approach: A case study in the Tertiary basin of Puy-en-Velay (Massif central, France). *Geomorphology*. 216:(1):208-224.

Pradhan, B., and Buchroithner, M. (2010). Weights-of-evidence model applied to landslide susceptibility mapping in a tropical hilly area. *Geomatics, Natural Hazards and Risk*. 1:199-223.

Pradhan, B., and Pirasteh, S. (2010). Comparison between prediction capabilities of neural network and fuzzy logic techniques for landslide susceptibility mapping. *Disaster Advances Journal*. 3(2):19-25.

Pradhan, R. P., Singh, R. P., and Buchroithner, M. F. (2006). Estimation of stress and its use in evaluation of landslide prone regions using remote sensing data. *Advanced Space Research*. 37:698-709.

Prokop, A., and Panholzer, H. (2009). Assessing the capability of terrestrial laser scanning for monitoring slow moving landslides. *Natural Hazards Earth System Sciences*. 9:1921-1928.

Rajabi, A. M., Mahdavifar, M. R., Khamehchiyan, M., and Del Gaudio, V. (2011). A new empirical estimator of coseismic landslide displacement for Zagros Mountain region (Iran). *Natural Hazards*. 59:1189-1203.

Rau, J. Y., Jhan, J. P., Lo, C. F., and Lin, Y. S. (2011). Landslide mapping using imagery acquired by a fixed-wing UAV. International Archives of the Photogrammetry, Remote Sensing and Spatial Information Sciences, Volume *XXXVIII-1/C22, 2011 ISPRS* Zurich 2011 Workshop; 2011 September 14-16; Zurich, Switzerland.

Rau, J.-Y., Jhan, J.-P., and Rau, R.-J. (2014). Semiautomatic object-oriented landslide recognition scheme from multisensor optical imagery and DEM. *IEEE Transactions Geoscience and Remote Sensing*. 52(2):1336-1349.

Ren, F., Wu, X., Zhang, K., and Niu, R. (2014). Application of wavelet analysis and a particle swarm-optimized support vector machine to predict the displacement of the Shuping landslide in the Three Gorges, China. *Environmental Earth Sciences*. 73 (8): 4791-4804.

Renee, S. V. M. (2012). Comparison of bivariate and multivariate statistical approaches in landslide susceptibility mapping at a regional scale. *Geomorphology*. 161-162:40-45.

Roering, J. J., Stimely, L. L., Mackey, B. H., and Schmidt, D. A. (2009). Using DInSAR airborne LIDAR and archival air photos to quantify landsliding and sediment transport. *Geophysics Research Letter*. 36:L19402.

Safaiee, M., Omar, H., Yousof, Z. B. M., and Vahed, G. (2010). Applying geospatial technology to landslide susceptibility assessment. *Electron Journal Geotechnical Engineering*. 15:667-696.

Safari, H. O., Pirasteh, S., and Pradhan, B. (2009). Upliftment estimation of the Zagros Transverse Fault in Iran using geoinformatics technology. *Remote Sensing*. 1:1240-1256.

Sarkar, S., and Kanungo, D. P. (2004). An integrated approach for landslide susceptibility mapping using remote sensing and GIS. *Photogrammetric Engineering and Remote Sensing*. 70(5):617-625.

Sassa K. (2017a). Monthly publication of Landslides: *Journal of International Consortium on Landslides (ICL)*.

Sassa K. (2017b). Participants in the Fourth World Landslide Forum and call for ICL members, supporters, and associates. *Landslides.* 14(5):1839-1842. Sassa K. (2017c). The Fifth World Landslide Forum-implementing and monitoring the ISDR-ICL Sendai Partnerships. *Landslides*. 14(5):1857-1859.

Schicker, R., and Moon, V. (2012). Comparison of bivariate and multivariate statistical approaches in landslide susceptibility mapping at a regional scale. *Geomorphology*. 161-162:40-57.

Schulz, W. H. (2007). Landslide susceptibility revealed by LIDAR imagery and historical records, Seattle, Washington. *Engineering Geology*. 89:67-87.

Seefelder, C. L. N., Koide, S., and Mergili, M. (2016). Does parameterization influence the performance of slope stability model results? A case study in Rio de Janeiro, Brazil. *Landslides*. 14 (4): 1389–1401.

Shan, J., and Toth, C.K. (2008). *Topographic Laser Ranging and Scanning: Principles and Processing*. CRC Press. *Taylor and Francis*.

Sherrod, B. L., Brocher, T. M., Weaver, C. S., Bucknam, R. C., Blakely, R. J., Kelsey, H. M., Nelson, A. R., and Haugerud, R. (2004). Holocene fault scarps near Tacoma, Washington, USA. *Geology*. 32(1):9-12.

Shirzadi, A., Bui, D. T., Pham, B. T., Solaimani, K, Chapi, K., Kavian, A., Shahabi, H., and Revhaug, I. (2017). Shallow landslide susceptibility assessment using a novel hybrid intelligence approach. *Environmental Earth Sciences*.76:60.

Siyahghalat, S., Saraf, A. K., Pradhan, B., Jebur, N. M., and Shafapour, T. M. (2016). Rule-based semi-automated approach for the detection of landslides induced by 18 September 2011 Sikkim, Himalaya, earthquake using IRS LISS3 satellite images. *Geomatics, Natural Hazards Risk*. 7:326-344.

Soeters, R., van Westen, C. J. (1996). Slope stability: Recognition, analysis and zonation. In A. K. Turner and R. L. Schuster (Eds.), *Landslides Investigation and Mitigation* (). Springer, Special Report 247, pp. 129-177.

Solaimani, K., Mousavi, S. Z., and Kavian, A. (2013). Landslide susceptibility mapping based on frequency ratio and logistic regression models. *Arabian Journal Geosciences*. 6:2557-2569.

Spaete, L. P., Glenn, N. F., Derryberry, D. R., Sankey, T., Mitchell, J., and Hardegree, S. P. (2011). Vegetation and slope effects on accuracy of a LiDAR-derived DEM in the sagebrush steppe. *Remote Sensing Letters*. 2:317-326.

Streutker, D. R., and Glenn, N. F. (2006). LiDAR measurement of sagebrush steppe vegetation heights. *Remote Sensing of Environment*. 102 (1-2):135-145.

Su, C., Wang, L., Wang, X., Huang, Z., and Zhang, X. (2015). Mapping of rainfall-induced landslide susceptibility in Wencheng, China, using support vector machine. *Natural Hazards*. 76:1-23.

Su, J. G., Bork, E. W. (2006). Influence of vegetation, slope and LiDAR sampling angle on DEM accuracy. *Photogrammetric Engineering and Remote Sensing*. 72:1265-1274.

Su, W. J., and Stohr, C. (2000). Aerial photointerpretation of landslides along the Ohio and Mississippi Rivers. *Environmental and Engineering Geoscience*. VI(4):311-323.

Tarchi, D., Casagli, N., Fanti, R., Leva, D. D., Luzi, G., Pasuto, A., Pieraccini, M., and Silvano, S. (2003). Landslide monitoring by using ground-based SAR interferometry: An example of application to the Tessina landslide in Italy. *Engineering Geology*. 68:15-30.

Taylor, F. E., Malamud, B. D., and Witt, A. (2015). What shape is a landslide? Statistical patterns in landslide length to width ratio. *Geophysical Research Abstracts*. 17:EGU2015-10191.

Teza, G., Galgaro, A., Zaltron, N., and Genevois, R. (2007). Terrestrial laser scanner to detect landslide displacement fields: A new approach. *International Journal of Remote Sensing*. 28:3425-3446.

Tian, Y., XiaO, C., Liu, Y. et al. Sci. China Ser. E-Technol. Sci. (2008). Effects of raster resolution on landslide susceptibility mapping: A case study of Shenzhen. *Science in China*. 51(Suppl 2): 188-198.

Travelletti, J., Oppikofer, T., Delacourt, C., Malet, J., and Jaboyedoff, M. (2008). Monitoring landslide displacements during a controlled rain experiment using a long-range terrestrial laser scanning (TLS). *International Archives of the Photogrammetry Remote Sensing*. 37:485-490.

Tsutsui, K., Rokugawa, S., Nakagawa, H., Miyazaki, S., Cheng, Chin-Tung, Shiraishi, T., and Yang, Shiun-Der. (2007). Detection and volume estimation of large-scale landslides based on elevation-change analysis using DEMs extracted from high-resolution satellite stereo imagery. *IEEE Transactions on Geosciences and Remote Sensing*. 45(6): 1681-1696.

Van Den Eeckhaut, M., Poesen, J., Verstraeten, G., Vanacker, V., Moeyersons, J., Nyssen, J., and Van Beek, L. P. H. (2005). The effectiveness of hillshade maps and expert knowledge in mapping old deep-seated landslides. *Geomorphology*. 67:351-363.

Varnes, D. J. (1978). Slope movement types and processes. In R. L. Schuster and R. J. Krizek (Eds.), *Special Report 176: Landslides: Analysis and Control*. Washington, D.C.: National Academy of Science.pp:11-33.

Watts, P. (2004). Probabilistic predictions of landslide tsunamis off Southern California. *Marine Geology*. 203:281-301.

Wehr, A., and Lohr, U. (1999). Airborne laser scanning: An introduction and overview. *ISPRS Journal Photogrammetry Remote Sensing*. 54:68-82.

Wen, F., Xin, S., Cao, W.Y., Zheng, B. (2017). Landslide susceptibility assessment using the certainty factor and analytic hierarchy process. *Journal of Mountain Science*. 14 (5): 906-925.

Westen, C. J., Van, C. E., and Kuriakose, S. L. (2008). Spatial data for landslide susceptibility,

hazard, and vulnerability assessment: An overview. *Engineering Geology*. 102:112-131.

Wu, S., Li, J., and Huang, G. H. (2008). Study on DEM-derived primary topographic attributes for hydrologic applications: Sensitivity to elevation data resolution. *Applied Geography*. 28: 210-223.

Wu, W., and Sidle, R. C. (1995). A distributed slope stability model for steep forested watersheds. *Water Resources Research*. 31:2097-2110.

Yalkin, A. (2008). GIS-based landslide susceptibility mapping using analytical hierarchy process and bivariate statistics in Ardesen (Turkey): Comparisons of results and confirmations. *Catena*. 72:1-12.

Yang, X., and Li, J. (2013); Advances in Mapping from Remote Sensor Imagery: Techniques and Applications. CRC Press. *Taylor and Francis*. USA. pp:33-55.

Yilmaz, I., and Yildirim, M. (2006). Structural and geomorphological aspects for the Kat Landslides (Tokat-Turkey) and susceptibility mapping by means of GIS. *Environmental Geology*. 50:461-472.

Yilmaz, I. (2010). The effect of the sampling strategies on the landslide susceptibility mapping by conditional probability (CP) and artificial neural network (ANN). *Environmental Earth Sciences*. 60:505-519.

Youssef, A. M., Al-Kathery, M., Pradhan, B. , and El-Sahly, T. (2016). Debris flow impact assessment along the Al-Raith Road, Kingdom of Saudi Arabia, using remote sensing data and field investigations. *Geomatics, Natural Hazards Risk*. 7(2): 620-638.

Youssef, A. M., Pourghasemi, H. R., El-Haddad, B.A, Dhahry, B. K. (2015). Landslide susceptibility maps using different probabilistic and bivariate statistical models and comparison of their performance at Wadi Itwad Basin, Asir Region, Saudi Arabia. *Bulletin of Engineering Geology Environment*. 75(1): 63-87.

Yousef, A. M., Pourghasemi, H. R., El-Haddad, B. A., and Dhahry, B. K. (2015). Landslide susceptibility maps using different probabilistic and bivariate statistical models and comparison of their performance at Wadi Itwad Basin, Asir Region, Saudi Arabia. *Bulletin of Engineering Geology Environment*. 75:63-87.

Zare, M., Pourghasemi, H. R., Vafakhah, M., and Pradhan, B. (2013). Landslide susceptibility mapping at Vaz Watershed (Iran) using an artificial neural network model: A comparison

between multilayer perceptron (MLP) and radial basic function (RBF) algorithms. *Arabian Journal Geosciences*. 6:2873-2888.

Zhou, C. H., Lee, C. F., Li, J., and Xu, Z. W. (2002). On the spatial relationship between landslides and causative factors on Lantau Island, Hong Kong. *Geomorphology*. 43:197-207.

Zhou, G., Esaki, T., Mitani, M., Xie, M., and Mori, J. (2003). Spatial probabilistic modelling of slope failure using integrated GIS Monte Carlo simulation approach. *Engineering Geology*. 68:373-386.